



**NATIONAL AND KAPODISTRIAN UNIVERSITY OF ATHENS**

**SCHOOL OF SCIENCE  
FACULTY OF BIOLOGY**

**MSc in Microbial Biotechnology**

**MASTER THESIS**

**The peroxisomal WscA protein function in *Aspergillus  
nidulans***

**Sofia N Dimou**

**Supervisor**            **G. Diallinas, Professor, UoA**

**ATHENS**

**JULY 2019**



**ΕΘΝΙΚΟ ΚΑΙ ΚΑΠΟΔΙΣΤΡΙΑΚΟ ΠΑΝΕΠΙΣΤΗΜΙΟ ΑΘΗΝΩΝ**

**ΣΧΟΛΗ ΘΕΤΙΚΩΝ ΕΠΙΣΤΗΜΩΝ  
ΤΜΗΜΑ ΒΙΟΛΟΓΙΑΣ**

**ΠΜΣ ΜΙΚΡΟΒΙΑΚΗ ΒΙΟΤΕΧΝΟΛΟΓΙΑ**

**ΔΙΠΛΩΜΑΤΙΚΗ ΕΡΓΑΣΙΑ**

**Ο ρόλος της υπεροξεισωμικής πρωτεΐνης WscA στον  
*Aspergillus nidulans***

**Σοφία Ν Δήμου**

**Επιβλέπων**

**Γ. Διαλλινάς, Καθηγητής, ΕΚΠΑ**

**ΑΘΗΝΑ**

**Ιούλιος 2019**

# MASTER THESIS

The peroxisomal WscA protein function in *Aspergillus nidulans*

**Sofia N.Dimou**

**S.N.: 81707**

**Supervisor**            **G.Diallinas**, Professor, UoA

**EXAMINING COMMITTEE**    **G.Diallinas**, Professor, UoA  
   **D.Hatzinikolaou**, Assistant Professor, UoA  
   **P. Syntichaki**, Assistant Professor, BRFAA

July 2019

## **ΔΙΠΛΩΜΑΤΙΚΗ ΕΡΓΑΣΙΑ**

Ο ρόλος της υπεροξεισωμικής πρωτεΐνης WscA στον *Aspergillus nidulans*

**Σοφία Ν. Δήμου**

**A.M.: 81707**

**Επιβλέπων**

**Γ. Διαλλινάς, Καθηγητής, ΕΚΠΑ**

**ΕΞΕΤΑΣΤΙΚΗ ΕΠΙΤΡΟΠΗ**

**Γ. Διαλλινάς, Καθηγητής, ΕΚΠΑ**

**Δ. Χατζηνικολάου, Αναπληρωτής Καθηγητής, ΕΚΠΑ**

**Π. Συντυχάκη, Αναπληρώτρια Καθηγήτρια, ΙΙΒΕΑ**

Ιούλιος 2019

## ABSTRACT

Peroxisomes are highly metabolic organelles involved in key functions in eukaryotic cells. One of them is the well-studied purine assimilation pathway in *Aspergillus nidulans*, where part of the purine catabolic enzymes is located inside peroxisomes. Since certain steps of the pathway occur inside these organelles, while others in the cytoplasm, there needs to be a transport of purine metabolites across the peroxisomal membrane. As these intermediates are unable to diffuse freely through lipid bilayers, specific transporters must exist for their passage membrane across the peroxisomal membrane. In order to identify them, we conducted an *in silico* search for evolutionarily correlated gene loss associated with fungal peroxisomal uric acid oxidase (UOX), where PMP22-like proteins, found to be the most promising candidates, as some of them function as promiscuous channels in organellar membranes. To investigate whether PMP22 channels actually have a role in peroxisomal uric acid transport and catabolism, we functionally analyzed the relevant *Aspergillus nidulans* protein, WscA, which is encoded by the uncharacterized gene *AN7258*. We confirmed that WscA is a peroxisomal membrane protein that co-localizes with PTS1-tagged mRFP, UOX or HexA, the latter considered a protein of Woronin bodies (WBs), organelles originating from peroxisomes that dynamically plug septal pores in filamentous ascomycetes. Our results suggest that in *A. nidulans*, unlike some other ascomycetes, there is no strict protein segregation of peroxisomal and WB-specific proteins. Importantly, genetic deletion of *wscA*, but not of *hexA*, led to lack of peroxisomal localization at septal pores, suggesting that WscA is a key factor for septal pore functioning. Additionally,  $\Delta wscA$  resulted in increased sensitivity to oxidative stress, apparently as a consequence of not only the inability for septal pore plugging, but also a recorded reduction in peroxisome biogenesis. However, deleting *wscA* had no effect on uric acid or purine utilization, as we hypothesized, a result in also line with the observation that expression of WscA was not affected by regulatory mutants and conditions known to control purine catabolic enzymes. Our results are discussed within the frame of previous studies of WscA homologues in other fungi, as well as, the observed gene losses of PMP22 and peroxisomal uric acid oxidase.

**SUBJECT AREA:** purine transporter

**KEYWORDS:** filamentous fungi, uric acid, urate oxidase, Woronin bodies, septa

## ΠΕΡΙΛΗΨΗ

Τα υπεροξεισώματα είναι μεταβολικά οργανίδια που εμπλέκονται σε διάφορες σημαντικές λειτουργίες στα ευκαρυωτικά κύτταρα. Μία από αυτές είναι το καλά μελετημένο μονοπάτι καταβολισμού των πουρινών στον μύκητα *Aspergillus nidulans*, καθώς ορισμένα από τα ένζυμα που συμμετέχουν σε αυτό βρίσκονται μέσα στα υπεροξεισώματα. Εφόσον κάποια από τα βήματα του μονοπατιού πραγματοποιούνται μέσα σε αυτά τα οργανίδια, ενώ άλλα στο κυτταρόπλασμα, είναι λογικό να διεξάγεται μεταφορά των ενδιάμεσων μεταβολικών κατά μήκος της υπεροξεισωμικής μεμβράνης. Λαμβάνοντας υπόψη ότι οι μεταβολίτες αυτοί δεν μπορούν να διαχυθούν ελεύθερα μέσω της λιπιδικής στοιβάδας των υπεροξεισωμάτων, ειδικοί μεταφορείς πρέπει να βρίσκονται εκεί επιτελώντας αυτό το ρόλο. Για τον εντοπισμό τους πραγματοποιήσαμε *in silico* αναζήτηση γονιδίων που 'χάνονται' εξελικτικά μαζί με την υπεροξεισωμική οξειδάση του ουρικού οξέος (UOX) στους μύκητες. Κατά την αναζήτηση αυτή, οι πρωτεΐνες της οικογένειας PMP22 εμφανίστηκαν ως οι καλύτεροι δυνατοί υποψήφιοι, καθώς μερικές από αυτές λειτουργούν ως κανάλια σε μεμβράνες οργανιδίων. Για να διερευνήσουμε αν τα PMP22 κανάλια έχουν πράγματι κάποιο ρόλο στη μεταφορά ουρικού οξέος, αναλύσαμε τη λειτουργία της σχετικής πρωτεΐνης στο μύκητα *Aspergillus nidulans*, την οποία ονομάσαμε WscA και η οποία κωδικοποιείται από το μη χαρακτηρισμένο γονίδιο AN7258. Επιβεβαιώσαμε ότι η WscA βρίσκεται στη μεμβράνη των υπεροξεισωμάτων και συνεντοπίζεται μαζί με mRFP συντηγμένη με υπεροξεισωμικό πεπτιδίο οδηγό PTS1, την UOX και την HexA, η οποία είναι βασική πρωτεΐνη εξειδικευμένων υπεροξεισωμάτων, των λεγόμενων σωματίων Woronin, τα οποία φράσσουν τους πόρους των διαφραγμάτων στους νηματοειδείς ασκομύκητες. Η γενετική διαγραφή του *wscA* γονιδίου οδήγησε σε αυξημένη ευαισθησία σε μεταβολικό ή οξειδωτικό στρες, πιθανόν ως συνέπεια της παρατηρούμενης μείωσης στη βιογένεση των υπεροξεισωμάτων αλλά και της ανικανότητας του συγκεκριμένου στελέχους να φράξει τους πόρους των διαφραγμάτων. Παρ' όλο το σχεδόν απόλυτο συνεντοπισμό της WscA με την HexA, η διαγραφή του *hexA* γονιδίου δεν οδήγησε σε τέτοια αδυναμία τοποθέτησης των υπεροξεισωμάτων στους πόρους των διαφραγμάτων, δείχνοντας πως η WscA αποτελεί βασικό παράγοντα για αυτή τη διαδικασία. Επιπλέον, πληθώρα δεδομένων αποδεικνύουν πως η WscA δεν ρυθμίζεται σε απόκριση της παρουσίας πουρινών και δεν είναι απαραίτητη για τη μεταφορά ουρικού οξέος, όπως είχαμε αρχικά υποθέσει. Τα αποτελέσματά μας αναλύονται μέσα στο πλαίσιο προηγούμενων μελετών για ομόλογες πρωτεΐνες της WscA σε άλλους νηματοειδείς μύκητες, καθώς σε ό,τι αφορά στις παρατηρούμενες απώλειες των PMP22 και των υπεροξεισωμικών ενζύμων που είναι απαραίτητα για τον καταβολισμό του ουρικού οξέος.

**ΘΕΜΑΤΙΚΗ ΠΕΡΙΟΧΗ:** μεταφορείς πουρινών

**ΛΕΞΕΙΣ ΚΛΕΙΔΙΑ:** νηματοειδείς μύκητες, ουρικό οξύ, οξειδάση του ουρικού οξέος, σωματία Woronin, διαφράγματα.

## **ACKNOWLEDGMENTS**

The completion of this thesis could not have been possible without the support and encouragement of several people. Hence, I would like to take this opportunity to show my gratitude to those who have assisted me.

First and foremost, I would like to thank my supervisor, Professor George Diallinas, for the guidance and advice he has provided me throughout my time as his student. I have been extremely lucky to have a supervisor who cared so much about my work, and who responded to my queries so promptly. His passion and enthusiasm not only about science but also about life in general is something refreshing and inspiring.

I am deeply grateful to Dr Sotiris Amillis for his help with molecular cloning and for always being there, willing to answer to all my questions. His valuable suggestions and ideas have contributed greatly to the improvement of this thesis.

I would also wish to express my gratitude to professor Riccardo Percudani for his work on the evolutionary analysis of this study. He laid the foundations of this idea and without him, this project could not be completed.

Last, but not least, I owe a special thanks to all my fellow labmates, Georgia, Anzie, Pothos, Mariangela and Olga for the excellent collaboration we had throughout this year. Thank you all for the amazing time we shared in the lab and I wish to each one of you all the best in every aspect of your life.

# CONTENTS

<b>ABSTRACT .....</b>	<b>5</b>
<b>ΠΕΡΙΛΗΨΗ .....</b>	<b>6</b>
<b>1. INTRODUCTION .....</b>	<b>16</b>
<b>1.1 <i>Aspergillus nidulans</i> .....</b>	<b>16</b>
1.1.1 Classification .....	16
1.1.2 Basic features.....	16
<b>1.2 Nitrogen metabolism in fungi .....</b>	<b>18</b>
1.2.1 General aspects.....	18
1.2.2 Purine assimilation pathway .....	19
<b>1.3 Peroxisomes.....</b>	<b>21</b>
1.3.1 General features .....	21
1.3.2 Peroxisome life cycle.....	21
1.3.3 Physiological functions.....	26
1.3.4 Transport across the peroxisomal membrane .....	30
<b>1.4 Aim of this study .....</b>	<b>31</b>
<b>2. MATERIALS AND METHODS .....</b>	<b>33</b>
<b>2.1 Strains, culture media, growth and storage conditions .....</b>	<b>33</b>
2.1.1 Strains used in this study .....	33
2.1.2 Culture media.....	34
2.1.3 Growth and storage conditions .....	35
<b>2.2 Genetic crosses and progeny analysis in <i>Aspergillus nidulans</i> .....</b>	<b>36</b>
<b>2.3 Epifluorescence microscopy and Statistical analysis .....</b>	<b>36</b>
<b>2.4 DNA manipulations &amp; construction of replacement cassettes .....</b>	<b>37</b>
2.4.1 <i>Aspergillus nidulans</i> genomic DNA extraction .....	37
2.4.2 Agarose gel electrophoresis.....	37
2.4.3 Polymerase Chain Reaction (PCR) .....	38
2.4.4 Molecular cloning .....	38
2.4.5 <i>Aspergillus nidulans</i> transformation .....	39

<b>2.5</b>	<b>Protein manipulations.....</b>	<b>40</b>
2.5.1	Total protein extraction .....	40
2.5.2	Protein quantification .....	40
2.5.3	SDS-PAGE electrophoresis and Western blot .....	40
<b>2.6</b>	<b>Analysis of correlated gene loss .....</b>	<b>42</b>
<b>3.</b>	<b>RESULTS .....</b>	<b>43</b>
<b>3.1</b>	<b>Purine catabolic enzymes show a correlated gene loss with Pmp22-like proteins.....</b>	<b>43</b>
<b>3.2</b>	<b><i>In silico</i> analysis of WscA.....</b>	<b>46</b>
<b>3.3</b>	<b>WscA is localized in peroxisomes .....</b>	<b>48</b>
<b>3.4</b>	<b>Growth defects of <math>\Delta wscA</math> null mutant.....</b>	<b>49</b>
<b>3.5</b>	<b>Genetic interactions of <i>wscA</i> with mutants affected in uric acid catabolism .....</b>	<b>53</b>
<b>3.6</b>	<b>WscA expression does not depend on transcriptional regulation of purine catabolism .....</b>	<b>56</b>
<b>3.7</b>	<b>WscA is essential for peroxisome localization on septal pores .....</b>	<b>58</b>
<b>4.</b>	<b>DISCUSSION .....</b>	<b>65</b>
	<b>ABBREVIATIONS .....</b>	<b>68</b>
	<b>APPENDIX.....</b>	<b>70</b>
	<b>REFERENCES.....</b>	<b>71</b>

## LIST OF FIGURES

Figure 1.1 (A) Scan of copper-engraving 91 from Micheli's <i>Nova plantarum</i> , showing his drawings of <i>Aspergillus</i> conidiophores. (B) Scanning electron micrograph of the conidiophore of <i>Aspergillus nidulans</i> (C) Epifluorescence microscopy of <i>A.nidulans</i> conidiophores, where nuclei are stained with DAPI. Photomicrograph [6], retrieved by [5].	18
Figure 1.2 Overview of <i>A. nidulans</i> life cycles. [10]	20
Figure 1.3 Nitrogen regulation by global and pathway-specific regulator. AreA is a global transcription factor that binds in specific sites of AreA-regulated nitrogen utilization genes and activates transcription during nitrogen limitation/starvation. A pathway-specific activator (A) responds to a specific induction signal [13].	21
Figure 1.4 The complete pathway of purine degradation to ammonium in <i>Aspergillus nidulans</i> is shown. Arrows connect the metabolic intermediate. Adjacent to each arrow the corresponding enzymatic reaction is shown, together with the name and identifier of the cognate gene. The transporters involved in the uptake of different metabolites are also shown to the left of the figure. Genes and their cognate proteins involved in cofactor synthesis or modification are shown in grey. They are connected by a squiggly line to the relevant enzymes [17].	22
Figure 1.5 Appearance of peroxisomes in different organisms. (a,b) Electron micrographs of peroxisomes in the indicated organisms. Bar, 1 $\mu$ m. (ER, endoplasmic reticulum; K, kinetoplast; L, lipid droplet; M, mitochondrion; N, nucleus; P, peroxisome.) [19].	23
Figure 1.6 Schematic overview of peroxisome biogenesis. Numbers indicate PEX gene products. Pex16 is present in mammals, plants and filamentous fungi but not in yeast [26].	25
Figure 1.7 Import of peroxisomal membrane proteins. The cytosolic chaperonin TriC protects the cargo protein from aggregation. Peroxisomal targeting of many membrane proteins is mediated by their cytosolic receptors, P40 and Pex19. After targeting cargo proteins to the membrane, the cytosolic receptors are recycled [19].	26
Figure 1.8 Import of matrix proteins into peroxisomes in (a) mammalian and (b) yeast cells [19]	27
Figure 1.9 Peroxisomal degradation pathways (A) Macropexophagy (B) Micropexophagy (C) Degradation by the activity of 15-LOX [28]	27
Figure 1.10 Peroxisomal respiration via H <sub>2</sub> O <sub>2</sub> [26]	28
Figure 1.11 (a) Enzymes and intermediates of the glyoxylate cycle. Enzyme abbreviations: ACO, aconitase; CIT, citrate synthetase; ICL, isocitrate lyase; MDH, malate dehydrogenase; MLS, malate synthetase (b) Enzymes of the glyoxylate cycle are located on both sides of the peroxisomal membrane. [26, 32].	29
Figure 1.12 The end product of purine metabolism varies in different species [34].	30

Figure 1.13 The final four reactions of the biotin biosynthetic pathway and involved enzymes from fungi and plants [20].	31
Figure 1.14 Overview of secondary metabolite synthesis in fungal peroxisomes. Rectangles and ovals represent transporters and enzymes, respectively. Continuous arrows indicate reactions well characterized, whereas dashed arrows indicate reactions that are still under investigation [37].	31
Figure 1.15 (A) Transmission electron microscopic observation of WBs (arrows) in <i>Aspergillus oryzae</i> . Bar: 500 nm (B) Schematic representation of septal tethering of WBs via LAH in <i>Aspergillus oryzae</i> [39].	32
Figure 1.16 Schematic overview of peroxisomal membrane transporters in mammals. The exchange of small metabolites is permitted through the Pxmp2/PMP22 protein and probably by a second unidentified pore. The import of very long-chain (VLCFAs) and long-chain fatty acids (LCFAs) is mediated by three ABC transporters (ABCD 1-3), which shuffle various fatty acyl-CoAs across the peroxisomal membrane, whereas the export of these bulky molecules occurs through shuttle systems exchanging the bulky CoA with carnitine. The transport of ATP remains still unidentified, while PMP34 is supposed to be responsible for NAD <sup>+</sup> and CoA import into peroxisomes AMP: adenosine monophosphate. FMN: flavine mononucleotide. PAP: adenosine-30 50 – diphosphate [27].	33
Figure 2.1 Schematic representation of the integrations of gfp in the N- and C-terminal regions of the corresponding ORFs [16]. The same procedure was followed for the construction of mrfp- tagged genes.	41
Figure 3.1 Comparison of the organism distribution of AN7258 with that of UOX (UaZ), HIU hydrolase (UaX), and UapA. The presence (gray) or absence (white) of genes is shown along a list of 540 fungal species ordered by taxonomic classification.	46
Figure 3.2 Phylogeny of the Mpv17/PMP22 family. The mid-point rooted neighbour-joining tree was based on the alignment of the complete set of homologous sequences in <i>A. nidulans</i> , <i>Arabidopsis thaliana</i> (At), <i>Danio rerio</i> (Dr), <i>Dictyostelium discoideum</i> (Dd), <i>Fusarium graminearum</i> (Fg), <i>Homo sapiens</i> (Hs), <i>Mus musculus</i> (Mm), <i>Neurospora crassa</i> (Nc), <i>Saccharomyces cerevisiae</i> (Sc), <i>Schizosaccharomyces pombe</i> (Sp). <i>A. nidulans</i> sequences are indicated with the genename in red; other sequences are indicated with Genbank accession codes preceded by the abbreviated scientific name. Node bootstrap support over 1000 replicates is indicated.	47
Figure 3.3 Topology prediction of WscA using TMHMM ( <a href="http://www.cbs.dtu.dk/services/TMHMM/">http://www.cbs.dtu.dk/services/TMHMM/</a> ) or TopRed ( <a href="https://embnet.vital-it.ch/software/TMPRED_form.html">https://embnet.vital-it.ch/software/TMPRED_form.html</a> ) programs.	48
Figure 3.4 Amino acid sequence alignment of WscA orthologues from selected fungi using <a href="http://espript.ibcp.fr/ESPrIPT/cgi-bin/ESPrIPT.cgi">http://espript.ibcp.fr/ESPrIPT/cgi-bin/ESPrIPT.cgi</a>	49
Figure 3.5 Growth test confirming the functionality of WscA tagged C-terminally with GFP or mRFP on several nitrogen sources (3 days at 37°C). N sources shown are: 10 mM ammonium (NH <sub>4</sub> <sup>+</sup> ), 0.5 mM adenine (ADE), 0.5 mM uric acid (UA), 0.5 mM allantoin (ALL), 10 mM urea. In all N source tests, 1% glucose is used as a C source.	50

Figure 3.6 (A) Epifluorescence microscopy of germlings of strains co-expressing GFP-UaZ and WscA-mRFP. Both markers label small motile and larger immotile peroxisome-like structures. Arrows indicate peroxisomal structures that seal septal pores. (B) The apparent high co-localization of these molecular markers is confirmed and quantified at ~65% for WscA-mRFP with GFP-UaZ and at ~80% for GFP-UaZ with mRFP-PTS1 by calculating Pearson's Correlation Coefficient (PCC) for n=12 hyphae. P-value for both cases is  $p < 0.0001$ .....51

Figure 3.7 Comparative growth rates and morphology of  $\Delta wscA$  and isogenic wild-type control on various N or C sources after 3 days at 37°C at pH 6.8. N sources shown are: 10 mM ammonium ( $\text{NH}_4^+$ ), 10 mM sodium nitrate ( $\text{NO}_3^-$ ), 10 mM L-proline (PRO), 0.5 mM adenine (ADE), 0.5 mM uric acid (UA), 0.5 mM allantoin (ALL), 10 mM urea. In all N source tests, 1% glucose is used as a C source. Other C sources shown, in the presence of  $\text{NH}_4^+$  as an N source, are 2% acetate or 2% oleate. Notice the reddish colony coloration, particularly evident, on uric acid or urea, but also visible on  $\text{NO}_3^-$  and PRO media. ....52

Figure 3.8 Comparative growth rates and morphology of  $\Delta wscA$  and wildtype control after prolonged growth (8 days at 37°C at pH 6.8). The picture shows single colonies growing on an entire petri dish. Notice the reduced colony diameter  $\Delta wscA$  mostly evident on ADE and ALL. ....52

Figure 3.9 Comparative growth rates and morphology of  $\Delta wscA$  and isogenic wild-type control on (A) media with different pH values (3 days at 37°C). N source: 10 mM sodium nitrate ( $\text{NO}_3^-$ ) (B) different temperatures ranging from 25 to 42°C for 3 days at 37°C. N source: 10 mM sodium nitrate ( $\text{NO}_3^-$ ).....53

Figure 3.10 Comparative resistance/sensitivity of  $\Delta wscA$  and wild-type control after 3 days at 37°C on media (10 mM  $\text{NO}_3^-$  and 1% glucose) containing known oxidative agents: 2 mM  $\text{H}_2\text{O}_2$ , 0.5 mM Paraquat (PAR), 50  $\mu\text{M}$  Congo Red (CR), 0.02 mM Methylene Blue (MB) and 0.02mM  $\text{CdCl}_2$  (Cd). Notice that  $\Delta wscA$  proved hypersensitive to most of these agents. ....53

Figure 3.11 Synthetic growth phenotypes of  $\Delta wscA$  genetically combined with other null mutants ( $\Delta AN5660$ ,  $\Delta AN4674$ ,  $\Delta aloA$ ) related to oxidative or stress sensitivity. AN5660 and AN4674 are PM stress sensors involved in hypo-osmotic and acidic pH stress tolerance whereas AloA is D-Arabinono-1,4-lactone oxidase, catalyzing the production of D-erythroascorbic acid, an important antioxidant molecule in fungi. In all cases, 1% glucose was used a C source, while 10 mM  $\text{NO}_3^-$  were used as N source, unless otherwise noted. Oxidizing agents and cell wall stressors were used at final concentrations: Paraquat 0.5 mM,  $\text{H}_2\text{O}_2$  2 mM,  $\text{CdCl}_2$  0.02 mM, Methylene Blue (MB) 50  $\mu\text{M}$ , Congo Red (CR) 50 $\mu\text{g}/\text{ml}$ , Caffeine 7 mM. For hyperosmotic conditions NaCl 500 mM was used. All strains were incubated for 3 days at 37°C. ....55

Figure 3.12 Growth test showing that the double  $\Delta wscA \Delta uaZ$  mutant is slightly more sensitive to uric acid toxicity, compared to an isogenic single  $\Delta uaZ$  mutant (3 days at 37°C). *uaZ* is the gene encoding UOX in *A. nidulans*. Knock-out of *uaZ* is known to lead to UA accumulation and severe cytotoxicity .....55

Figure 3.13 Epifluorescence microscopy of germlings of strains expressing UaZ or UaX tagged either N-terminally (GFP-UaZ, GFP-UaX, GFP <sup>(no PTS2)</sup> -UaX) or C-terminally (UaZ-GFP). Notice that the N-terminally tagged versions of UaZ and UaX are localized in cytoplasmic structures that correspond to peroxisomes, confirming previous observations [16]. In contrast, a C-tagged version of UaZ and a N-tagged version of UaX, along with a PTS2 deletion, show a cytoplasmic diffused fluorescent signal. The bar indicates 5 $\mu$ m. ....	56
Figure 3.14 Comparative growth tests of a standard wild-type control strain with isogenic strains expressing the cytoplasmic versions of UaZ or UaX, named Cyt UaZ and Cyt UaZ, respectively (3 days at 37°C). N sources shown are: 10 mM ammonium (NH <sub>4</sub> <sup>+</sup> ), 0.5 mM adenine (ADE), 0.5 mM uric acid (UA), 0.5 mM allantoin (ALL), 10 mM urea. In all N source tests, 1% glucose is used as a C source. ....	56
Figure 3.15 Prolonged growth (7 days at 37°C) of a standard wild-type control strain with isogenic strains expressing the cytoplasmic versions of UaZ or UaX, named Cyt UaZ and Cyt UaZ. Media are prepared as shown in Figure 3.14.....	57
Figure 3.16 Apparent synthetic effect of genetic absence of interaction of WscA ( $\Delta$ wscA) with cytoplasmically expressed UaZ. Notice the suppression of reddish coloration in the double mutant cyt-UaZ $\Delta$ wscA compared to the single mutant $\Delta$ wscA (3 days at 37°C). N sources used were: 10 mM sodium nitrate (NO <sub>3</sub> <sup>-</sup> ) and 0.5 mM uric acid (UA).....	57
Figure 3.17 Growth phenotypes of strains expressing cytoplasmic UaZ in the $\Delta$ wscA background after prolonged 7-day growth at 37°C on purine related metabolites as N sources. Notice that the reddish appearance due to the $\Delta$ wscA allele becomes apparent also the in strain expressing cytoplasmically UaZ. N sources used were: 10 mM sodium nitrate (NO <sub>3</sub> <sup>-</sup> ) and 0.5 mM uric acid (UA). ....	58
Figure 3.18 (A) Expression and subcellular localization of WscA and UaZ, as followed by epifluorescence microscopy, under conditions affecting the transcriptional regulation of transporters and enzymes involved in purine uptake and catabolism. Notice that, as previously shown [16], UaZ is strongly expressed and marks peroxisomes only under conditions of purine catabolism induction by UA, while it is hardly expressed in non-inducing (NO <sub>3</sub> <sup>-</sup> ) or repressing (NH <sub>4</sub> <sup>+</sup> ) conditions. Contrastingly, WscA is strongly expressed under all conditions tested. (B) Quantification of expression levels in the right panel, where peroxisomal surface in WscA and UaZ under the three different N sources is depicted. Only UaZ is induced by the presence of uric acid in the medium, as we can see in the diagram. ....	59
Figure 3.19. Putative UaY binding site of the wscA gene. ....	59
Figure 3.20 Expression and subcellular localization of WscA and UaZ, followed by epifluorescence microscopy, in wild-type and mutant backgrounds uaY462c and uaY2 leading to constitutive induction or non-induction of purine catabolic genes, respectively [51, 52], under repressing (NH <sub>4</sub> <sup>+</sup> ) or inducing (UA) conditions. Notice the WscA expression and subcellular localization, unlike UaZ, is practically the same in all genetic backgrounds and under all conditions tested.....	60

Figure 3.21. Quantification of peroxisomal surface in each strain under repressing ( $\text{NH}_4^+$ ) or inducing (UA) conditions confirms the constitutive purine catabolism-independent expression of WscA. ....	60
Figure 3.22 Growth tests (3 days at 37°C) showing that GFP-HexA is not fully functional, as judged by the reddish appearance of relative strains and the similarity to the phenotype of a $\Delta\text{hexA}$ mutant, shown in Figure 3.24. N sources shown are: 10 mM ammonium ( $\text{NH}_4^+$ ), 10 mM sodium nitrate ( $\text{NO}_3^-$ ), 0.5 mM adenine (ADE), 0.5 mM uric acid (UA), 0.5 mM allantoin (ALL), 10 mM urea. 1% glucose is used as a C source. ....	61
Figure 3.23 (A) Epifluorescence microscopy of germlings of strains of strains co-expressing WscA-mRFP and GFP-HexA. Notice the very high colocalization of the two peroxisomal markers. Bar = 5 $\mu\text{m}$ (B) Quantification of co-localization between WscA-mRFP and GFP-HexA, by calculating Pearson's Correlation Coefficient (PCC) for n=12 hyphae. P-value is $p < 0.00014$ .....	61
Figure 3.24 Comparative growth phenotypes of the $\Delta\text{hexA}$ and $\Delta\text{wscA}$ mutants and isogenic wild-type control strains (3 days at 37°C). N sources shown are: 10 mM ammonium ( $\text{NH}_4^+$ ), 0.5 mM adenine (ADE), 0.5 mM uric acid (UA), 0.5 mM allantoin (ALL), 10 mM urea. As C source, 1% glucose is used. ....	62
Figure 3.25 Epifluorescence microscopy of germlings of strains expressing GFP-UaZ, under transcriptional inducing conditions, in isogenic strain deleted for <i>wscA</i> and/or <i>hexA</i> , compared to a control strain. Bar = 5 $\mu\text{m}$ .....	63
Figure 3.26. (A) Quantification of the number of apparently open versus closed septal pores shows that WscA, but not HexA, is essential for pore sealing by peroxisomes. Septa were counted as closed, if UaZ was found on both sides of the septal pore. The percentages of closed septa were determined based on the analysis of 120 septa for each strain. (B) Quantification of the total number of peroxisomes per 40 $\mu\text{m}$ of hypha length in relative strains. Notice the nearly 50% reduction in strains that <i>wscA</i> is deleted. ....	63
Figure 3.27. Quantification of the number of closed septal pores in a strain expressing WscA-mRFP under various N sources (CM, $\text{NH}_4^+$ , Uric acid, Urea and Nitrogen starvation). Septa were counted as closed, if WscA was found on both sides of the septal pore. The percentages of closed septa were determined based on the analysis of 150 septa for each strain. ....	64
Figure 3.28. (A) Epifluorescence microscopy of WscA-GFP H1-mRFP, <i>nimA5</i> WscA-GFP H1-mRFP and <i>bimE7</i> WscA-GFP H1-mRFP expressing strains after a 4h shift at the restrictive temperature (42°C) (B) Quantification of the percentage of closed septa of each strain at permissive (25°C) and restrictive temperature (42°C). Notice the difference on septal pore sealing at 42°C on the cell cycle mutants, <i>nimA5</i> (fewer plugged septa) and <i>bimE7</i> (all septa plugged). The percentages of closed septa were determined based on the analysis of 60 septa for each strain.....	65
Figure 3.29 Western blot analysis of WscA-GFP in wt, <i>nimA5</i> and <i>bimE7</i> genetic backgrounds. ....	66

## LIST OF TABLES

Table 1.1 PEX genes and their main functions [24].....	22
Table 1.2 Purine degrading enzymes in vertebrates and invertebrates [31].....	28
Table 2.1 List of strains .....	33
Table 2.2 Media used for <i>A. nidulans</i> growth.....	35
Table 2.3 Solutions used in culture media.....	35
Table 2.4 Composition of conventional and high fidelity PCR reactions.....	38
Table 2.5 Conditions for conventional and high fidelity PCR reactions.....	38
Table 2.6 Solutions used for total protein extraction.....	40
Table 2.7 Composition of separating and stacking layers of polyacrylamide gels .....	41
Table 2.8 Solutions for Western blot.....	41
Table 3.1 Fungal genes with correlated loss with uric acid oxidase (uricase) .....	43

# 1. INTRODUCTION

## 1.1 *Aspergillus nidulans*

### 1.1.1 Classification

*Aspergillus nidulans* is a homothallic filamentous fungus belonging to the genus *Aspergilli*. According to the modern classification, the genus is placed in the phylum Ascomycota, subphylum Pezizomycotina, class of Eurotiomycetes, order Eurotiales and family Aspergillaceae. Unlike the past classification, where *A. nidulans* was regarded as the telomorph of *Emericella nidulans*, the single named but pleomorphic nomenclatural and taxonomical system classifies both anamorphic and telomorphic states in *Aspergillus*, while *Emericella* is considered synonymus to the latter [1].

Ascomycota comprise the largest phylum of the Fungi Kingdom, consisting of more than 64000 species, ranging from unicellular yeasts to the fairly large morels [2]. The basic morphological feature that distinguishes members of Ascomycota from all other fungi is the ascus, a saclike cell containing the ascospores, which are produced by a combination of meiosis and a subsequent mitotic division [3].

Based on phylogenetic studies and molecular sequence data, the phylum Ascomycota is divided into three subphyla, the Pezizomycotina, containing almost all ascomycetes that produce ascocarps, the Saccharomycotina, consisting of most of the true yeasts, including *Saccharomyces cerevisiae* and the basal group Taphrinomycotina [2,4].

The genus *Aspergilli* was first described and catalogued in 1729 by the Italian priest and botanist Pietro Antonio Micheli. When he first viewed the mold under the microscope, the morphology of the spores radiating from the conidiophore resembled him the aspergillum, which is an instrument used in the Roman Catholic mass to sprinkle holy water over the head of the faithful [5].

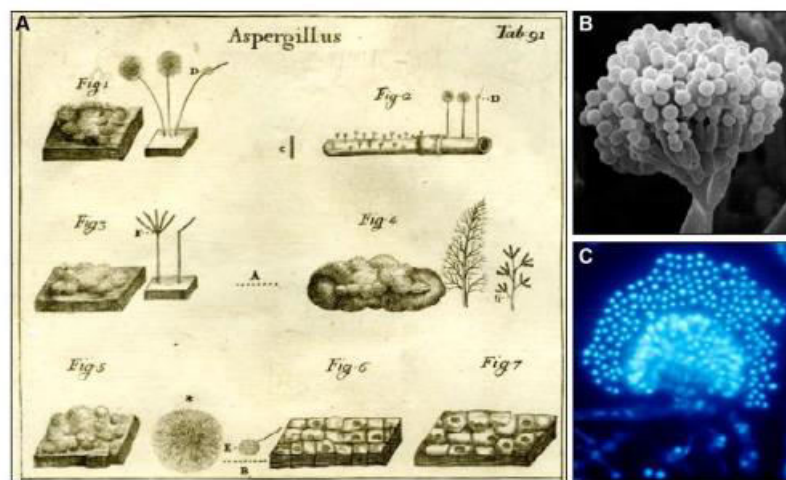


**Figure 1.1** (A) Scan of copper-engraving 91 from Micheli's *Nova plantarum*, showing his drawings of *Aspergillus* conidiophores. (B) Scanning electron micrograph of the conidiophore of *Aspergillus nidulans* (C) Epifluorescence microscopy of *A.nidulans* conidiophores, where nuclei are stained with DAPI. Photomicrograph [6], retrieved by [5].

### 1.1.2 Basic features

The aspergilli comprise a diverse group of filamentous fungi spanning over 200 million years of evolution [7]. Among the over 185 members are several that can be harmful, such as *A. fumigatus* towards immunocompromised individuals as well as species of

industrial interest, like *A. oryzae*. Within this genus, *A. nidulans* possesses a unique role as a model organism.

Its power as a genetic model was recognized by Pontecorvo et al. [8] and it is been used since then as a longstanding laboratory organism of high value for research and teaching genetic principles. Half a century of *A. nidulans* research has advanced the study of eukaryotic cellular physiology, contributing to our understanding of a wide range of biological processes [9].

*A. nidulans* has considerable advantages as a model organism. It has eight sequenced chromosomes with many auxotrophic, drug resistance and color markers. It is homothallic, meaning it is capable of sexual reproduction without a mating partner, thus allowing both selfing and outcrossing [9]. It is normally haploid but heterokaryons and stable diploids can be produced under stress, enabling the complementation analysis for mutations. The conidiospores are in haploid form, which enables the direct screening of mutants or transformants by plating on appropriate media. Moreover, it grows rapidly on inexpensive media under a variety of nutritional conditions and produces conidia or ascospores that can be stored for long periods of time. Last but not least, it can be efficiently and easily transformed in an integrative and site-specific manner and generate stable transformants.

#### **1.1.2.1 Life cycle**

*A. nidulans* has a complex life cycle, having the ability to reproduce through sexual, asexual or parasexual cycle.

During, the asexual cycle, a conidiospore germinates under favorable conditions, producing haploid vegetative filamentous hyphae. Under the appropriate environmental conditions, some hyphal cells can differentiate into specialized foot cells, from which will rise the conidiophore, on which more conidia will be produced. At the end of the conidiophore, a vesicle is formed and two layers of uninucleate sterigmata, metulae and phialides are elaborated. The repeated asymmetric division of each phialide will produce long chains of uninucleate conidiospores, which can further disperse from the stalk, initiating another asexual cycle [9].

When conditions are restraining for vegetative growth, then hyphae can enter the sexual cycle. Sexual ascospores are recruited for long-term survival of the fungus. This developmental process starts with simultaneous mitotic division of the two nuclei at the tip cell of an ascogenous hypha. Nuclear divisions, along with septa formation, lead to the creation of a uninucleate tip cell, a binucleate penultimate cell and a uninucleate basal cell. Differentiation and enlargement of the penultimate cell, fusion of the two haploid nuclei (karyogamy), following meiosis of the diploid nucleus and consequent mitotic divisions, lead to the generation of eight haploid binucleate ascospores, contained within an ascus. The asci are dispersed in closed fruting bodies, called cleistothecia, which are surrounded by thick-walled nurse cells, termed "Hülle cells" Germination of the ascospores leads to reinitiation of the vegetative growth [9].

*A. nidulans*, has also a parasexual cycle, where a heterokaryon is formed, through anastomoses of extending hyphal branched from two different strains. The haploid nuclei fuse in the vegetative cells of the heterokaryon and continue to divide mitotically. The parasexual cycle offers the genetic benefits of meiosis achieved through a mitotic route [10].

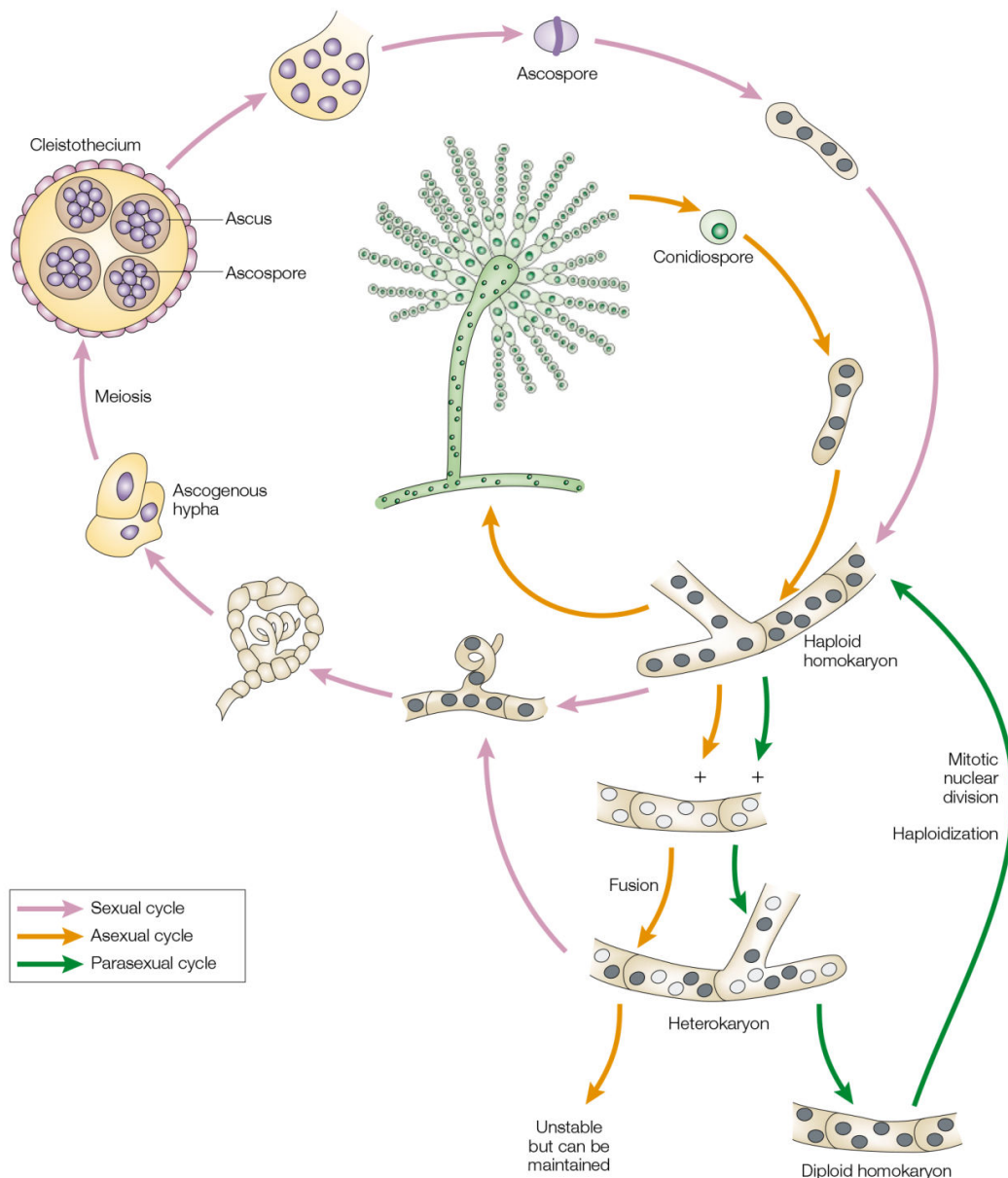


**Figure 1.2** Overview of *A. nidulans* life cycles. [10]

## 1.2 Nitrogen metabolism in fungi

### 1.2.1 General aspects

Nitrogen, as a major component of nearly all of the complex macromolecules, is essential to the structure and function of all living organisms. Fungi can use a surprisingly diverse array of compounds as nitrogen sources and are capable of expressing upon demand the catabolic enzymes of many different pathways. Therefore, extensive studies of nitrogen metabolism and its regulation have been conducted in fungal model organisms, such as *A. nidulans* [11].

Generally, some nitrogenous compounds, such as ammonium or glutamine, are more easily metabolized by fungi and thus preferentially used as nitrogen sources. However, when these primary sources are not available or are present in limiting for growth concentrations, many other nitrogen sources, like nitrite, nitrate or purines can be used. Utilization of any of these secondary nitrogen sources is highly regulated, mainly at transcriptional level. The activation of their catabolic pathways often requires two distinct positive signals: a global acting signal, due to absence of the primary nitrogen

source and a pathway specific one, indicative of the presence of a secondary source, which acts as a substrate or intermediate of the pathway [12].

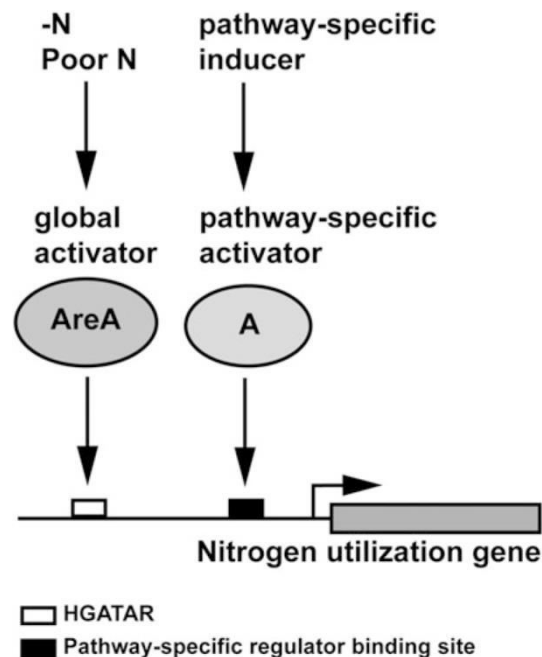


**Figure 1.3** Nitrogen regulation by global and pathway-specific regulator. AreA is a global transcription factor that binds in specific sites of AreA-regulated nitrogen utilization genes and activates transcription during nitrogen limitation/starvation. A pathway-specific activator (A) responds to a specific induction signal [13].

In *A. nidulans*, purine catabolism requires the synthesis of a set of catabolic enzymes and permeases. This can only happen upon nitrogen derepression, mediated by AreA, a global GATA-type zinc finger transcription factor and upon simultaneous induction with uric acid, mediated by the pathway-specific transcription factor UaY [12, 14].

## 1.2.2 Purine assimilation pathway

Fungi, as well as other organisms, have the ability to take up purines, which can be used either for nucleotide biosynthesis or for catabolic purposes, as being fairly good nitrogen sources. The latter is due to their degradation first to ureides (allantoin, allantoic acid) and eventually to urea, via several enzyme-catalysed oxidations. The complete purine catabolic pathway is present in most filamentous fungi and is the same as that of most bacteria and plants, in contrast to most yeast, where degenerate variations of the purine degradation pathway exist [15].

Several yeasts, including *Saccharomyces cerevisiae*, lack xanthine dehydrogenase (HxA or purine hydroxylase I), the major enzyme-oxidizing hypoxanthine to xanthine and xanthine to uric acid, and urease (UreA), the last enzyme-oxidizing allantoinic acid to urea [14, 15]. However, some yeasts, like *Candida albicans* and *Schizosaccharomyces pombe*, can use purines as nitrogen sources through XanA (xanthine  $\alpha$ -ketoglutarate-dependent dioxygenase). *S. cerevisiae* lacks all the necessary enzymes for purine oxidation, while conserving the ability to break down ureides to urea. Thus, it can grow on allantoin or allantoic acid, but not on purines as sole nitrogen sources [15].

In *A. nidulans* the purine utilization pathway has been thoroughly characterized. This conforms to the classical purine degradation pathway, with the addition that xanthine hydroxylation to uric acid can be catalyzed besides xanthine dehydrogenase also by xanthine dioxygenase, an exclusive fungal enzyme [16].

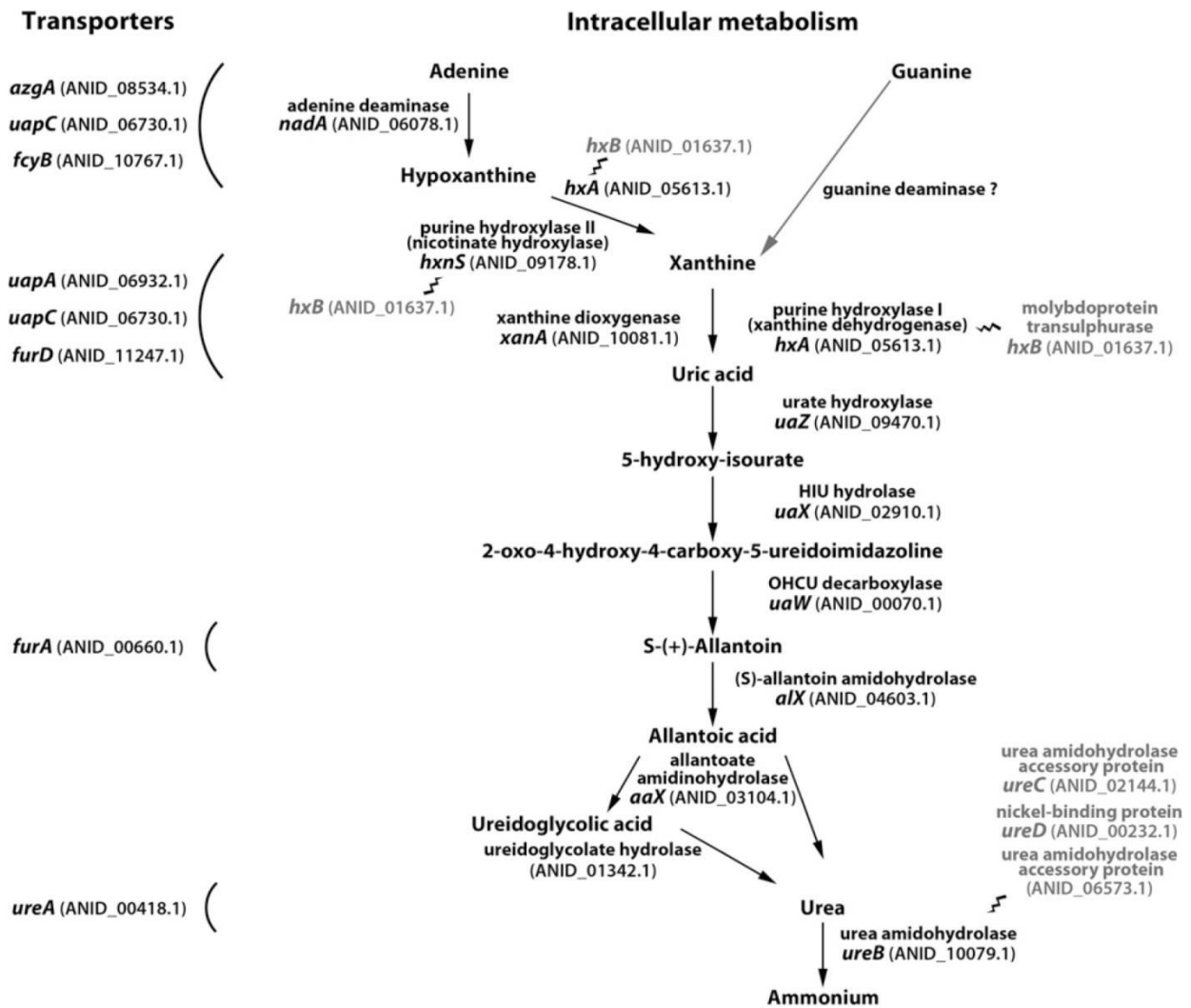


**Figure 1.4** The complete pathway of purine degradation to ammonium in *Aspergillus nidulans* is shown. Arrows connect the metabolic intermediate. Adjacent to each arrow the corresponding enzymatic reaction is shown, together with the name and identifier of the cognate gene. The transporters involved in the uptake of different metabolites are also shown to the left of the figure. Genes and their cognate proteins involved in cofactor synthesis or modification are shown in grey. They are connected by a squiggly line to the relevant enzymes [17].

Although purine catabolism is generally well conserved from animals and fungi, to plants and bacteria, enzymes involved in this pathway show variable cell localization throughout the evolutionary tree [18]. While urate oxidase has been found to be a peroxisomal enzyme in every eukaryote where its localization has been studied, no such statement could be made about other enzymes of the pathway. Several variations could be found not only among different phyla, but also within the same phylum [16, 18].

In *A. nidulans*, the intracellular localization of the specific enzymes of the purine utilization pathway was recently established [16]. The subcellular distribution of xanthine dehydrogenase (HxA), allantoinase (AIX), allantoicase (AaX), ureido imidazoline decarboxylase (UaW) and  $\alpha$ -ketoglutarate Fe(II)-dependent dioxygenase (XanA) is cytosolic, while urate oxidase (UaZ), 5-hydroxy-isourate hydrolase (UaX) and ureidoglycolate lyase (UglA) are peroxisomal [16].

## 1.3 Peroxisomes

### 1.3.1 General features

Peroxisomes are ubiquitous organelles that are present in almost all eukaryotic cells. They are spherical in transmission electron micrographs, ranging in diameter from 0.1  $\mu\text{m}$  to 1.0  $\mu\text{m}$  (Figure 1.5). These organelles are delimited by a single unit membrane and contain a fine granular matrix and occasionally a paracrystalline core [19].

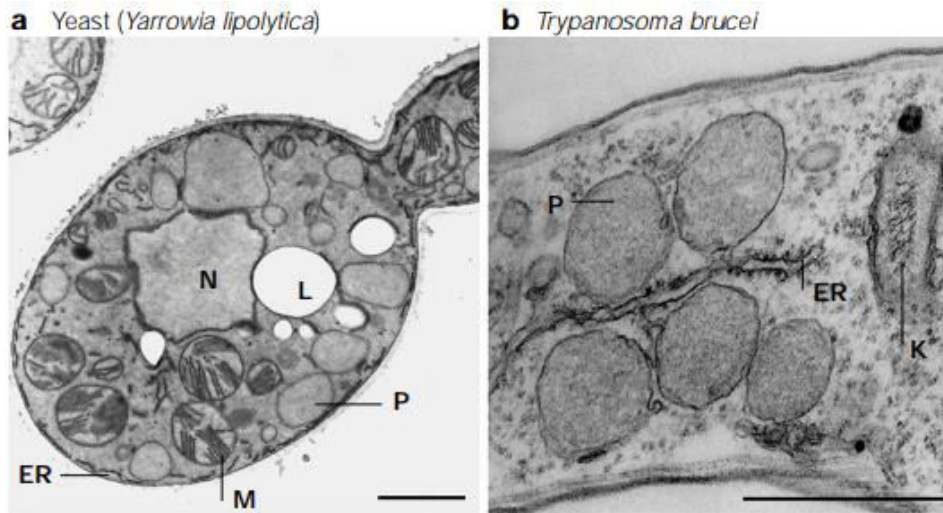


**Figure 1.5 Appearance of peroxisomes in different organisms.** (a,b) Electron micrographs of peroxisomes in the indicated organisms. Bar, 1  $\mu\text{m}$ . (ER, endoplasmic reticulum; K, kinetoplast; L, lipid droplet; M, mitochondrion; N, nucleus; P, peroxisome.) [19].

They typically contain enzymes involved in the  $\beta$ -oxidation of fatty acids and detoxification of reactive oxygen species, but are also known to have complex physiological functions based on their roles in diverse metabolic activities [20]. For instance, peroxisomes in plants are involved in a vast array of processes, including the glyoxylate cycle, the synthesis of phytohormones and photorespiration [21], while in higher eukaryotes they are involved in lipid biosynthesis and in the oxidation of polyamines and amino acids [22].

### 1.3.2 Peroxisome life cycle

#### 1.3.2.1 Biogenesis

The biogenesis of peroxisomes involves the formation of the peroxisomal membrane, the targeting and insertion of peroxisomal membrane proteins (PMPs), the import of soluble matrix proteins and the modulation of peroxisomal number, shape, and cellular position. Unlike mitochondria, peroxisomes do not contain DNA or independent protein synthesis machinery, and accordingly all peroxisomal proteins are encoded by nuclear genes and imported post-translationally from the cytosol [23].

The proteins which are essential for the assembly, division and inheritance of peroxisomes demonstrate a broad level of similarity from yeast to man and have been named “peroxins”. Peroxins collaborate in the translocation from the cytosol into the peroxisomal matrix, catalyze membrane protein assembly and are involved in proliferation and division. These proteins are encoded by the *PEX* genes, which are generally evolutionary conserved [24]. Thirty-three *PEX* genes have been identified so far (Table 1.1).

**Table 1.1 PEX genes and their main functions [24].**

PEX genes-peroxin functions			
<i>Process</i>	<i>Gene</i>	<i>Protein function</i>	
<b>Transport of newly synthesized enzymes through the cytosol to peroxisomes:</b>			
PTS receptors	Pex5	Shuttling receptor for PTS1 proteins	
Co-receptors	Pex7	Shuttling receptor for PTS2 proteins	
	Pex18	Co-receptor for PTS2 proteins in <i>Saccharomyces cerevisiae</i>	
	Pex21	Co-receptor for PTS2 proteins in several yeasts	
	Pex20	Co-receptor for PTS2 proteins in other fungi	
<b>Translocation of newly synthesized enzymes into peroxisomes:</b>			
Receptor docking complex	Pex13	Site for shuttling receptors to dock on exterior of membrane	
	Pex14		
	Pex17		
Translocation through the membrane	Pex33	Functional homolog of Pex17	
	Pex5	Formation of transient pore	
Linkage of docking and ubiquitination complexes	Pex14		
	Pex8		
Ubiquitination	Pex2	Ubiquitin ligases	
	Pex10		
	Pex12		
	Pex4		
Receptor reexport	Pex22	Ubiquitin conjugating enzyme	
	Pex1	Membrane anchor for Pex4	
	Pex6	ATP-dependent export of receptor	
<b>Membrane protein assembly:</b>	Pex15	Membrane anchor for Pex1 and Pex6 in <i>S. cerevisiae</i>	
	Pex26	Membrane anchor for Pex1 and Pex6 in <i>H. sapiens</i>	
	Transport and insertion of newly synthesized proteins into the peroxisome membrane	PEX19	Soluble chaperone and shuttling receptor
	Transport of membrane proteins via the ER and vesiculation	PEX3	Docking of Pex19 on the peroxisome membrane
		PEX16	Insertion of Pex3 into the peroxisome membrane
PEX16		Recruits Pex3 in mammals	
PEX3		May recruit other proteins	
<b>Proliferation and division:</b>	PEX19	Budding of vesicles containing Pex3 (and 16)	
	PEX15	unknown	
	Proliferation, fission	PEX11	Proliferation and membrane elongation, recruitment of fission proteins
		PEX25	Proliferation and elongation in yeasts; required for peroxisome reintroduction in <i>S. cerevisiae</i>
	Proliferation	PEX27	Negative effector in <i>S. cerevisiae</i>
PEX34		Fission in <i>S. cerevisiae</i>	
PEX23		Proliferation in <i>Yarrowia lipolytica</i>	
PEX24			
PEX28, 29			
Omitted	PEX30, 31, 32	Proliferation in <i>S. cerevisiae</i>	
	PEX9	Proliferation, ER contact in <i>S. cerevisiae</i>	
		None	

Despite decades of research on peroxisome biogenesis, the origin of the organelle remains controversial. In the past, several models for peroxisomal formation have been proposed. Classic morphologic work pointed to an origin of peroxisomal membranes from the endoplasmic reticulum (ER). A following shift in the scientific thinking came later towards a “growth and fission” model in which peroxisomes were considered autonomous organelles that derive from preexisting ones [25]. It is now generally accepted that peroxisome biogenesis can occur through both the classical route of growth and division of pre-existing organelles, or through an alternate route of *de novo* formation of nascent peroxisomes with a help from the ER. Peroxisomal numbers are, however, primarily controlled by growth and division [23].

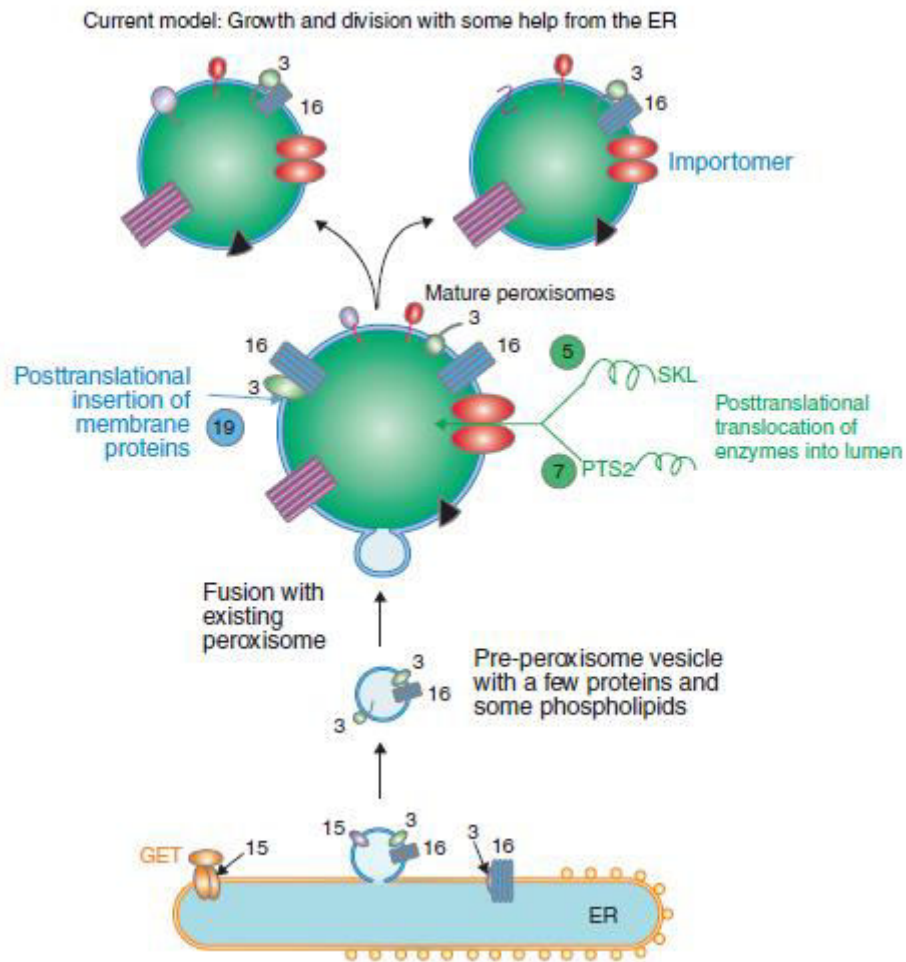


**Figure 1.6** Schematic overview of peroxisome biogenesis. Numbers indicate PEX gene products. Pex16 is present in mammals, plants and filamentous fungi but not in yeast [26].

Peroxisomes undergo both constitutive and regulated division. During the cell cycle, they divide independently of extracellular stimuli in order to maintain their number in a growing cell population. Additionally, they can undergo a regulated division in response to an external signal to accommodate increased amounts of peroxisome-housed enzymes. While the latter is well characterized in several model organisms, the mechanism for constitutive division remains to be established. Members of the Pex11 family function as positive regulators of peroxisome division and seem to be the key players in this process. Nevertheless, they are not required for peroxisomal protein import [19].

### 1.3.2.1.1 Peroxisomal protein import

Analysis of various model organisms has revealed some general rules governing peroxisomal protein import, without excluding the existence of organism-specific differences during this process. First, all membrane and matrix proteins are targeted to peroxisomes post-translationally. Second, matrix proteins are targeted to peroxisomes by at least two targeting signals, peroxisomal targeting signal 1 and 2, named PTS1 and PTS2, respectively. Third, the majority of integral membrane proteins are sorted to peroxisomes directly from the cytosol by the peroxisomal membrane targeting signal 1, mPTS1, while a limited set can be targeted to these organelles, indirectly, through the ER, by mPTS2. Fourth, the peroxisomal import machineries and targeting signals are distinct between membrane and matrix proteins. Last, but not least, into the peroxisomal matrix are imported both folded and unfolded polypeptides [19].

The targeting and insertion of membrane proteins into the peroxisomal membrane seems to occur post-translationally. This process involves the protection of transmembrane segments from aggregation, the targeting of proteins to the peroxisomal membrane via mPTS1 or/and cytosolic receptor(s), the docking to the peroxisomal membrane, which involves membrane-bound proteins and the insertion of proteins into the peroxisomal membrane, followed by their assembly within the membrane [19]. The mPTSs are internal sequences, consisting of a cluster of positively charged amino acids, but no clear sequence consensus has ever been reported [19, 26].

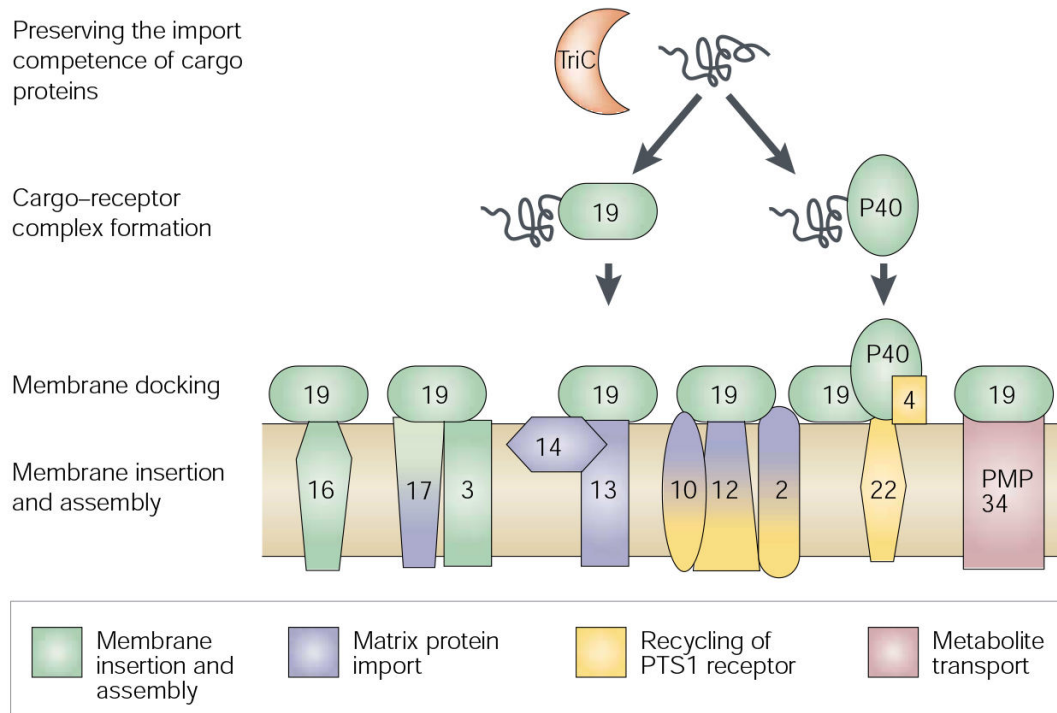


**Figure 1.7** Import of peroxisomal membrane proteins. The cytosolic chaperonin TriC protects the cargo protein from aggregation. Peroxisomal targeting of many membrane proteins is mediated by their cytosolic receptors, P40 and Pex19. After targeting cargo proteins to the membrane, the cytosolic receptors are recycled [19].

The protein import of peroxisomal matrix proteins can be categorized in four consecutive steps, with some mechanistic differences between higher and lower eukaryotes [19, 27]:

1. The cargo is recognized via peroxisomal targeting sequences—PTS1 and PTS2—by their correspondent receptors Pex5 and Pex7, respectively. PTS1 is a carboxy-terminal tripeptide with the consensus motif (S/A/C)(K/R/H)(L/M/I), while PTS2 is a nonapeptide with the consensus motif (R/K)(L/V/I)<sub>5</sub>(H/Q)(L/A). Most matrix proteins contain PTS1.
2. The cargo-receptor complexes dock to Pex13/14 (mammals) and Pex17 for Pex7 (yeast) at the peroxisomal membrane.
3. Pex14 and Pex5 interact to translocate the cargo across the peroxisomal membrane.
4. The cargo-receptors are recycled into the cytosol via an ubiquitination-dependent mechanism.

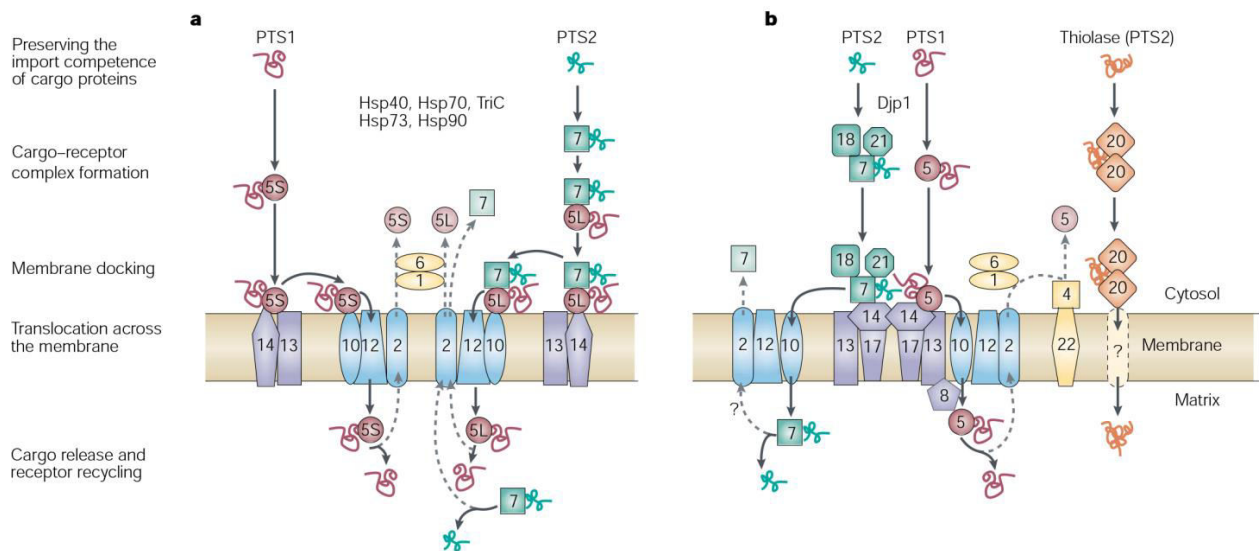


**Figure 1.8** Import of matrix proteins into peroxisomes in (a) mammalian and (b) yeast cells [19]

### 1.3.2.2 Degradation

The actual number of the peroxisomes that is present in the cell is tightly regulated by both biogenic and degradative processes [28]. The organelles are subject to quality control mechanisms and a constitutive degradation process, not only to maintain a healthy and juvenile organelle population, but also as a response to changes in environmental and developmental conditions like nutrient availability or stress [27, 28]. There are several mechanisms that control the turnover of peroxisomes.

Autophagy is a cellular degradative pathway which is conserved in eukaryotes. It can be divided into two non-selective autophagic mechanisms for sequestering of cytoplasmic components (proteins and lipids) and organelles: micro- and macroautophagy. Microautophagy occurs through the engulfment of cytoplasm and organelles by the lysosomal/vacuolar membrane followed by internalization and degradation, while macroautophagy involves the formation of double membrane vesicles (autophagosomes) which transport the cargo to the vacuole/lysosomes [27].

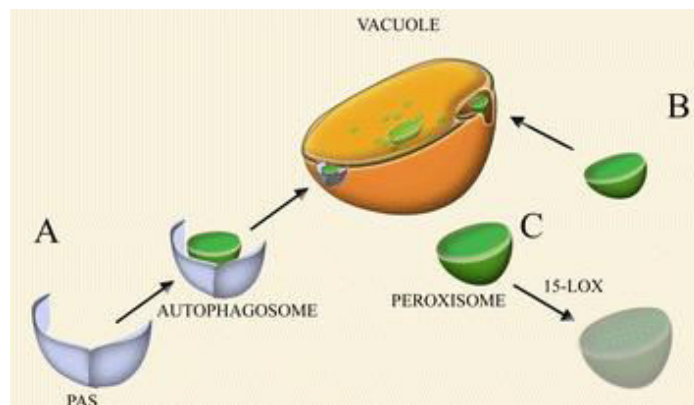


**Figure 1.9** Peroxisomal degradation pathways (A) Macropexophagy (B) Micropexophagy (C) Degradation by the activity of 15-LOX [28]

Additionally to non-selective autophagy, peroxisomes can be specifically degraded, when appropriate, by micro- and macropexophagy [27]. In macropexophagy a pre-autophagosomal structure (PAS), probably formed from the ER, engulfs the peroxisome thus forming an autophagosome that fuses with the vacuole, delivering the organelle for degradation by vacuolar hydrolases. In micropexophagy the peroxisome is directly

engulfed by the vacuolar membrane and subsequently degraded in the vacuolar lumen [28].

Besides autophagic processes, there are two other peroxisomal degradation mechanisms: degradation by the effect of 15-lipoxygenase (15-LOX), which disturbs the integrity of peroxisomal membrane and by the peroxisomal Lon protease (PSLP), with the latter bearing a PTS1 motif and showing protease activity as well as a chaperone-like activity [27, 28]. Peroxisomal LON2 protease plays a role in the degradation of unfolded, non-assembled or damaged peroxisomal matrix proteins, but an additional role was revealed in Arabidopsis, where loss of function of LON2 accelerates pexophagy [29].

### 1.3.3 Physiological functions

Peroxisomes are dynamic, multifunctional organelles that contribute to numerous anabolic and catabolic pathways and are thus vital for every eukaryote. Common function in plants, mammals and fungi include the metabolism of hydrogen peroxide and the oxidation of fatty acids. However, several specialized biological functions also exist, leaving the list of peroxisomal tasks far from being complete. In general, peroxisomal functions can be divided into those that are distributed among all eukaryotic organisms and are evolutionary ancient and those which are specific to one or more branches of the evolutionary tree [27].

#### 1.3.3.1 Conserved biochemical pathways present in most peroxisomes

##### 1.3.3.1.1 Reactive oxygen and nitrogen metabolism

The enzymes that were identified from the first isolation of peroxisomes were oxidases and catalase [30]. The oxidases use molecules of oxygen ( $O_2$ ) to oxidize a plethora of substrates, such as D-amino acids, L-a-hydroacids and uric acid with the formation of hydrogen peroxide ( $H_2O_2$ ), which is decomposed subsequently by the catalase (Figure 1.10) [26]. Hydrogen peroxide is toxic and can damage organic molecules. Thus putting the enzymes that make large amounts of it in the same compartment with the enzyme that destroys it protects the cell from its harmful effects. However, it must be noted that some hydrogen peroxide is useful for the cell, by modifying the activity of signaling molecules and employing in cellular defense [26]. This is also true for all ROS species.

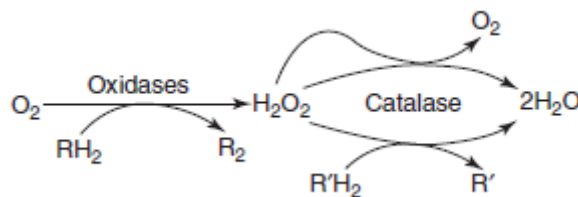


Figure 1.10 Peroxisomal respiration via  $H_2O_2$  [26]

Besides hydrogen peroxide, there are also other reactive oxygen and nitrogen species that are produced inside peroxisomes. These include superoxide ( $O_2^-$ ), hydroxyl radicals ( $\bullet OH$ ) and nitric oxide (NO) which affect the redox state both inside peroxisomes and in other cells compartments. Peroxisomes manage to maintain the balance between production and destruction of reactive molecules, by encompassing several ROS scavenging enzymes, like superoxide dismutase, epoxide hydrolase, peroxiredoxin, as well as catalase [26].

##### 1.3.3.1.2 Fatty acid $\beta$ -oxidation

The  $\beta$ -oxidation of long and very long chain fatty acids (LCFAs and VLCFAs, respectively) is probably the most prominent pathway of peroxisomes [31]. While in mammals the breakdown of fatty acids is distributed between peroxisomes and mitochondria, it appears to be exclusively peroxisomal in plants and in many fungi [26, 31]. In general, the architecture of the peroxisomal  $\beta$ -oxidation system is comparable to that of mitochondria and consists of the following subsequent steps: dehydrogenation, hydration, dehydrogenation again and thiolitic cleavage [32]. However, the enzymes that catalyze these four reactions in peroxisomes are distinct from their mitochondrial counterparts [26].

### 1.3.3.1.3 The glyoxylate cycle and glyoxylate metabolism

The glyoxylate cycle, a variation of the tricarboxylic acid cycle in plants, protozoans and fungi centers on the conversion of acetyl-CoA to succinate for the synthesis of carbohydrates. This permits *de novo* gluconeogenesis from fatty acids along with the utilization of ethanol and acetate as sole carbon sources by yeasts. In the last step of the pathway [Figure 1.11(a)], isocitrate is cleaved to produce succinate and reform glyoxylate, for which the cycle is named [26].

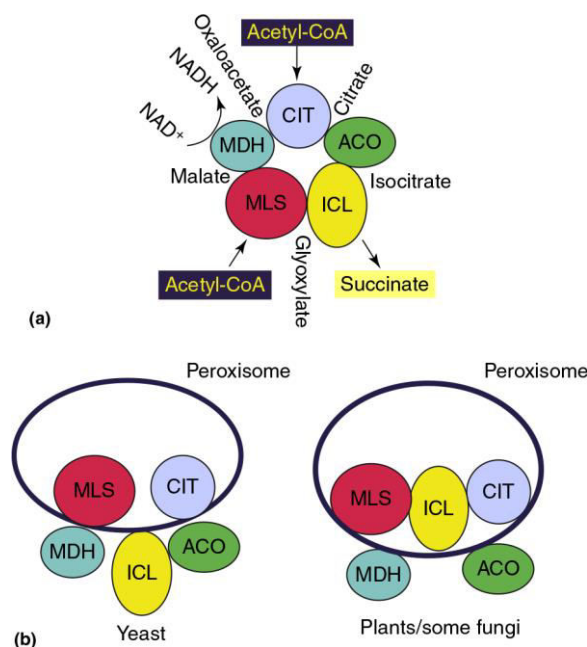


**Figure 1.11** (a) Enzymes and intermediates of the glyoxylate cycle. Enzyme abbreviations: ACO, aconitase; CIT, citrate synthetase; ICL, isocitrate lyase; MDH, malate dehydrogenase; MLS, malate synthetase (b) Enzymes of the glyoxylate cycle are located on both sides of the peroxisomal membrane. [26, 32].

### 1.3.3.1.4 Purine catabolism

Purine catabolism is generally well conserved throughout organisms ranging from animals to fungi. Whereas the degradation of purines to uric acid is common to all kingdoms of life, the resulting uric acid can either be excreted or further degraded by uric acid catabolic enzymes in the peroxisomes. The various end products are a result of loss-of function mutations during evolution in urate oxidase, allantoinase and allantoinase (Figure 1.12) [34]. Most mammals excrete allantoin having lost the capability to express allantoinase and allantoinase. Additionally, primates as well as birds and reptiles, do not possess a functional gene for uricase, consequently excreting uric acid [31]. As uric acid is a potent antioxidant and protects cells by scavenging

reactive oxygen species, it has been proposed that the loss of urate oxidase may have been selected for due to it promoting longevity [33].

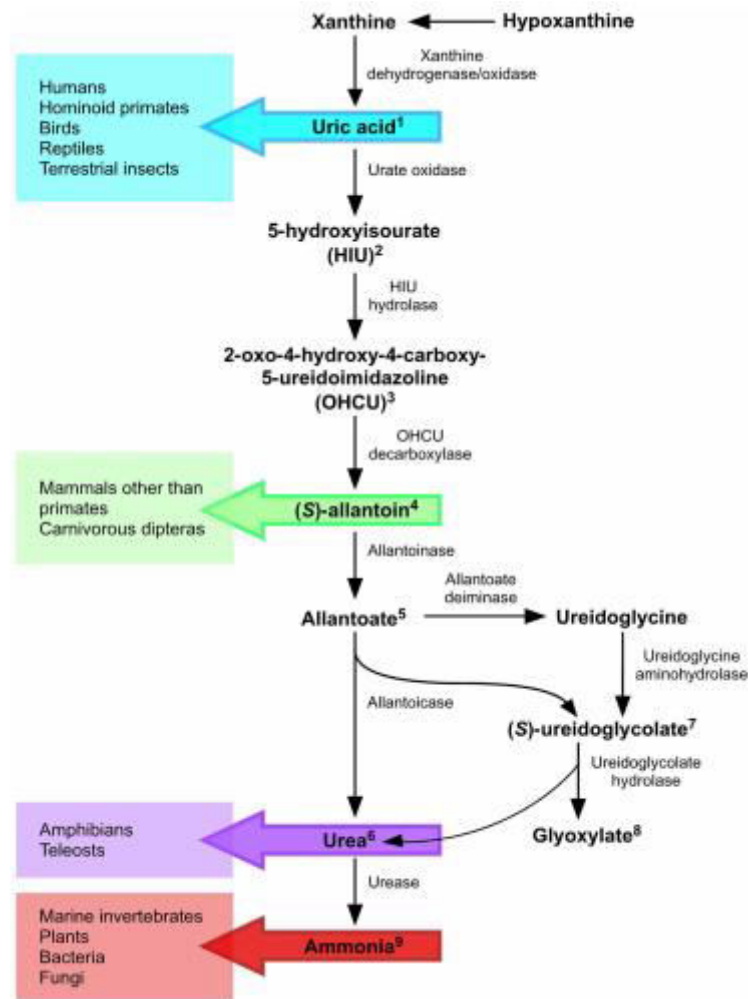


**Figure 1.12** The end product of purine metabolism varies in different species [34].

In parallel to this evolutionary truncation of the pathway several subcellular reallocations of the corresponding enzymes have occurred: potentially, all enzymes with the exception of allantoinase may have been originally localized in or adjacent to peroxisomes since throughout eukaryotes, peroxisomal localizations can be found for all proteins [30].

**Table 1.2 Purine degrading enzymes in vertebrates and invertebrates [31].**

Purine degrading enzymes in different species.

	Xanthine oxidase	Urate oxidase	Allantoinase	Allantoicase
<b>Invertebrates</b>				
Mytilus	+ (Cyt)			
Diptera	+ (Po)	+ (Po)	+ (Cyt <sup>a</sup> )	+ (?) Po-
Amphioxus	Po?			
Marine fish	+ (Cyt)	+ (Po)	+ Po/Cyt	+ (Po)
Freshwater fish	+ (Cyt)	+ (Po)	+ Cyt	+ (Po)
Amphibia	+ (Po)	+ (Po)	+ (Mito)	+ (Cyt, Mito)
Reptiles	+	+/-	-	-
Birds	+ (Po)	-	-	-
Mammals	+ (Po)	+ (Po)	-	-
Primates	+ (Cyt)	-	-	-

+ gene is present and expressed; intracellular localization in brackets; Po, peroxisomes; Cyt, cytosol; Mito, mitochondria.

### 1.3.3.2 Specialized functions in fungi

#### 1.3.3.2.1 Biotin synthesis

Numerous fungal species, as well as plants, have the ability to synthesize biotin, an essential cofactor involved in a number of carboxylation and decarboxylation reactions [35]. The final four reactions in the biosynthetic process, which convert pimeloyl-CoA to biotin, are conserved, throughout these organisms (Figure 1.13) [20].

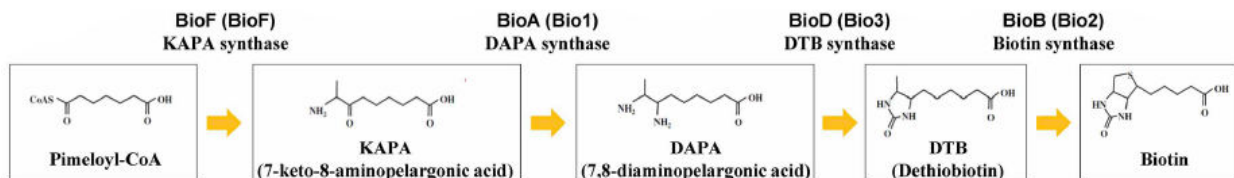


**Figure 1.13** The final four reactions of the biotin biosynthetic pathway and involved enzymes from fungi and plants [20].

While the final three reactions converting KAPA to biotin occur in mitochondria, the BioF enzyme has a C-terminal PTS1 sequence and localizes to peroxisomes [20, 36]. Thus functional coupling between peroxisomes and mitochondria appears to be required for biotin biosynthesis [20].

#### 1.3.3.2.2 Biosynthesis of secondary metabolites

Beside their prominent role in primary metabolism, fungal peroxisomes are also involved in secondary metabolism. There are a lot of biosynthetic pathways of this diverse group of metabolites that are partially located inside peroxisomes (Figure 1.14) [37].

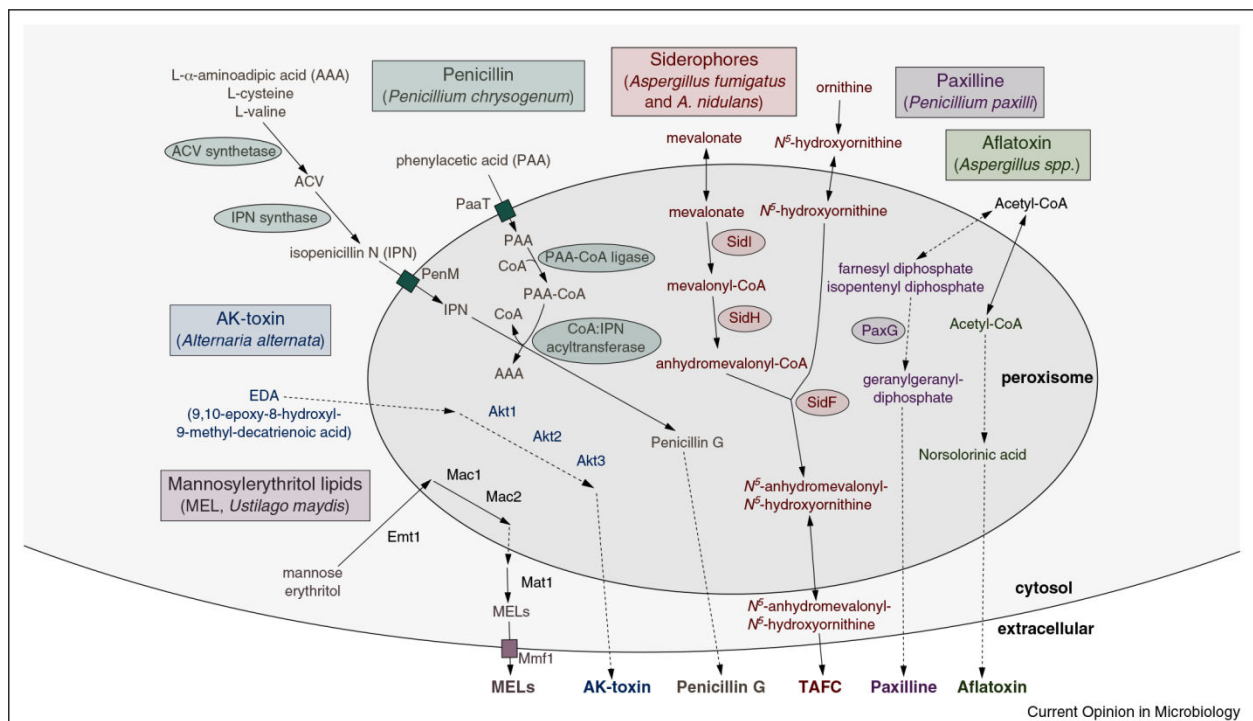


**Figure 1.14** Overview of secondary metabolite synthesis in fungal peroxisomes. Rectangles and ovals represent transporters and enzymes, respectively. Continuous arrows indicate reactions well characterized, whereas dashed arrows indicate reactions that are still under investigation [37].

Peroxisomal enzymes are crucial for the synthesis of  $\beta$ -lactam antibiotics in filamentous fungi [28]. Penicillin and cephalosporin are synthesized in *Penicillium chrysogenum* by a

collaboration of cytosolic with peroxisomal enzymes, with the latter belonging to the family of fatty acid metabolizing enzymes [26]. In addition, peroxisomes in fungi are involved in the biosynthesis of several toxins. During contact of *Aspergillus* species with plant seeds, fungi synthesize seed-contaminating polyketide mycotoxins, such as aflatoxin from the acetyl-coA produced in peroxisome [26, 37]. The AK-toxin that attacks Japanese pears is also produced by peroxisomal enzymes in *Alternaria alternata* [26, 37].

### 1.3.3.2.3 Woronin bodies

Woronin bodies (WBs) are dense-core organelles that are found exclusively in species of Pezizomycotina (filamentous ascomycetes) and evolved over 400 million years ago in the common ancestor of this clade [38, 40]. These organelles rapidly seal the septal pore in response to wounding, allowing the rest of the hypha to continue growth and also reversibly plug the pore under normal growth [41]. WBs range in size from 100 nm to more than 1  $\mu\text{m}$  and can be seen with a light microscope in some species. They form by budding from peroxisomes, in the growing apical without their biogenesis being completely understood [38]. Three genetic loci are known to be essential for WB assembly. These encode the core matrix protein HEX, which self-assembles to hexagonal crystals that form the dense core of the organelle, its membrane receptor WSC (Woronin sorting complex), and the cytoplasmic tether Leashin (LAH), which is localized near the septal pore and in some species promotes equitable WB inheritance by providing a link to the cell cortex, as described in *N.crassa* [38, 42].

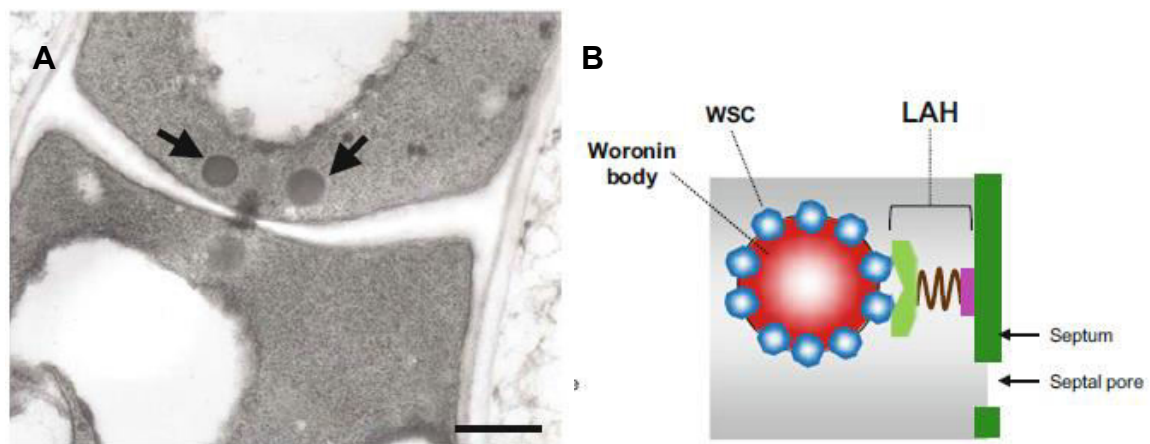


**Figure 1.15** (A) Transmission electron microscopic observation of WBs (arrows) in *Aspergillus oryzae*. Bar: 500 nm (B) Schematic representation of septal tethering of WBs via LAH in *Aspergillus oryzae* [39].

Within the Pezizomycotina, patterns of WB distribution vary systematically; in most species, WBs are tethered to the septal pore at a distance of 100 nm–200 nm and associate with the pore rim through the elastic tether protein Leashin [38, 39]. In contrast, in a group defined by *Neurospora* and *Sordaria*, WBs occur at the cell cortex in a delocalized pattern, suggesting that a new pattern evolved in the common ancestor of these genera [42].

### 1.3.4 Transport across the peroxisomal membrane

As in peroxisomes several anabolic and catabolic pathways exist, there has to be a stable exchange of metabolites, cofactors and ions for the maintenance of intraperoxisomal reactions [27]. Recent experimental data suggest that peroxisomes seem to be permeable to small metabolites up to a size of 300–400 Da, whereas “bulky” substrates require active transport. This implies the coexistence of unselective membrane channels as well as specific transport proteins in the peroxisomal membrane

[27, 43]. During the last few years, unselective channels have been described in yeast and mammals, such as Pxmp2/PMP22 in mammalian peroxisomes [44]. Pxmp2 appears to form a general diffusion pore in the peroxisomal membrane that function as a size selective-filter with an exclusion limit of approximately 400 Da for hydrophilic solutes [44]. Even though peroxisomes are more or less permeable to small metabolites, molecules that approach the exclusion limit, such as NADH, ATP, CoA or fatty acids diffuse very slowly across the membrane, suggesting the existence of active transporters [45]. It is well established that three members of the ATP-binding cassette (ABC) subfamily D catalyze the import of fatty acids for the peroxisomal  $\beta$ -oxidation. These transporters act as homo- as well as heterodimers to ensure import of a broad range of fatty acids [46]. Few other candidates for the transport of other small metabolites have been described recently, acting as ATP transporters: Ant1p in yeast [47], PMP34 in mammals [48] and PNC1/PNC2 in plants [49]. Besides ATP, there are also other cofactors highly required in peroxisomal reactions, like FAD or  $\text{NAD}^+$  that have to be shuffled inside these organelles and reduced there in several reactions [27]. Peroxisomal enzymes such as lactate, malate dehydrogenase and glycerol-3-phosphate dehydrogenase can both recycle them and participate in shuttle systems for their transport [27, 45].

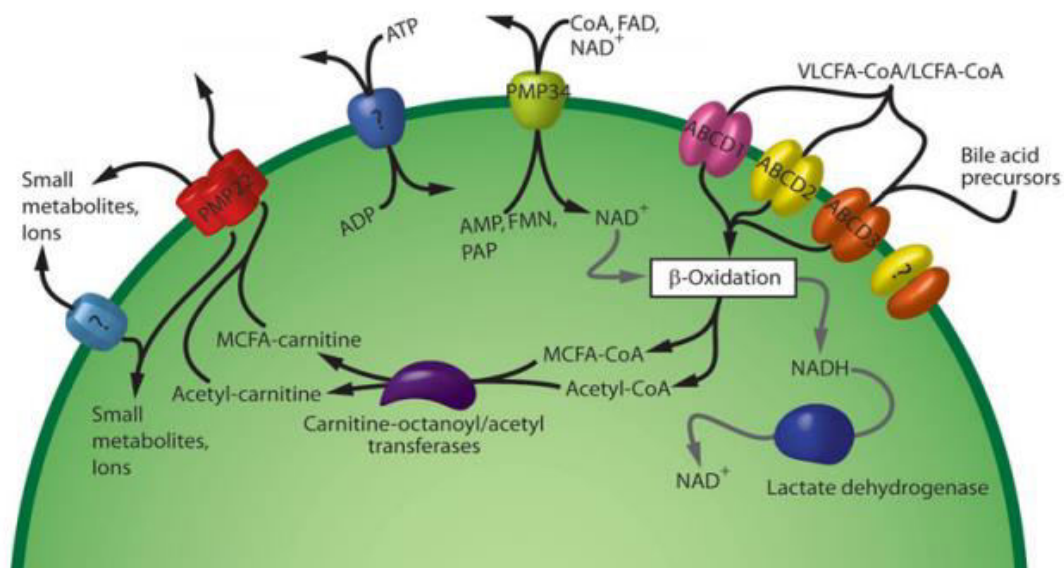


**Figure 1.16** Schematic overview of peroxisomal membrane transporters in mammals. The exchange of small metabolites is permitted through the Pxmp2/PMP22 protein and probably by a second unidentified pore. The import of very long-chain (VLCFAs) and long-chain fatty acids (LCFAs) is mediated by three ABC transporters (ABCD 1-3), which shuffle various fatty acyl-CoAs across the peroxisomal membrane, whereas the export of these bulky molecules occurs through shuttle systems exchanging the bulky CoA with carnitine. The transport of ATP remains still unidentified, while PMP34 is supposed to be responsible for  $\text{NAD}^+$  and CoA import into peroxisomes AMP: adenosine monophosphate. FMN: flavine mononucleotide. PAP: adenosine-30 50 -diphosphate [27].

Taken together, much light has been shed the last years about the bimodal transport system of peroxisomes [27]. However the unique permeability properties of these organelles still remain a mystery.

#### 1.4 Aim of this study

The purpose of the current study is the investigation of the mechanism by which purine metabolites cross the peroxisomal membrane. So far, no such transporter or channel has been identified. The only experimental data involving this topic relies on the work of Rokka et al. [44] on Pxmp2 knock-out mice, who found upon deletion of Pxmp2 a partial restriction of peroxisomal membrane permeability to uric acid.

In order to gain insight into this process, we used an unbiased *in silico* approach to identify, and subsequently functionally characterize, proteins that show correlated gene loss with uric acid oxidase (UOX) in fungi. The rationale of this approach was based on the hypothesis that in cases where peroxisomal UOX is lost in evolution cells cannot metabolize uric acid and thus might be “relaxed” from the need to transport uric acid in peroxisomes, and consequently the machinery for uric acid transport into peroxisomes might also be lost. An analogous well-correlated gene loss has been observed in *Saccharomycotina*, which have lost both UOX and the specific transporter, which mediates uric acid uptake from the growth medium.

*Aspergillus nidulans* serves as a great organism for this kind of study, as its purine assimilation pathway has been thoroughly studied over the last fifty years. Furthermore, several different transporters responsible for the uptake of nitrogenous compounds have been characterized in detail. All the above, combined with the excellent knowledge concerning the physiology and cellular mechanisms of *A. nidulans*, the easy handling of this organism and the availability of various experimental protocols, qualify *A. nidulans*, as the best model for the identification of putative peroxisomal transporters.

## 2. MATERIALS AND METHODS

### 2.1 Strains, culture media, growth and storage conditions

#### 2.1.1 Strains used in this study

All strains carry the *veA1* mutation affecting sporulation. *pyroA4*, *riboB2*, *argB2*, *pyrG89*, *pantoB100*, and *biA1* are auxotrophic mutations for pyridoxine, riboflavin, arginine, uracil/uridine, D-pantothenic acid and biotin respectively. *ptrA* and *aurA* are pyrithiamine and aureobasidin A resistance genes, respectively. *yA2* and *wA3* are mutations resulting in yellow and white conidiospore colors, respectively. The genes *AN5660* and *AN4674* are also called *wscA* and *wscB*, respectively [50]. To avoid confusion with the peroxisomal gene/protein analyzed in this work, called *wscA/WscA*, we kept in the text the original annotation codes (<https://fungidb.org>).

**Table 2.1 List of strains**

Name	Genotype	Reference
TNO2A7	<i>nkuAΔ::argB pyrG89 pyroA4 riboB2</i>	[51]
ΔwscA	(AN7258) <i>wscAΔ::AFpyrG nkuAΔ::argB pyrG89 pyroA4 riboB2</i>	This study
wscA-GFP	<i>wscA::wscA<sup>-(5xGA)</sup>GFP/AFpyrG nkuAΔ::argB pyrG89 pyroA4 riboB2</i>	This study
wscA-mRFP	<i>wscA::wscA<sup>-(5xGA)</sup>mRFP/AFpyrG nkuAΔ::argB pyrG89 pyroA4 riboB2</i>	This study
ΔAN5660	<i>AN5660Δ::ptrA akuBΔ::aurA argB2 biA1</i>	[50]
ΔAN4674	<i>AN4674Δ::ptrA akuBΔ::aurA argB2 biA1</i>	[50]
ΔAN5660 ΔAN4674	<i>AN5660Δ::ptrA AN4674Δ::argB akuBΔ::aurA argB2 biA1</i>	[50]
ΔAN5660 ΔAN4674 ΔwscA	<i>AN5660Δ::ptrA AN4674Δ::argB wscAΔ::AFpyrG pyroA4</i>	This study
ΔaloA	(AN0836) <i>aloAΔ::AFpyrG nkuAΔ::argB pyrG89 pyroA4 riboB2</i>	This study
ΔaloA ΔwscA	<i>aloAΔ::AFpyrG wscAΔ::AFpyrG nkuAΔ::argB pyroA4</i>	This study
ΔuaZ	<i>uaZ14 nkuAΔ::argB pantoB100 pyroA4</i>	[16]
ΔuaZ ΔwscA	<i>uaZ14 wscAΔ::AFpyrG nkuAΔ::argB pyroA4 pantoB100</i>	This study
CytUaZ	<i>uaZ::uaZ<sup>-(5xGA)</sup>GFP/AFpyrG nkuAΔ::argB pyrG89 pyroA4 riboB2</i>	This study
CytUaX	<i>uaX::GFP-uaX<sup>ATG2</sup>/AFpyrG nkuAΔ::argB pyrG89 pyroA4</i>	[16]
Cyt UaZ ΔwscA	<i>uaZ::uaZ<sup>-(5xGA)</sup>GFP/AFpyrG wscAΔ::AFpyrG nkuAΔ::argB pyroA4</i>	This study
GFP-uaX	<i>uaX::GFP-uaX<sup>ATG1</sup>/AFpyrG nkuAΔ::argB pyrG89 pyroA4</i>	[16]
GFP-uaZ wscA- mRFP	<i>uaZ14::GFP-uaZ wscA::wscA<sup>-(5xGA)</sup>mRFP/AFpyrG nkuAΔ::argB pyroA4</i>	This study
GFP-uaZ mRFP- AKL	<i>uaZ14::GFP-uaZ pGEM-gpdAp:mRFP<sup>AKL</sup>::panB nkuAΔ::argB pantoB100 pyroA4</i>	[16]

GFP-uaZ	<i>uaZ14::GFP-uaZ nkuAΔ::argB pyroA4 pantoB100</i>	[16]
uaY462c	<i>uaY462<sup>c</sup> pantoB100 wA3</i>	[52]
uaY2	<i>uaY2 pantoB100 biA1 yA2</i>	[53]
uaY462c wscA-GFP	<i>uaY462<sup>c</sup> wscA::wscA<sup>-(5xGA)</sup>GFP/AFpyrG pyroA4 wA3</i>	This study
uaY2 wscA-GFP	<i>uaY2 wscA::wscA<sup>-(5xGA)</sup>GFP/AFpyrG pyroA4</i>	This study
uaY462c GFP-uaZ	<i>uaY462c uaZ14::GFP-uaZ pGEM-gpdAp-mRFP<sup>AKL</sup>-trpC-panB pyroA4 wA3</i>	This study
uaY2 GFP-uaZ	<i>uaY2 uaZ14::GFP-uaZ pGEM-gpdAp-mRFP<sup>AKL</sup>-trpC-panB pyroA4</i>	This study
GFP-hexA	<i>hexA::GFP-hexA/AFpyrG nkuAΔ::argB pyrG89 pyroA4 riboB2</i>	This study
ΔhexA	<i>(AN4695)hexAΔ::AFpyrG nkuAΔ::argB riboB2 pyroA4 pyrG89</i>	This study
GFP-hexA wscA-mRFP	<i>hexA::GFP-hexA/AFpyrG wscA::wscA<sup>-(5xGA)</sup>mRFP/AFpyrG nkuAΔ::argB pyroA</i>	This study
ΔhexA ΔwscA	<i>hexAΔ::AFpyrG wscAΔ::AFpyrG nkuAΔ::argBpyroA</i>	This study
H1-mRFP	<i>LO:1516 H1-mRFP::AFriboB nkuAΔ::argB pyrG89 pyroA4 riboB2</i>	[54]
nimA5	<i>S06: nimA5 pyrG89 cnxE16 cS12 chaA1 yA2 choA1 wA2</i>	[55]
bimE7	<i>DBE4: bimE7 pyrG89 riboA2</i>	[56]
H1-mRFP WscA-GFP	<i>H1-mRFP::AFriboB riboB2 wscA::wscA<sup>-(5xGA)</sup>GFP/AFpyrG pyroA4</i>	This study
nimA5 WscA-GFP	<i>nimA5 wscA::wscA<sup>-(5xGA)</sup>GFP/AFpyrG yA2 chaA</i>	This study
nimA5 H1-mRFP WscA-GFP	<i>nimA5 H1-mRFP::AFriboB riboB2 wscA::wscA<sup>-(5xGA)</sup>GFP/AFpyrG wA2</i>	This study
bimE7 WscA-GFP	<i>bimE7 wscA::wscA<sup>-(5xGA)</sup>GFP/AFpyrG pyroA4</i>	This study
bimE7 H1-mRFP WscA-GFP	<i>bimE7 H1-mRFP::AFriboB riboB2 wscA::wscA<sup>-(5xGA)</sup>GFP/AFpyrG pyroA4</i>	This study

### 2.1.2 Culture media

Standard complete (CM) and minimal media (MM) supplemented with appropriate auxotrophies for *A. nidulans* were used (<http://www.fgsc.net>). CM contains all the nutrients and auxotrophies required for fungal growth, while MM contains only the minimum nutritional supplements possible. These are salt solution, carbon source (glucose, fructose or sucrose), nitrogen source and the appropriate auxotrophies, according to the requirements of each strain. Composition of all media and solutions used in this study are shown in Table 2.2 and Table 2.3 respectively. For solid growth mediums, 1-2 % agar was added to the liquid medium, before autoclaving. Media and supplemented auxotrophies were at the concentrations given in FGSC (<http://www.fgsc.net>). Media and chemical reagents were obtained from Sigma-Aldrich (Life Science Chemilab SA, Hellas) or AppliChem (Bioline Scientific SA, Hellas).

**Table 2.2 Media used for *A. nidulans* growth**

	Complete medium (CM)	Minimal medium (MM)
Salt solution	20mL	20mL
Vitamin solution	10mL	-
Glucose	10g	10g
Casamino acids	1g	-
Bactopeptone	2g	-
Yeast extract	1g	-
H <sub>2</sub> O <sub>distilled</sub>	Up to 1L	Up to 1L

**Table 2.3 Solutions used in culture media**

Salt solution	Vitamin solution	Trace elements (1 L)
KCl 26 g	p-aminobenzoic acid 20 mg	Na <sub>2</sub> B <sub>4</sub> O <sub>7</sub> x 10 H <sub>2</sub> O 40 mg
MgSO <sub>4</sub> 7H <sub>2</sub> O 26 g	D-pantothenic acid 50 mg	CuSO <sub>4</sub> x 5 H <sub>2</sub> O 400 mg
KH <sub>2</sub> PO <sub>4</sub> 76 g	pyridoxine 50 mg	FeO <sub>4</sub> P x 4 H <sub>2</sub> O 714 mg
Trace elements 50 mL	riboflavin 50 mg	MnSO <sub>4</sub> x 1 H <sub>2</sub> O 728 mg
Chloroform 2 mL	biotin 1 mg	Na <sub>2</sub> MoO <sub>4</sub> x 2 H <sub>2</sub> O 800 mg
H <sub>2</sub> O <sub>distilled</sub> Up to 1L	H <sub>2</sub> O <sub>distilled</sub> Up to 1L	ZnSO <sub>4</sub> x 7 H <sub>2</sub> O 8 mg

The pH was adjusted to 6.8 with the addition of NaOH 3M. Unless otherwise stated, growth was tested on media containing 1% (w/v) Glucose, as mentioned above, CH<sub>3</sub>COONa 0.2% (w/v) or Oleic acid 0.1% (v/v) as carbon sources. Nitrogen sources were used at final concentrations: urea 5 mM, NaNO<sub>3</sub> 10 mM, Ammonium L-(+)-tartrate 10 mM, purines 0.1 mg/mL. Amino acids (proline, L-glutamate) were used at 5 mM. Uracil and uridine were used at 5 mM and 10 mM respectively.

Oxidizing agents and cell wall stressors were used at final concentrations: Paraquat 0.5 mM, H<sub>2</sub>O<sub>2</sub> 2 mM, CdCl<sub>2</sub> 0.02 mM, Methylene Blue (MB) 50 µM, Congo Red (CR) 50 µg/ml, Caffeine 7 mM. For hyperosmotic conditions NaCl 500 mM was used in the presence of NaNO<sub>3</sub> as sole nitrogen source.

### 2.1.3 Growth and storage conditions

For the inoculation of *A. nidulans* cultures, conidiospores were harvested from sporulating culture plates with the use of sterile toothpicks. Solid cultures were incubated in 37°C or 25°C for 2-4 days and liquid cultures were incubated overnight at 37°C or 25°C, 140-150 rpm.

*Escherichia coli* bacterial cultures (strain DH5a) were grown on Luria-Bertani (LB) medium (Bacto Tryptone 10 g, NaCl 10 g, BactoYeast Extract 5 g for 1L). The pH was

adjusted to 7.0 with NaOH 1M. For the selection of transformed colonies ampicillin was added in a final concentration of 100 µg/mL. Solid cultures were incubated overnight at 37°C, whereas liquid cultures were incubated in the same conditions, plus agitated at 200 rpm.

For short term storage agar plates were stored at 4°C. For long-term storage, glycerol stocks were prepared. *A. nidulans* conidiospores were harvested from ¼ of a fresh 100 mm CM plate, in 700 µL glycerol and 700 µL PBS (NaCl 8 g, KCl 0.2 g, Na<sub>2</sub>PO<sub>4</sub> 1.44 g, KH<sub>2</sub>PO<sub>4</sub> 0.24 g, pH 7.4 with 1 N HCl), in a sterile eppendorf tube. After vortexing, glycerol stocks were stored at -80°C.

## **2.2 Genetic crosses and progeny analysis in *Aspergillus nidulans***

For the sexual crossing of *A. nidulans*, the two parental strains were inoculated 1cm apart on a minimal medium plate containing the appropriate supplements and incubated for 2-3 days at 37°C. Small parts of media in the contact area between the two parental strains, where an heterokaryon was formed, were cut out and transferred to small Petri dishes with selective medium, which contained nitrate as nitrogen source and only the auxotrophies required for both strains. After 2 days of incubation at 37°C, the dishes were sealed with masking tape and incubated at the same temperature for further 15-17 days, in order to form cleistothecia.

The plates were unsealed and 8 single cleistothecia were selected under the stereoscope with a sterile toothpick. Hulle cells, aerial hyphae and any conidiophores were removed by rolling cleistothecia on an agar plate. Each cleistothecium was transferred to a sterile eppendorf tube containing 500 µL sterile water and ruptured against the wall of the tube with a toothpick to release the asci. The asci were disrupted by vortexing to generate an ascospore suspension. An aliquot (~10 µL) of each suspension was plated on minimal media selecting against both parental types and was incubated at 37°C for 3 days, so that only recombinant progeny would grow. In order to obtain single colonies, 5-10 µL of the ascospore suspension from a recombinant cleistothecium were plated. Several colonies were then selected and analyzed for their genetic background.

## **2.3 Epifluorescence microscopy and Statistical analysis**

Conidiospores were incubated overnight in glass bottom 35 mm µ-dishes (ibidi, Lab Supplies Scientific SA, Hellas) in liquid minimal media, for 18-22 h at 25°C, under described conditions (0.1% glucose and 10 mM NaNO<sub>3</sub> or 10 mM ammonium tatratre or 0.5 mM uric acid). Images were obtained using an inverted Zeiss Axio Observer Z1 equipped with an Axio Cam HR R3 camera. Contrast adjustment, area selection and color combining were made using the Zen lite 2012 software. Scale bars were added using the FigureJ plugin of the ImageJ software. Images were further processed and annotated in Adobe Photoshop CS4 Extended version 11.0.2.

Quantification of Peroxisomal Surface (total surface of peroxisomes containing GFP or mRFP/hypha) was performed using the Area Selection Tool of the ICY application. Tukey's Multiple Comparison Test (One-Way ANOVA) was performed to test the statistical significance of the results for 5 Regions of Interest (ROIs), using Graphpad Prism 6. For the quantification of colocalization, Pearson's correlation coefficient (PCC) above thresholds, for a selected Region of interest (ROI) was calculated using the ICY colocalization studio plugin (pixel-based method) (<http://icy.bioimageanalysis.org/>). One sample t-test was performed to test the significance of differences in PCCs, using the Graphpad Prism software. Confidence interval was set to 95%.

## 2.4 DNA manipulations & construction of replacement cassettes

### 2.4.1 *Aspergillus nidulans* genomic DNA extraction

Genomic DNA extraction for PCR reactions was performed as described in FGSC (<http://www.fgsc.net>). CM culture plates were incubated for 4-5 days at 37°C. Conidiospores were harvested from 1/4 of a plate in 25 mL of MM liquid media containing  $\text{NH}_4^+$  and all the necessary supplements required by the strain used. The cultures were incubated at 37°C, 140 rpm overnight. Then, they were filtered through a blutex, dried and immediately frozen in liquid nitrogen. The mycelia were pulverized in a mortar with a pestle in the presence of liquid nitrogen and ~200 mg of the fine powder were transferred in a 2 mL eppendorf tube. The powder was resuspended in 800  $\mu\text{L}$  of DNA extraction buffer (0.2 M Tris-HCl pH 8.0, 1% SDS, 1 mM EDTA pH 8.0) mixed by vortexing and incubated on ice for ~20 min. 800  $\mu\text{L}$  of pure phenol were then added and the mixture was shaken vigorously and centrifuged for 7 min at 12000 rpm. The upper phase, containing the DNA, was transferred to a new 2 mL eppendorf tube, where an equal volume of chloroform was added and the mixture was shaken again vigorously and centrifuged for 7 min at 12000 rpm. The upper phase was recovered and transferred once again to a new 2 mL eppendorf tube, where DNA was precipitated by adding equal volume of isopropanol and 1/10 volume of 3 M Sodium acetate ( $\text{CH}_3\text{COONa}$ ) pH 5.3. The mixture was mixed by inverting the tube several times and after that, it was centrifuged for 10 min at 12000 rpm. The pellet was washed with 200  $\mu\text{L}$  70% ethanol without mixing and after a 2 min centrifugation at 12000 rpm ethanol was removed with a pipette. The pellet was dried for 10 min at 50°C. Finally it was resuspended in 80  $\mu\text{L}$  of sterile distilled water containing 0.2 mg/mL RNaseA and incubated at 37°C for 30 min.

In order to estimate quantitatively and qualitatively the extracted DNA, agarose gel electrophoresis was performed using 3  $\mu\text{L}$  of the DNA solution.

### 2.4.2 Agarose gel electrophoresis

For the analysis of size and conformation of DNA in a sample, quantification of DNA, as mentioned above, or separation and extraction of DNA fragments, 0.8% agarose was dissolved in 1x TAE buffer (242 g Tris-Base, 57.1 mL glacial  $\text{CH}_3\text{COOH}$ , 100 mL 0.5 M EDTA pH 8.0 for 1L 50x buffer) by warming up the solution until it was transparent. After cooling down, 0.5 mg/mL ethidium bromide was added and the solution was poured into a casting tray. 45 min-1h later, DNA samples were mixed with loading buffer and loaded to the gel. In order to determine the size of the fragments, a molecular weight marker was also loaded to the gel. The gel was run for 20-40 min, according to the expected DNA sample size at 100 V. Then, it was exposed to UV light with a UV transilluminator and DNA bands were either photographed or excised from the gel for cloning purposes.

In the latter case, DNA bands were extracted and purified from the gel using the Nucleospin Extract II kit (Macherey-Nagel, Labsupplies Scientific SA, Hellas). The samples were mixed with Binding Buffer NTI (Guanidinium thiocyanate 30–60 %) and heated at 50°C for 5-10 min in order to dissolve the agarose. In the presence of chaotropic salt, the DNA was bound to the silica membrane of a NucleoSpin® Gel and PCR Clean-up Column. Contaminations were removed by simple washing steps with ethanolic Wash Buffer NT3. Finally, the pure DNA was eluted under low salt conditions with slightly alkaline Elution Buffer NE (5 mM Tris/HCl, pH 8.5).

### 2.4.3 Polymerase Chain Reaction (PCR)

Conventional and High fidelity PCR reactions were carried out using the KAPATaq DNA polymerase or the KAPA HiFi HotStart ReadyMix (Kapa Biosystems), respectively. Components and conditions of these PCR reactions are described in the following Tables, according to manufacturer's instructions. All DNA fragments used in the various constructs were amplified from a TNO2A7 strain.

**Table 2.4 Composition of conventional and high fidelity PCR reactions.**

Components	Final concentrations	
	Conventional	High fidelity
10x KapaTaq buffer (MgCl <sub>2</sub> included)	1x	-
10x KapaHiFi buffer (MgCl <sub>2</sub> included)	-	1x
dNTPs	0.2 mM each	-
Forward primer	0.4 μM	0.3 μM
Reverse primer	0.4 μM	0.3 μM
DNA polymerase	0.5 U	0.5 U
DNA template	10-20 ng	10ng
H <sub>2</sub> O <sub>distilled</sub>	Up to 25 μL	Up to 25 μL

**Table 2.5 Conditions for conventional and high fidelity PCR reactions.**

Step	Conventional			High fidelity		
	Temperature	Duration	Cycles	Temperature	Duration	Cycles
Initial denaturation	95°C	3 min	1	95°C	3 min	1
Denaturation	95°C	30 sec	35	98°C	20 sec	15-35
Annealing	T <sub>m</sub> - 5°C	30 sec		60-75°C	15 sec	
Extension	72°C	1 min/kb		72°C	15-60 sec/kb	
Final extension	72°C	1 min/kb	1	72°C	1 min/kb	1
Hold	4-10°C	∞	1	-	-	-

### 2.4.4 Molecular cloning

Gene deletions and in locus integration of tagged gene fusions (Figure 2.1) were generated by one step ligations or sequential cloning of the relevant fragments in the plasmid pGEM, using oligonucleotides with additional restriction sites.

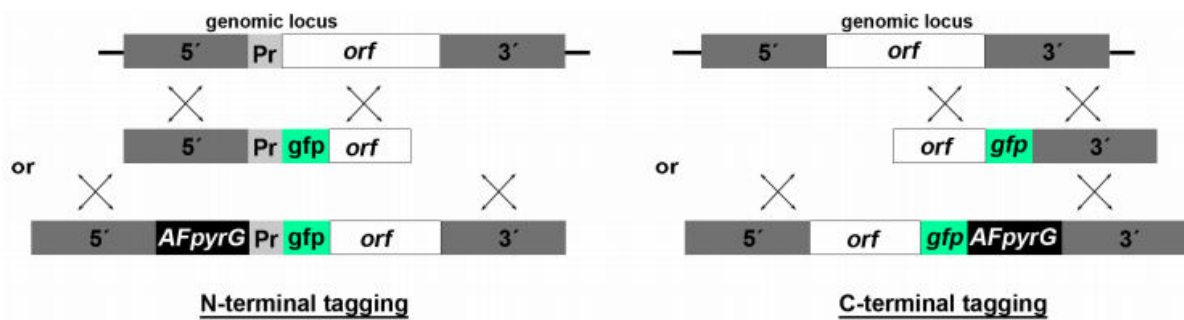


**Figure 2.1** Schematic representation of the integrations of *gfp* in the N- and C-terminal regions of the corresponding ORFs [16]. The same procedure was followed for the construction of *mrpf*-tagged genes.

For the construction of *wscA* and *hexA* null mutants, linear DNA cassettes containing flanking sequences of the relevant ORFs separated by *AFpyrG*, as selection marker, were generated. The C-terminal *wscA-gfp* or *mrpf* fusions were constructed by sequential cloning of the relevant fragments into the pGEM vector. These constructs carried also a 5x Gly-Ala (5xGA) linker, amplified together with *gfp* or *mrpf* and *AFpyrG* from plasmids p1439, or p1491 respectively [51]. In cases where cloning was performed with only one restriction enzyme, the digested vector was incubated with alkaline phosphatase (CIAP, TaKaRa) at 37°C for 15 min. Generation of recombinant DNA was mediated by DNA ligase, along with vector and insert at a 1:3 concentration, and 1x ligase buffer at 25°C for 1.5 h. The reaction mixture was used to transform *E. coli* competent cells (DH5a). The resulting plasmids were used as templates to amplify the linear cassettes by PCR and transform relevant strains.

The replacement cassette for the N-terminal *gfp*-tagged *hexA* was generated using Double Joint PCR [57] by fusing the *gfp-hexA* chimera with relevant fragments of the plasmid containing the *hexA* null cassette. Oligonucleotides used are listed in Appendix. In all cases, transformants selected by either auxotrophy or gene function complementation, were subjected to PCR analysis.

#### 2.4.5 *Aspergillus nidulans* transformation

Transformation was performed as described in Koukaki et al. [58]. Conidiospores from a full grown CM culture plate were harvested and filtered. 200 mL liquid MM with the appropriate auxotrophies and nitrogen source were inoculated with the spore solution and incubated at 37°C for 4-4.5 h, 140-150 rpm. For examining the entry of conidia to germinating phase, an aliquot of the culture was regularly observed under the microscope. Once conidia reached that phase, the culture was transferred into sterile falcons and centrifuged at 4000 rpm for 10 min. The pellet was resuspended in 20 mL of Solution I (1.2 M MgSO<sub>4</sub>, 10 mM orthophosphate pH 5.8), followed by the incubation with 200 mg of the lytic enzyme glucanex, together with a few crystals of Bovine Serum Albumin (BSA) for 1.5-2 h at 30°C, 60 rpm. Protoplasts concentration was achieved by centrifugation at 4000 rpm for 10 min. The pellet was then washed with 10 mL Solution II (1 M sorbitol, 10 mM Tris-HCl pH 7.5, 10 mM CaCl<sub>2</sub>) and resuspended in the same solution, at a volume depending on the number of transformations desired. Protoplasts, plasmid DNA (1.5-2 µg) and ¼ of the total volume Solution III (60% w/v PEG6000, 10 mM Tris-HCl pH 7.5, 10 mM CaCl<sub>2</sub>) were distributed in eppendorf tubes and incubated on ice for 15 min. A tube without DNA was included as a control, to estimate any possible contaminations of the protoplasts or the solutions. Furthermore, 500 µL of Solution III were added to the tubes, mixed and incubated for another 15 min at room temperature. Then, the tubes were centrifuged for 10 min at 6000 rpm, washed and resuspended with 1 mL and 200 µL of Solution II, respectively. The last step of the

transformation included the mix of protoplasts with 4 mL of melted Top Sucrose Minimal Media (0.45% agar, 20 mL salt solution, 10 g D-glucose, 342.4 g sucrose for 1 L) and the inoculation of previously prepared SM (sucrose minimal media; 1% agar). Plates were incubated at 37°C for 4-5 days. Transformants were isolated by streaking on MMG, containing the appropriate supplements and further analyzed by growth tests or PCR.

## 2.5 Protein manipulations

### 2.5.1 Total protein extraction

CM culture plates were incubated for 7 days at 25°C. Conidiospores from a full plate were harvested in 100 mL of liquid MM containing NaNO<sub>3</sub> as a nitrogen source and any supplements required, depending on the auxotrophies of each strain. The cultures were then incubated for 14-16 h at 25°C and at 37°C. Afterwards, they were filtered through blutex, dried and immediately frozen in liquid nitrogen. The mycelia were pulverized 5 times in a mortar with a pestle in the presence of liquid nitrogen, and ~ 500 mg of the fine powder were collected in a 2 mL eppendorf tube.

The pulverized mycelium was resuspended in 1 mL of ice cold precipitation buffer (Table 2.6), vortexed and incubated on ice for 10-30 min. After a centrifugation of the sample for 10 min, at 13000 rpm, 4°C, the pellet was collected and resuspended once in ice cold ethanol 100% and twice in ice old acetone, with each step followed by a centrifugation for 5 min, at 13000 rpm, 4°C. The supernatant was removed with a pipette and the pellet was air-dried for 30 min at 60°C. The pellet was then resuspended and dissolved in 500-600 µL of Protein Extraction Buffer I and the sample was centrifuged for 10-15 min, at 13000 rpm, 4°C. Finally, the supernatant was transferred in a pre-frozen eppendorfs and was stored at -80°C for further use.

**Table 2.6 Solutions used for total protein extraction**

Precipitation buffer	50 mM Tris-HCl pH 8.0, 50 mM NaCl, 12.5% (v/v) trichloroacetic acid (TCA), 1 mM PMSF, 1 x Protease Inhibitors Cocktail (PIC)
Extraction buffer I	100 mM Tris-HCl pH 8.0, 50 mM NaCl, 1% (v/v) SDS, 1 mM EDTA, 1 mM PMSF, 1 x PIC

### 2.5.2 Protein quantification

Protein concentration in the samples was determined using the Bradford method [59]. 1 mL of Bradford reagent (100 mg Coomassie Brilliant Blue G-250, 50 mL 100% EtOH, 100 mL H<sub>2</sub>PO<sub>4</sub>, 850 mL H<sub>2</sub>O) were mixed with 2 µL of the protein extract and mixed by vortexing and then transferred to a cuvette. The spectrophotometer was calibrated with 1 mL of the reagent only and then the optical density (OD) of the samples was measured in triplicates, at 595 nm. Protein concentration were quantified by comparing the average of the obtained OD values against the BSA standard curve, which was generated by plotting the average of various absorbance versus various known concentrations of BSA.

### 2.5.3 SDS-PAGE electrophoresis and Western blot

For the SDS-PAGE electrophoresis, a polyacrylamide gel was used, consisting of two gel parts of different acrylamide concentration; the separating gel (lower layer), which is

responsible for separating polypeptides by size and the stacking gel (upper layer), which is designed to stack the proteins into a thin layer before entering the separating gel. The density of the separating gel is the main factor that determines the migration pattern of the proteins based on their size. In this study, the polyacrylamide gels were prepared as indicated in Table 2.7. The gels were casted in casting glass plates (Biorad) and combs were used to form wells. After polymerization, the comb was removed, the wells were washed and the gels were placed into an electrophoresis apparatus (Mini PROTEAN™ Tetra Cell, Bio-Rad) containing electrophoresis running buffer [25 mM Tris, 192 mM Glycine, 0.1% (w/v) SDS pH 8.3].

Proteins (30-50 mg estimated by Bradford analysis) were incubated with 4x sample loading buffer [40% (v/v) glycerol, 250 mM Tris-HCl pH 6.8, 0.02% (w/v) bromophenol blue, 8% (v/v) SDS, 20% (v/v) β-mercaptoethanol] for 30 min at 37°C, loaded and run at 80 V through the stacking gel and afterwards at 100 V through the separating gel. A protein ladder was also loaded and run in parallel to estimate protein size as well as transfer efficiency during western blot.

**Table 2.7 Composition of separating and stacking layers of polyacrylamide gels**

	Separating gel 8% (for 10 mL)	Stacking gel 4% (for 5 mL)
<b>H<sub>2</sub>O<sub>distilled</sub></b>	4.09 mL	3.65 mL
<b>Acrylamide/Bisacrylamide 30 %</b>	3.3 mL	0.667 mL
<b>Upper Tris</b>	-	0.625 mL
<b>Lower Tris</b>	2.5 mL	-
<b>20% (w/v) SDS</b>	50 µL	25 µL
<b>10% (w/v) Ammonium persulfate (APS)</b>	50 µL	25 µL
<b>TEMED</b>	10 µl	10 µl

After electrophoresis, the SDS gel was equilibrated in Transfer Buffer for 30 min. Next it was placed in a cassette on a top of a sponge and a couple of filtered paper, followed by the methanol-activated PVDF membrane (Macherey-Nagel, Lab Supplies Scientific SA, Hellas), two more filter papers and another sponge. The cassette was inserted in a blotting apparatus (Mini PROTEAN™ Tetra Cell, Bio-Rad), filled with ice-cold Transfer Buffer, and electric current was applied for 1.5-2 h at 100 V, forcing the proteins to migrate on the membrane. After transfer, the membrane was stored in TBS-T buffer at 4°C.

**Table 2.8 Solutions for Western blot**

<b>Transfer Buffer</b>	25mM Tris, 192 mM Glycine, 20% methanol
<b>TBS</b>	20 mM Tris-HCl pH 7.5, 500 mM NaCl, 0.1% (v/v) Tween 20
<b>TBS-T</b>	10 mM Tris-HCl pH 7.5, 150 mM NaCl

In order to prevent the primary or secondary antibody from binding non-specifically to the remaining free protein sites on the membrane, blocking was performed using 2% (w/v) non-fat dry milk in TBS-T for 1h, RT, under gentle agitation. Immunodetection was performed using a primary anti-GFP monoclonal antibody (Roche Diagnostics, Hellas) diluted at 1:2000 in an aliquot of the blocking solution for 2h, at RT, under gentle agitation. After 3 x 10 min washing in TBS-T with vigorous shaking to remove non-specifically bound antibodies, the membrane was incubated for 1 h with secondary goat anti-mouse IgG HRP-linked antibody (Cell Signaling Technology Inc, Bioline Scientific SA, Hellas), diluted in blocking buffer (1:1000-1:3500), at RT, under gentle agitation. Once again, the membrane was washed with TBS-T 3 x 10 min as previously described.

After the last washing step, the membrane was subjected to chemiluminescence reaction using the LumiSensor Chemiluminescent HRP Substrate kit (Genscript USA, Lab Supplies Scientific SA, Hellas), according to manufacturer's instructions. Blots were developed in a dark room with Kodak developing reagents and SuperRX Fuji medical X-Ray films (FujiFILM Europe).

## **2.6 Analysis of correlated gene loss**

Gene orthologous groups were downloaded from OrthoDB release 10 (<http://www.orthodb.org>) as flat files. Genes classified at the fungi level (taxid=4751) were organized in a table containing 46160 gene groups (rows) and 540 species (columns) ordered by taxonomic classification. For the comparison of phylogenetic profiles, the presence or the absence of members of a gene group in a given species were coded as 1 or 0, respectively. Mutual information (MI) scores were calculated between UOX (249875at4751) and each profile in the dataset using the mutual information function of the R library infotheo (<https://cran.r-project.org/package=infotheo>). For the ten genes with higher MI scores, gene losses were estimated as the number of present to absent transitions along gene vectors. Since the vector order approximately reflects organism phylogeny, this method is expected to provide an overestimation of true losses equally affecting all genes.

### 3. RESULTS

#### 3.1 Purine catabolic enzymes show a correlated gene loss with Pmp22-like proteins

The investigation of the mechanism by which purine metabolites cross the peroxisomal membrane relied on the hypothesis that in cases where peroxisomal uric acid oxidase (UOX) is lost in evolution, the machinery for uric acid transport into peroxisomes might also be lost, as these organelles can no longer catabolize uric acid.

We compared the UOX distribution in 540 fungal species with complete genomes with that of 46160 gene groups classified by the OrthoDB database [60]. For the ten profiles most similar to UOX, as judged by the mutual information criterion [61] we inferred the number of correlated losses with UOX and ranked the list of genes accordingly (Table 3.1).

**Table 3.1 Fungal genes with correlated loss with uric acid oxidase (uricase)**

OrtoDB group ID	<i>A. nidulans</i> names	<i>A. nidulans</i> genes	Mutual information score	Inferred losses	correlated losses	OrthoDB definition
249875at4751	AN9470	uaZ	0.3331	21	21	Uricase
499960at4751	AN2910	uaX	0.1297	44	12	5-hydroxyisourate hydrolase
376025at4751	AN0077		0.1215	38	12	Oxidoreductase, 2OG-Fe(II) oxygenase family, putative
480625at4751	AN0070	uaW	0.1181	42	11	Oxo-4-hydroxy-4-carboxy-5-ureidoimidazoline decarboxylase
458012at4751	AN7258	wscA <sup>a</sup>	0.1187	25	10	Integral membrane protein
229636at4751	AN6932, AN6730	uapA, uapC	0.1213	28	9	Purine permease
297091at4751	AN8127, AN2783, AN1427		0.1162	21	8	Major facilitator superfamily
443385at4751	AN10863, AN7187, AN0174		0.1261	21	7	D-amino-acid oxidase
397940at4751	AN7042		0.1124	25	7	Mitochondrial 18kDa protein
289953at4751	AN6815, AN10903		0.1274	21	6	guanine deaminase
132324at4751	AN6095, AN6703	jenA, jenB	0.1202	21	6	Major facilitator, sugar transporter-like

<sup>a</sup> This work.

As we can see on the table above, among the highest-ranking entries of this list are genes with a known function in purine metabolism, including two enzymes following UOX in the degradation pathway (HIU hydrolase and OHCU decarboxylase), and the UapA purine transporter. The first entry in our list encoding a transmembrane protein corresponded to a group of orthologous genes represented in *A. nidulans* by AN7258 (WscA).

Comparison of the phylogenetic profile (Figure 3.1) shows that as in the case of UOX, genes of the AN7258 group are present in most fungal species. However, both genes were lost in some fungal lineages, often together with HIU hydrolase and UapA. Notable examples of co-losses of AN7258 and UOX are observed in Microsporidia, in some Ustilaginomycotina, in a group of Saccharomycotina that includes *S. cerevisiae*, and in some Taphirinomycotina.

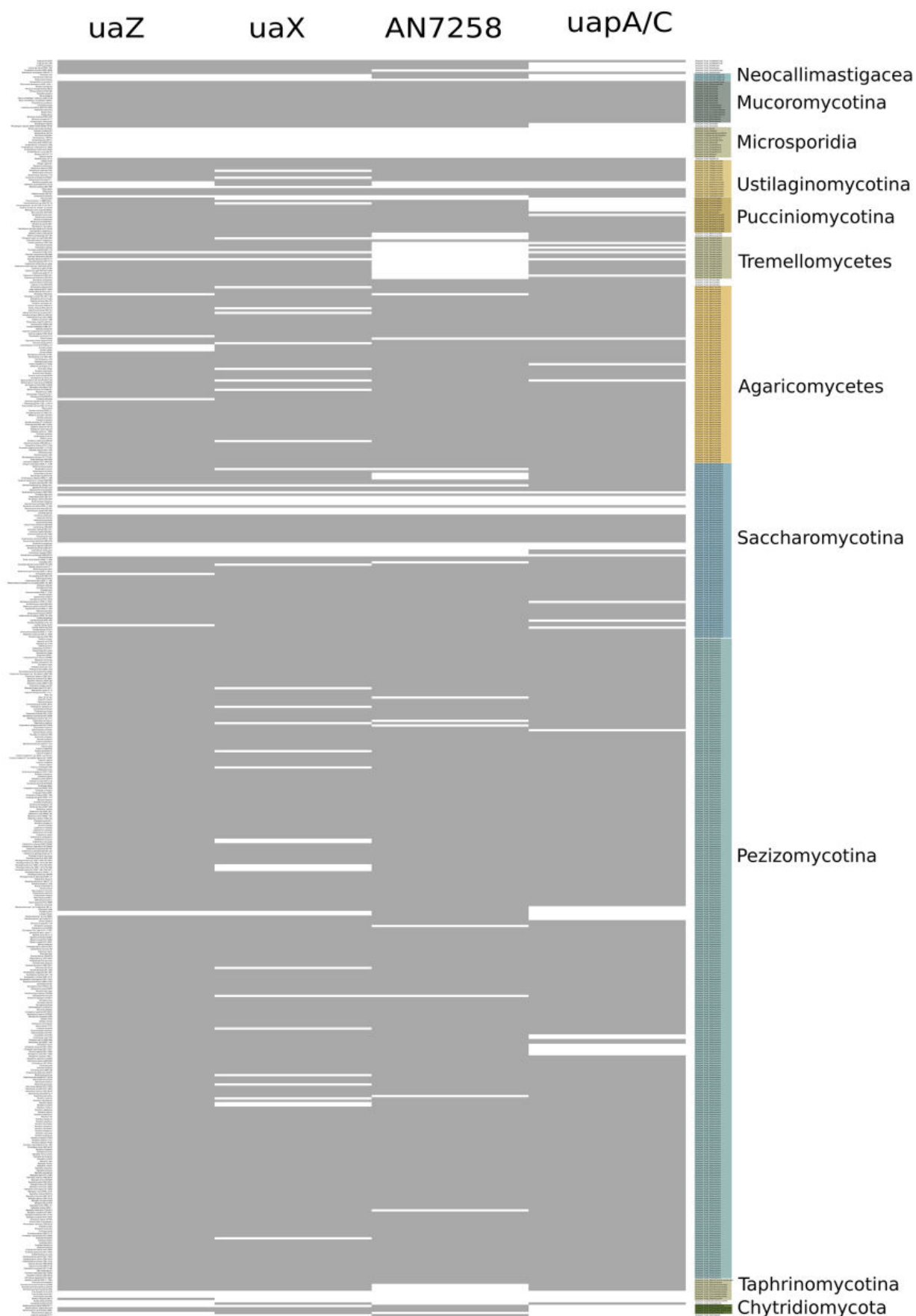


**Figure 3.1** Comparison of the organism distribution of AN7258 with that of UOX (UaZ), HIU hydrolase (UaX), and UapA. The presence (gray) or absence (white) of genes is shown along a list of 540 fungal species ordered by taxonomic classification.

Homology searches with AN7258 revealed significant similarity to protein annotated as belonging to the Mpv17/PMP22 family. To clarify the phylogenetic position of AN7258 within this family, we performed a phylogenetic analysis with all homologous protein collected in ten model eukaryotes. The phylogenetic tree suggests that among the six *A. nidulans* paralogous proteins with similarity to this family, AN7258 is the most closely related to characterized mammalian PMP22. However, orthologous relations between metazoan and fungal proteins in this family could not be assessed with confidence as the deep branches of the tree have low bootstrap support.

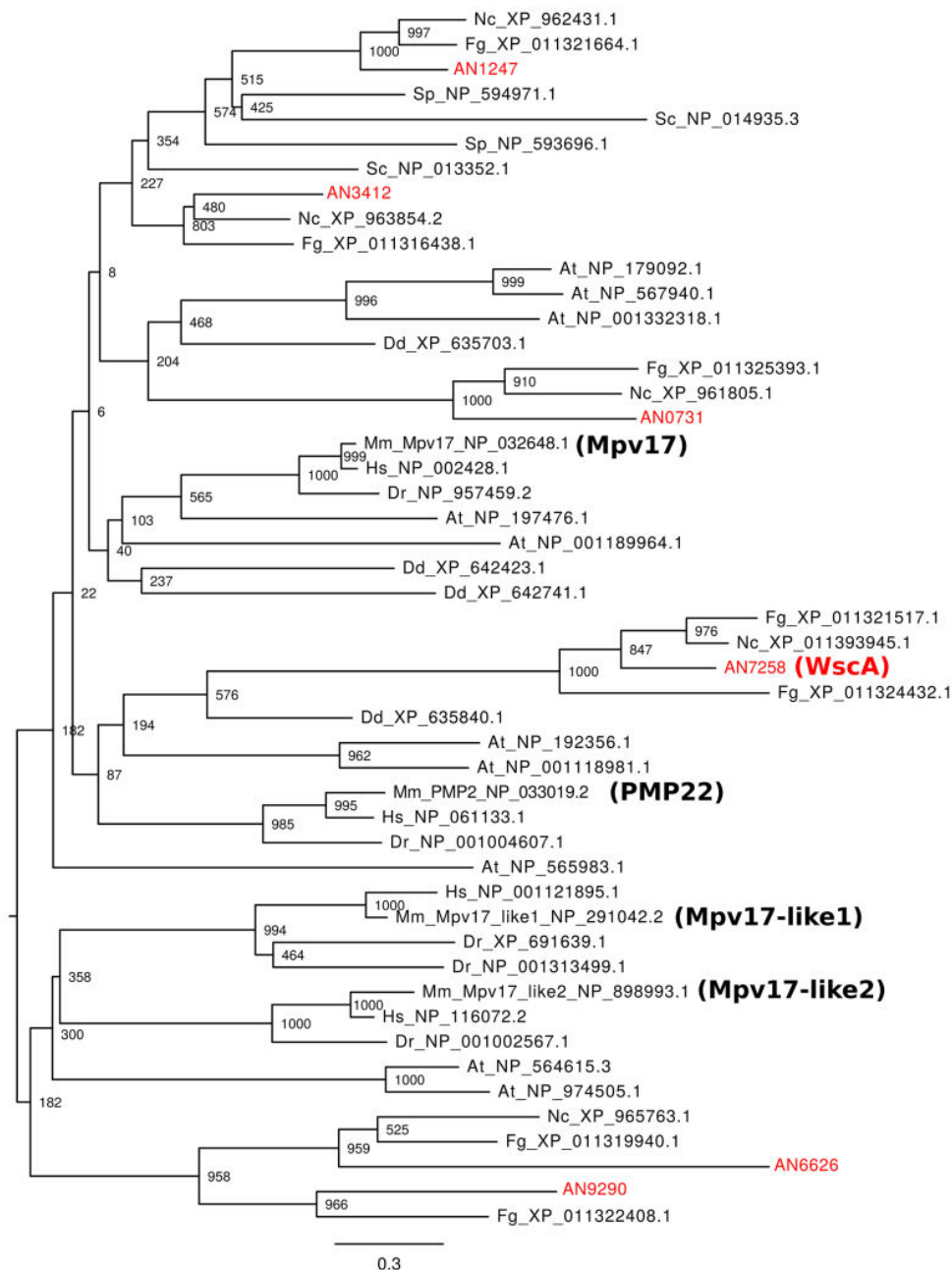


**Figure 3.2** Phylogeny of the Mpv17/PMP22 family. The mid-point rooted neighbour-joining tree was based on the alignment of the complete set of homologous sequences in *A. nidulans*, *Arabidopsis thaliana* (At), *Danio rerio* (Dr), *Dictyostelium discoideum* (Dd), *Fusarium graminearum* (Fg), *Homo sapiens* (Hs), *Mus musculus* (Mm), *Neurospora crassa* (Nc), *Saccharomyces cerevisiae* (Sc), *Schizosaccharomyces pombe* (Sp). *A. nidulans* sequences are indicated with the genename in red; other sequences are indicated with Genbank accession codes preceded by the abbreviated scientific name. Node bootstrap support over 1000 replicates is indicated.

### 3.2 *In silico* analysis of WscA

As shown in Figure 3.1, *A. nidulans* has a single gene, AN7258, encoding a putative Pxmp22 orthologue often lost together with UOX in fungi. The annotation of the gene predicts peroxisomal localization (<https://fungidb.org/fungidb/app/record/gene/AN7258>), but it has not been experimentally characterized. We named the product of this gene WscA (Woronin sorting complex A), in line with the name given for the homologous protein recently studied in *A. fumigatus* [62]. The *A. nidulans* WscA protein is 269 amino acids long and predicted to consist of 4  $\alpha$ -helical membrane spanning segments (TMS1-4), a long N-tail cytosolic tail of 98 residues, and a shorter cytosolic C-tail of 48 residues (Figure 3.3).

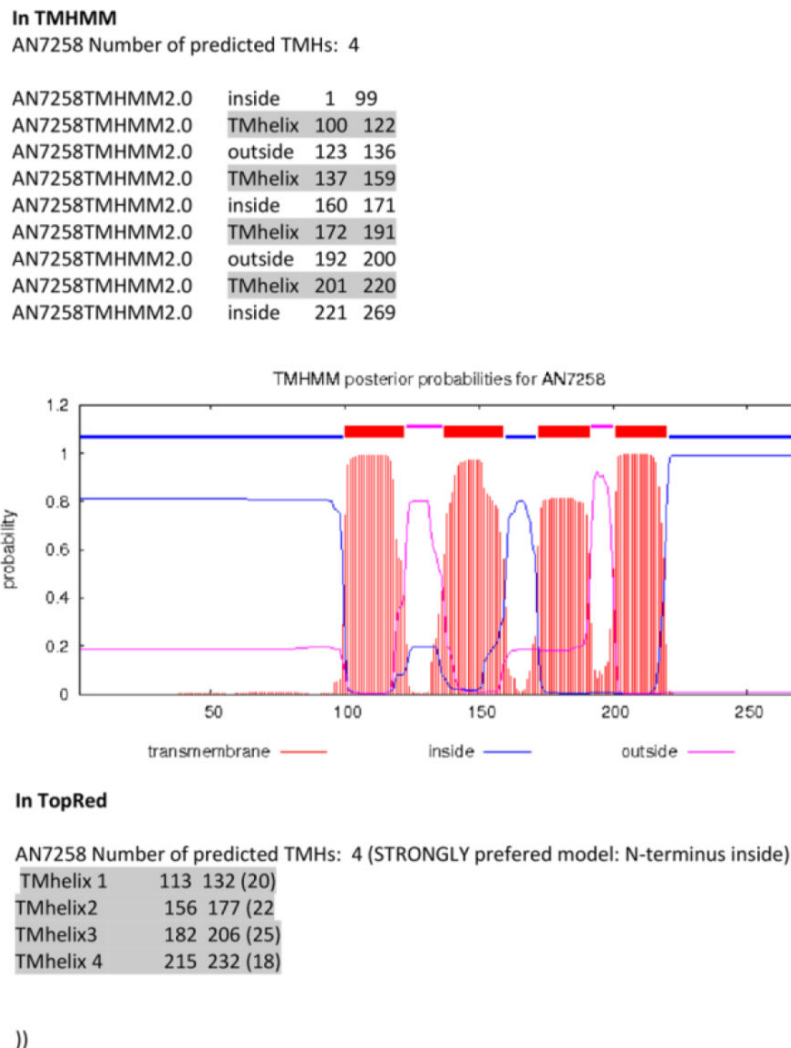


**Figure 3.3** Topology prediction of WscA using TMHMM (<http://www.cbs.dtu.dk/services/TMHMM/>) or TopRed ([https://embnet.vital-it.ch/software/TMPRED\\_form.html](https://embnet.vital-it.ch/software/TMPRED_form.html)) programs.

The WscA protein in *A. nidulans* is clearly a true orthologue of the very similar *A. fumigatus* and *A. oryzae* proteins (83.3% and 79.5% identical respectively), which have been functionally characterized and shown to be involved in Woronin body functioning [61, 62]. Woronin bodies are considered to be specialized peroxisomes, that form through the incorporation of a self-assembled matrix protein, called HexA in *Aspergillus* species or Hex-1 in *Neurospora crassa* [38, 40, 62]. These organelles function to seal the septal pore in response to hyphal wounding or stress, or dynamically during normal growth [38, 39]. Woronin body biogenesis takes place in the growing apex of hyphae, apparently as a consequence of apically-biased hexA gene expression [64].

Interestingly, when compared to their orthologue in *Neurospora crassa*, named WSC, the *Aspergillus* WscA proteins have an important sequence difference (64% identity in the transmembrane regions), which is noticed mainly on the C-terminal of the proteins. The WSC orthologue in *N. crassa* contains an extended C-terminal His-rich region (Figure 3.4) that has been proposed to play an important role in Woronin body function. It has been shown that WSC binds via its C-terminal to the tether protein LAH-1, which binds to the cell cortex [40]. However, *Aspergillus* WscA proteins are shorter and lack the C-terminal domain that mediates this interaction. In most filamentous Ascomycetes, including *Aspergillus*, Woronin bodies are positioned directly at the septum and are not anchored at the lateral cell wall like *Neurospora*. The different C-terminal sequences between WSC and WscA may reflect the distinct molecules and molecular interaction that are used by the two clades for the tethering of Woronin bodies [65]. Although, the molecular mechanism on how WscA proteins interact with other molecules like HexA or LAH interact in order to seal the septal pores remains obscure.

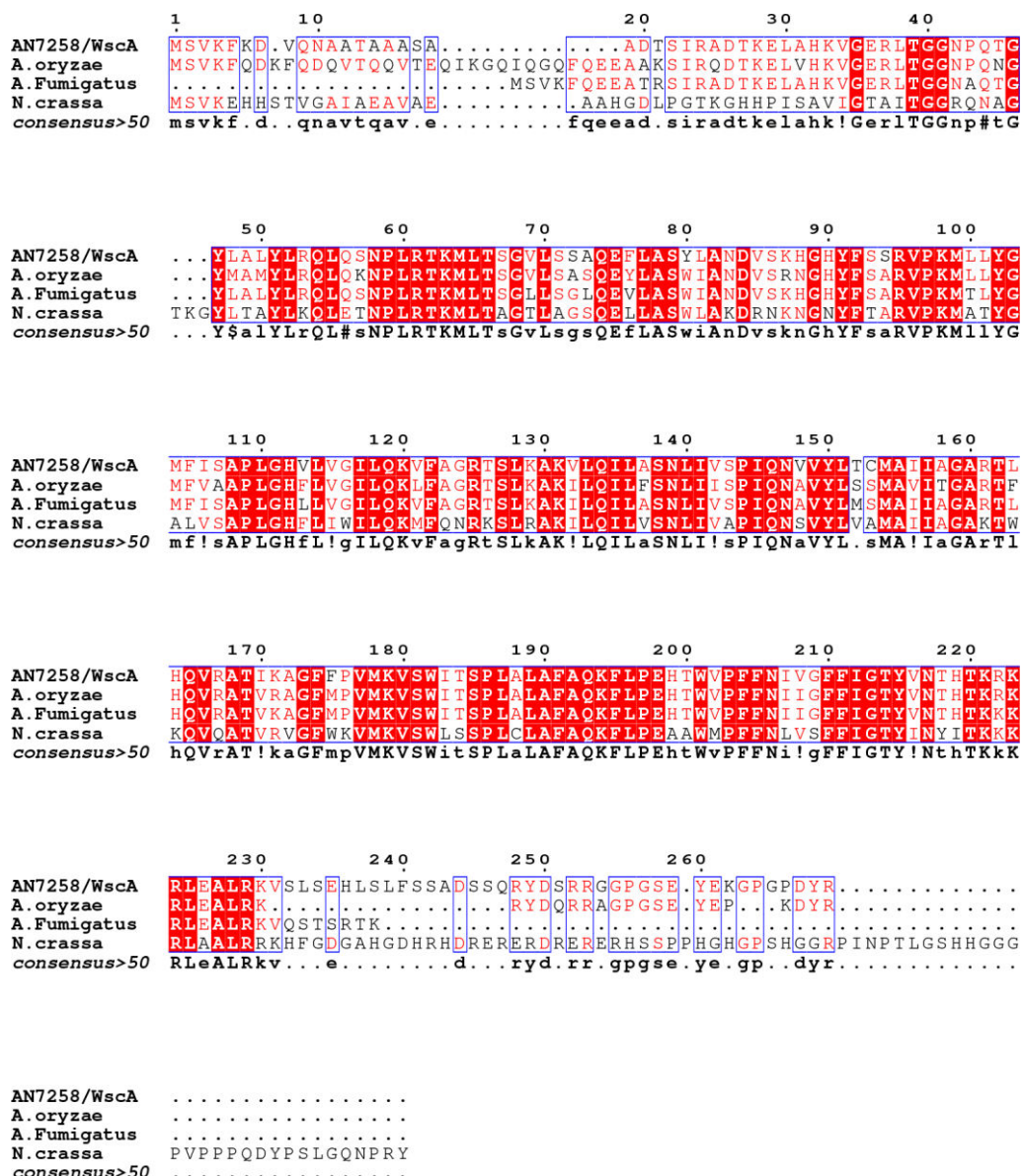


**Figure 3.4** Amino acid sequence alignment of WscA orthologues from selected fungi using <http://espript.ibcp.fr/ESPrIPT/cgi-bin/ESPrIPT.cgi>

As seen in Figure 3.2, true orthologues of WscA (48-92% sequence identity) seem to be present in most higher fungi (Dikarya). This is also supported by a high degree of synteny (<https://fungidb.org/fungidb/app/record/gene/AN7258>). Additionally,

*A. nidulans* has no close paralogue of WscA, as other similar proteins (i.e. AN0731, AN1247, AN3412, AN6626, and AN0731 and AN6626) have low sequence identity (< 28%) and are more closely related to the Mpv17 or Mpv17-like families. Plants and animals have distant homologues of fungal PMP22/Mpv17 proteins, sharing 24-30% identity, mostly in putative transmembrane regions. Transcriptomics of the *wscA* gene in *A. nidulans* suggested constitutive expression in media containing different N sources or under N starvation.

### 3.3 WscA is localized in peroxisomes

To formally show that WscA is a peroxisomal protein in *A. nidulans*, as shown in other *Aspergillus* species, we constructed strains expressing WscA tagged C-terminally with GFP or mRFP. From the *in silico* analysis, we couldn't predict a peroxisomal localization, as WscA is a membrane protein and there is no conserved mPTS for peroxisomal membrane proteins. The chimeric proteins proved functional, as evidenced from the nearly wild-type phenotype of the strains expressing WscA-GFP or WscA-mRFP, under all conditions tested (Figure 3.5).

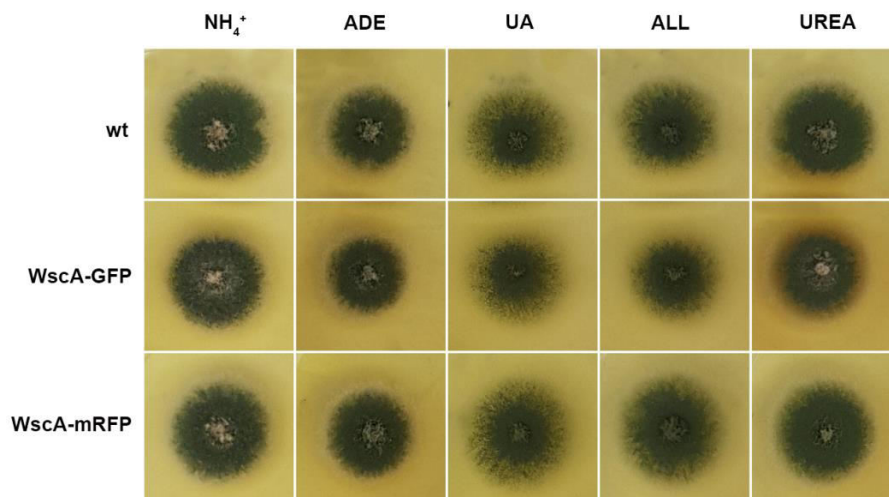


**Figure 3.5** Growth test confirming the functionality of WscA tagged C-terminally with GFP or mRFP on several nitrogen sources (3 days at 37°C). N sources shown are: 10 mM ammonium (NH<sub>4</sub><sup>+</sup>), 0.5 mM adenine (ADE), 0.5 mM uric acid (UA), 0.5 mM allantoin (ALL), 10 mM urea. In all N source tests, 1% glucose is used as a C source.

Most importantly, when these strains were examined by epifluorescence microscopy, the WscA-GFP or WscA-mRFP markers were both localized in cytoplasmic structures characteristic of peroxisomes. The evidence for peroxisomal localization was based not solely on the characteristic size, number and shape of *A. nidulans* peroxisomes, but also by the co-localization of WscA-mRFP with GFP-UaZ [Figure 3.6 (A)]. This was also confirmed by the co-localization of WscA-GFP with a peroxisome-targeted version of mRFP (mRFP-PTS1) as well as by the characteristic early endosome-driven motility of fungal peroxisomes. Despite the technical difficulty we faced trying to co-localize peroxisomal markers, due to their high motility, the level of co-localization detected between WscA-mRFP and GFP-UaZ was indicative of the high frequency the two proteins were found in close proximity [~65%, Figure 3.6 (B)]. In fact, this level of co-localization is certainly underestimated, as judged by the fact that even two markers that are unambiguously peroxisomal, such as GFP-UaZ and mRFP-PTS1, show a maximum of 80% apparent co-localization due to peroxisomal mobility [Figure 3.6 (B)]. Noticeably, however, the co-localized markers WscA and UaZ appeared as partially overlapping, suggesting that they represent a 'double organelle' with two distinct protein subdomains. A similar observation has been reported in *A. fumigatus* [71] for HexA (see 3.7 below)

and PTS1, characterizing these double organelles, as tandem structures. Importantly, however, the overall picture was that WscA despite being in all closed septal pores, it is also found in most other peroxisomes, found free in the cytoplasm [Figure 3.6 (A)], as observed also in *A. fumigatus* [62] but not in *N. crassa* [38]. This finding verifies previous observations made for the positioning of Woronin bodies [62, 83]. Besides the common purpose these organelles serve, two distinct patterns exist for their positioning: In the Sordaria clade, Woronin bodies are tethered to the cortical cell wall, while in other Pezizomycotina, represented by members of the genus *Aspergillus*, they are found anchored at the septal pores as well as distributed free all over the cytoplasm [62, 83].

The overall picture was that WscA is a major component of most, but not all peroxisomes, including however all peroxisomes that are localized on septal pores. In other words, WscA seems to be a component of Woronin bodies, as also shown previously in other filamentous ascomycetes. In agreement to most other Pezizomycotina, Woronin bodies are found anchored at septal pores as well as free in the cytoplasm [62].

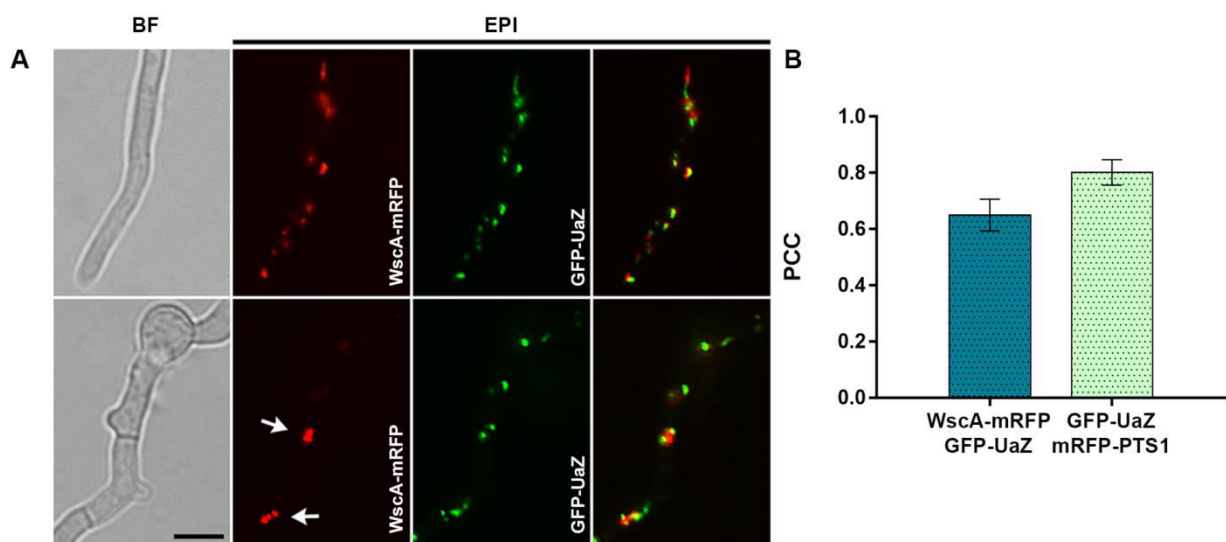


**Figure 3.6 (A)** Epifluorescence microscopy of germlings of strains co-expressing GFP-UaZ and WscA-mRFP. Both markers label small motile and larger immotile peroxisome-like structures. Arrows indicate peroxisomal structures that seal septal pores. **(B)** The apparent high co-localization of these molecular markers is confirmed and quantified at ~65% for WscA-mRFP with GFP-UaZ and at ~80% for GFP-UaZ with mRFP-PTS1 by calculating Pearson's Correlation Coefficient (PCC) for n=12 hyphae. P-value for both cases is  $p < 0.0001$ .

### 3.4 Growth defects of $\Delta wscA$ null mutant

Our next project was the inactivation of the *wscA* gene using standard reverse genetics methodology for *A. nidulans* [66]. The null mutant,  $\Delta wscA$ , proved viable and was subsequently analyzed by a series of growth tests. As we can see in Figure 3.7, the knock-out mutant had a distinct growth phenotype characterized by a reddish appearance, particularly evident in media containing uric acid, urea and to a lower degree  $\text{NO}_3^-$ , as sole nitrogen sources, in comparison to an isogenic wild-type control strain after 3 days at 37°C. Minor to none growth defects were detected in other N sources such as  $\text{NH}_4^+$ , proline and allantoin. That was also obvious in other C sources than glucose, where nearly no growth defect was observed.

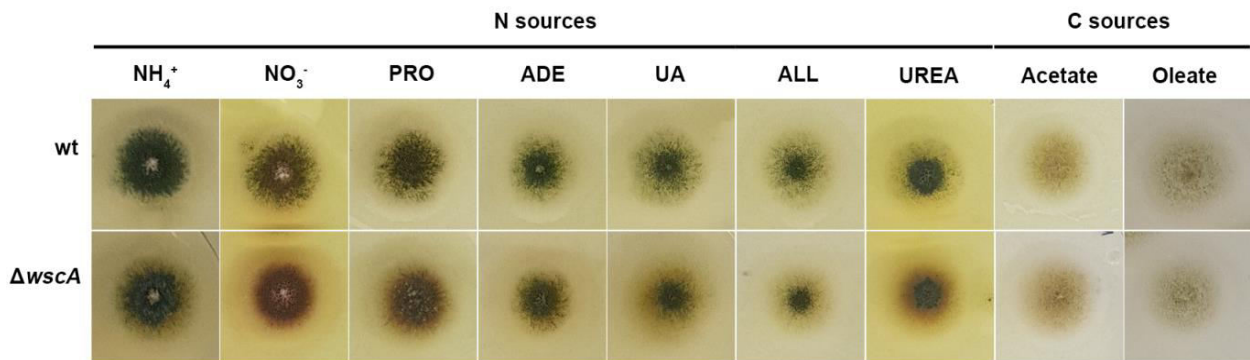


**Figure 3.7** Comparative growth rates and morphology of  $\Delta wscA$  and isogenic wild-type control on various N or C sources after 3 days at 37°C at pH 6.8. N sources shown are: 10 mM ammonium (NH<sub>4</sub><sup>+</sup>), 10 mM sodium nitrate (NO<sub>3</sub><sup>-</sup>), 10 mM L-proline (PRO), 0.5 mM adenine (ADE), 0.5 mM uric acid (UA), 0.5 mM allantoin (ALL), 10 mM urea. In all N source tests, 1% glucose is used as a C source. Other C sources shown, in the presence of NH<sub>4</sub><sup>+</sup> as an N source, are 2% acetate or 2% oleate. Notice the reddish colony coloration, particularly evident, on uric acid or urea, but also visible on NO<sub>3</sub><sup>-</sup> and PRO media.

However, after prolonged growth at the same conditions (7 days at 37°C), the characteristic reddish appearance of  $\Delta wscA$  became even more evident not only on urea and uric acid, but also on adenine and allantoin (Figure 3.8). Apparently, a reduction in the diameter of colonies (i.e. reduced rate of vegetative growth) and in conidiospore production was also observed for the  $\Delta wscA$  mutant.

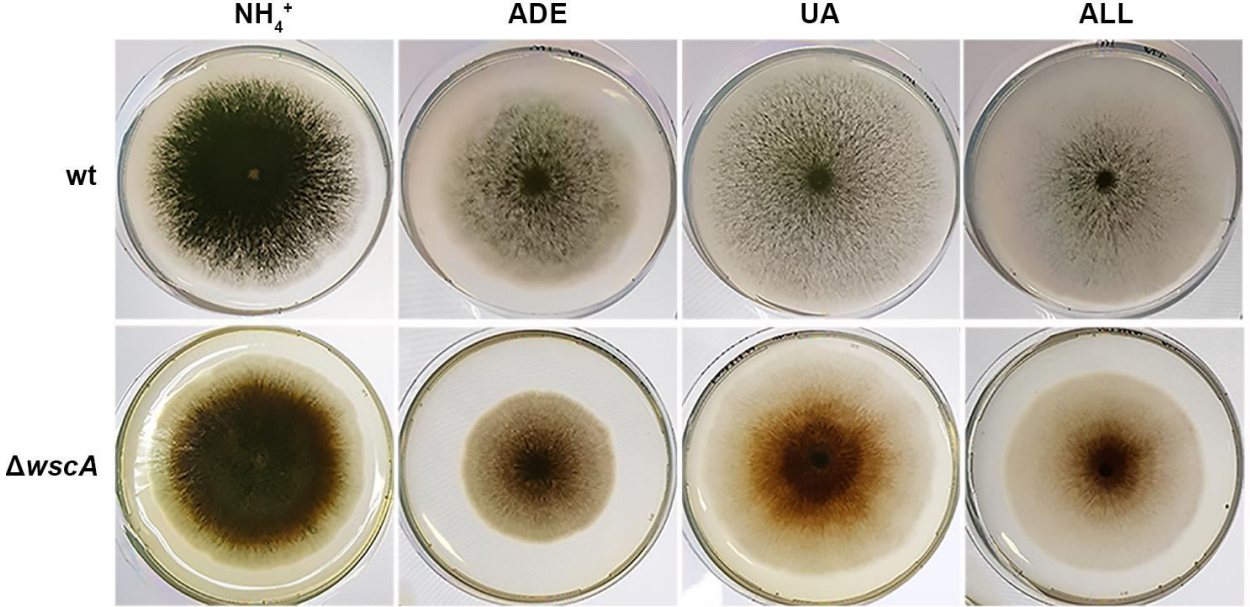


**Figure 3.8** Comparative growth rates and morphology of  $\Delta wscA$  and wildtype control after prolonged growth (8 days at 37°C at pH 6.8). The picture shows single colonies growing on an entire petri dish. Notice the reduced colony diameter  $\Delta wscA$  mostly evident on ADE and ALL.

Concerning the pH of the medium [Figure 3.9 (A)] or the temperature of growth [Figure 3.9 (B)], we did not detect any particular effect on the phenotype of  $\Delta wscA$ . A minor defect of  $\Delta wscA$  could be attributed to the N source used (NO<sub>3</sub><sup>-</sup>), as stated previously (Figure 3.7)

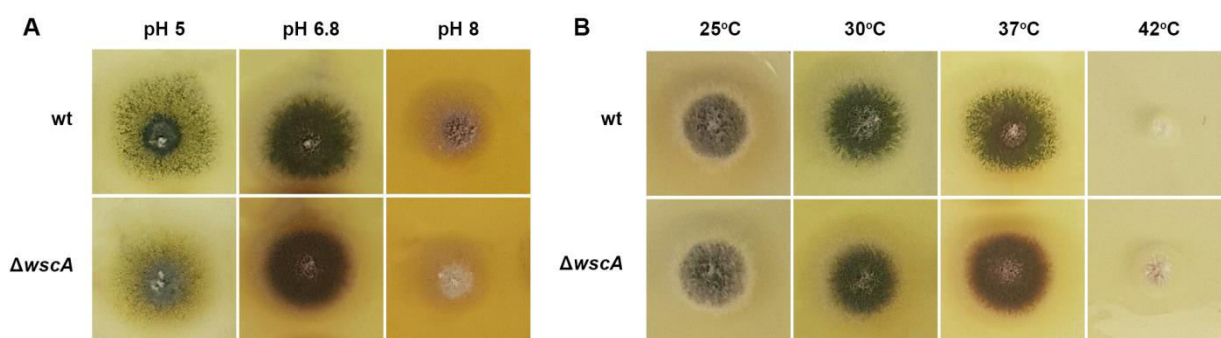


**Figure 3.9** Comparative growth rates and morphology of  $\Delta wscA$  and isogenic wild-type control on **(A)** media with different pH values (3 days at 37°C). N source: 10 mM sodium nitrate ( $\text{NO}_3^-$ ) **(B)** different temperatures ranging from 25 to 42°C for 3 days at 37°C. N source: 10 mM sodium nitrate ( $\text{NO}_3^-$ ).

Growth phenotypes related to a null *wscA* mutant have not been reported in great detail in other fungi. In *A. fumigatus*, under standard growth conditions, the null mutant had a normal growth and colony morphology, but showed an increased sensitivity to Calcofluor white, which interferes with cell wall assembly by binding to chitin [62]. In *N. crassa*, the *wsc* mutant colonies presented initially wild-type growth and morphology. However, with age, they began to present a poorly organized and irregular growth front [38]. To our knowledge, growth on purines for this mutant has not been studied in other Pezizomycotina.

The above growth tests suggest that *WscA* is not the major transporter of purines since its genetic deletion does not lead to inability for purine utilization, in spite of the correlated gene loss of *wscA* with genes involved in uric acid catabolism, which lead to the idea that *WscA* might act as a channel for transport of purines in and/or out of the peroxisome. This however, does not exclude the possibility that *WscA* is a promiscuous channel that facilitates the transport of purines along with other small solute across the peroxisomal membrane barrier, as reported for PMP22 channels in mammals [44].

Afterwards, we tested the phenotype of the  $\Delta wscA$  mutant under conditions of oxidative stress, in order to spot any effect on the peroxisomal function.  $\Delta wscA$  is significantly more sensitive, compared to an isogenic wild type strain, to  $\text{H}_2\text{O}_2$ , paraquat, Congo Red (CR), but not to Methylene Blue (MB) or Cd, the latter being much milder stress agents (Figure 3.10).

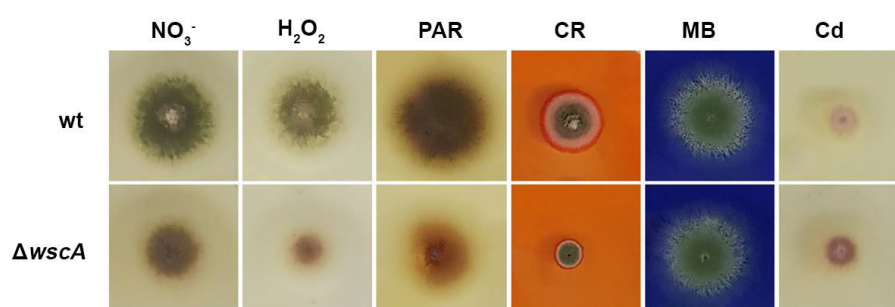


**Figure 3.10** Comparative resistance/sensitivity of  $\Delta wscA$  and wild-type control after 3 days at 37°C on media (10 mM  $\text{NO}_3^-$  and 1% glucose) containing known oxidative agents: 2 mM  $\text{H}_2\text{O}_2$ , 0.5 mM Paraquat (PAR), 50  $\mu\text{M}$  Congo Red (CR), 0.02 mM Methylene Blue (MB) and 0.02mM  $\text{CdCl}_2$  (Cd). Notice that  $\Delta wscA$  proved hypersensitive to most of these agents.

To gain a further insight into the role of *WscA* in stress response we constructed, by standard genetic crossing, double null mutants carrying  $\Delta wscA$  together with  $\Delta aloA$  ( $\Delta AN0836$ ),  $\Delta AN5660$  or  $\Delta AN4674$ . The gene *aloA* encodes the enzyme D-Arabinono-1,4-lactone oxidase, that catalyses the final step in the biosynthesis of D-erythroascorbic acid, which is an important antioxidant molecule in fungi [63]. This gene

however, remains uncharacterized in *A. nidulans*. The products of *AN5660* and *AN4674* are cell surface stress sensors involved in the cell wall integrity (CWI) signaling pathway under hypo-osmotic and acidic pH conditions in *A. nidulans* [50]. The  $\Delta AN5660$  strain is characterized by reduced colony and conidia formation and a high frequency of swollen hyphae under hypo-osmotic conditions [50]. A similar inhibition is described for the  $\Delta AN4674$  disruptant strain, but to a lesser extent. In addition, the double *AN5660* and *AN4674* disruptant ( $\Delta AN5660 \Delta AN4674$ ) strain is viable, but its growth is inhibited to a greater degree, indicating that the functions of the products of these genes are redundant [50]. At this point, to avoid any confusion, we must point out (noted also in Materials and Methods), that *AN5660* is annotated as *wscA*, standing for wall stress sensor, while we describe our gene of interest as *WscA* (Woronin sorting complex), in respect to its orthologue in *A. fumigatus*.

These observations are verified in our work, as  $\Delta AN5660$  shows reduced colony growth and reduction of conidiospore production, whereas  $\Delta AN4674$  exhibits a moderate mutant phenotype, compared to a wild type control strain (Figure 3.11). The double mutant seems even more sensitive to all conditions tested, as described also by Futagami et al. [50]. Concerning  $\Delta aloA$ , a minor deficiency is observed, especially in  $H_2O_2$ .

When it comes to the double mutants, lacking our gene of interest, *wscA*, along with the other genes involved in stress tolerance response, a stronger mutant phenotype than the corresponding single mutants in most to the imposed stress conditions is apparent in Figure 3.11.

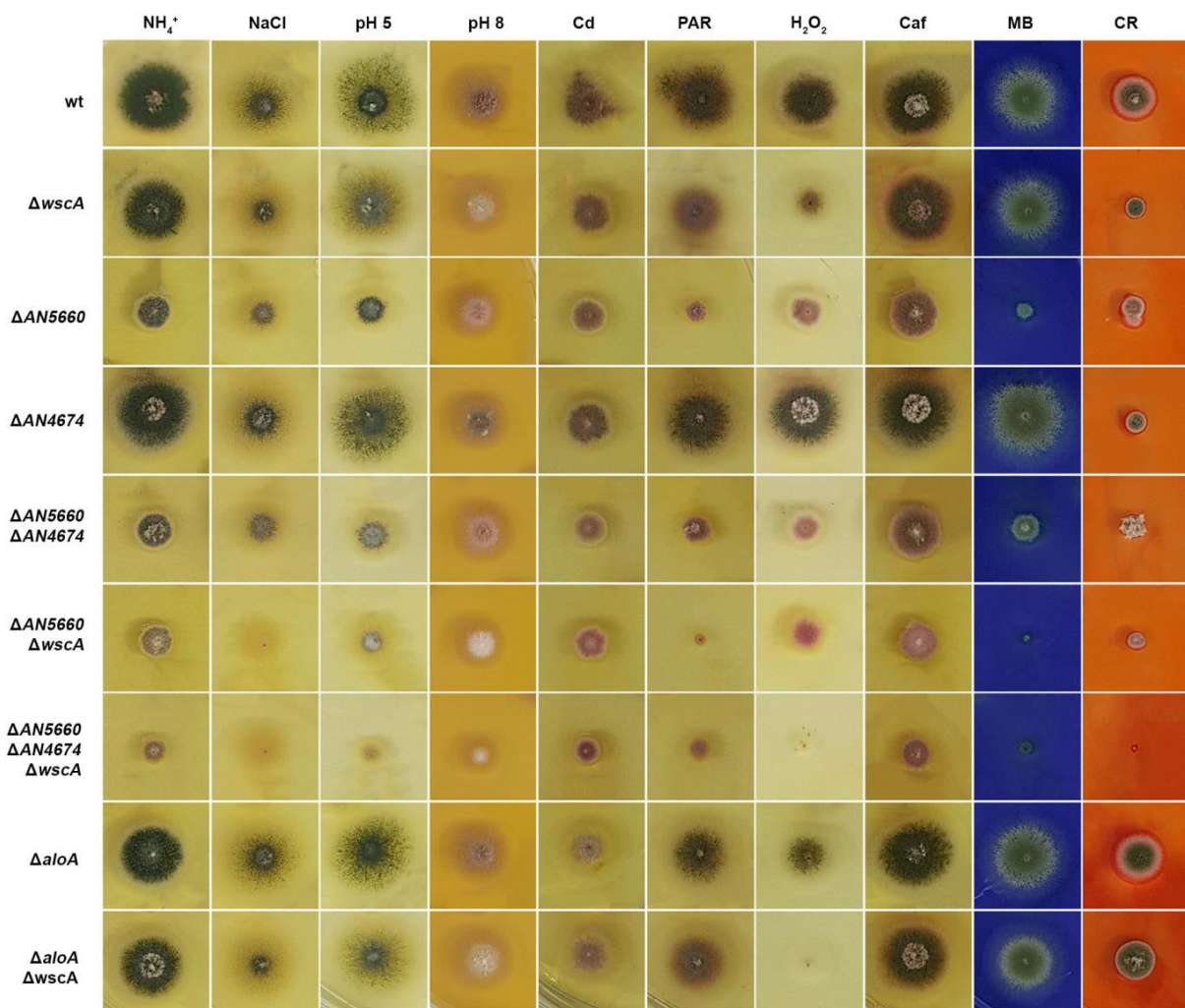


**Figure 3.11** Synthetic growth phenotypes of  $\Delta wscA$  genetically combined with other null mutants ( $\Delta AN5660$ ,  $\Delta AN4674$ ,  $\Delta aloA$ ) related to oxidative or stress sensitivity. AN5660 and AN4674 are PM stress sensors involved in hypo-osmotic and acidic pH stress tolerance whereas AloA is D-Arabinono-1,4-lactone oxidase, catalyzing the production of D-erythroascorbic acid, an important antioxidant molecule in fungi. In all cases, 1% glucose was used as a C source, while 10 mM  $NO_3^-$  were used as N source, unless otherwise noted. Oxidizing agents and cell wall stressors were used at final concentrations: Paraquat 0.5 mM,  $H_2O_2$  2 mM,  $CdCl_2$  0.02 mM, Methylene Blue (MB) 50  $\mu$ M, Congo Red (CR) 50  $\mu$ g/ml, Caffeine 7 mM. For hyperosmotic conditions NaCl 500 mM was used. All strains were incubated for 3 days at 37°C.

Taken all together, we came to the conclusion that WscA is redundant for purine utilization, but its loss affects negatively *A. nidulans* sensitivity to several stress factors.

### 3.5 Genetic interactions of *wscA* with mutants affected in uric acid catabolism

To further investigate the previously stated assumption, that WscA is not the major transporter of purines but may act as a channel for various small metabolites, including purines, we tested whether deletion of WscA might have an impact on the severe cytotoxicity purines have on *A. nidulans* mutant strains that are blocked in uric acid catabolism, due to deletion of genes encoding uricase (UaZ) or HIU hydrolase (UaX) [16]. The reason of cytotoxicity due to uric acid or HIU accumulation remains unknown, although it seems possible that as the relative enzymatic activities missing in *uaZ* or *uaX* mutants are peroxisomal, toxic uric acid or HIU accumulation takes place in this organelle. If so, in case WscA is a channel facilitating peroxisomal uric acid or HIU accumulation, then its deletion might partially alleviate or enhance purine cytotoxicity.

To test this hypothesis, we constructed a strain doubly inactivated for *wscA* and *uaZ*, ( $\Delta wscA \Delta uaZ$ ). This double mutant (Figure 3.12) was equally or slightly more sensitive to uric acid as the single  $\Delta uaZ$  mutant. This suggests that either uric toxicity is not related to its transport in the peroxisome, or that WscA is not the major transporter of uric acid and other purines in peroxisomes. However, the two explanations are not mutually exclusive.

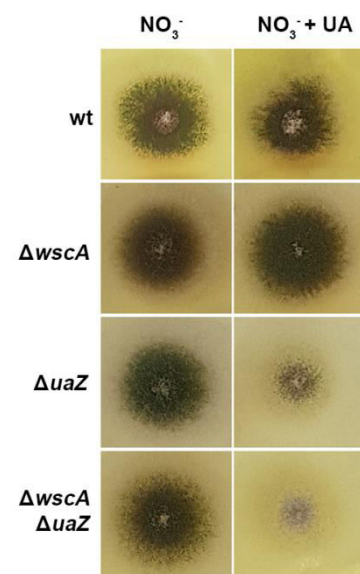


**Figure 3.12** Growth test showing that the double  $\Delta wscA \Delta uaZ$  mutant is slightly more sensitive to uric acid toxicity, compared to an isogenic single  $\Delta uaZ$  mutant (3 days at 37°C). *uaZ* is the gene encoding UOX in *A. nidulans*. Knock-out of *uaZ* is known to lead to UA accumulation and severe cytotoxicity

Given the inconclusive outcome of the above growth test, we tried next to understand better the basis of purine toxicity in strains lacking UaZ or UaX. To do so, we asked whether genetically-manipulated mislocalization of peroxisomal uric acid oxidase (UaZ) or HIU hydrolase (UaX) to the cytoplasm might lead to mutant phenotypes mimicking or resembling the total genetic absence of these enzymes.

To drive the localization of these enzymes to the cytoplasm, we mutated or deleted their peroxisomal targeting sites. For UaZ, a C-terminally tagged version with GFP, led to a cytosolic localization of the enzyme, due to the fact that the epitope masked the targeting signal. For UaX, which harbors a PTS2 N-terminal sequence, a N-terminal fusion with GFP upstream of PTS2 did not affect peroxisomal localization, while loss of its targeting signal resulted in its cytosolic diffusion. The successful construction and expression of the GFP-tagged versions of these two enzymes in the cytoplasm of *A. nidulans* is evident in Figure 3.13.

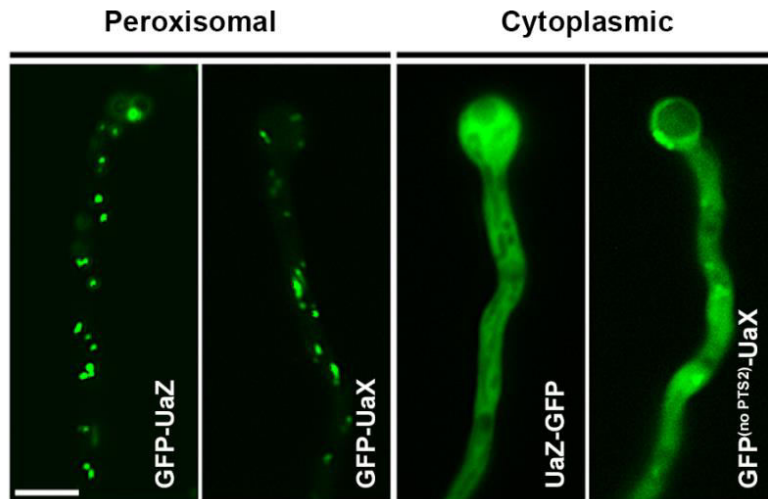


**Figure 3.13** Epifluorescence microscopy of germlings of strains expressing UaZ or UaX tagged either N-terminally (GFP-UaZ, GFP-UaX, GFP<sup>(no PTS2)</sup>-UaX) or C-terminally (UaZ-GFP). Notice that the N-terminally tagged versions of UaZ and UaX are localized in cytoplasmic structures that correspond to peroxisomes, confirming previous observations [16]. In contrast, a C-tagged version of UaZ and a N-tagged version of UaX, along with a PTS2 deletion, show a cytoplasmic diffused fluorescent signal. The bar indicates 5  $\mu$ m.

Surprisingly, both strains grew as wild-type strains on all purines, not only after growth for 3 days at 37°C (Figure 3.14), but also after prolonged growth on the same conditions (Figure 3.15). This means that the cytoplasmic expression of these two key peroxisomal enzymes for purine catabolism did not lead to any detectable phenotype, as strains expressing the cytoplasmic UaZ and UaX grow just like the isogenic wild-type control strain.

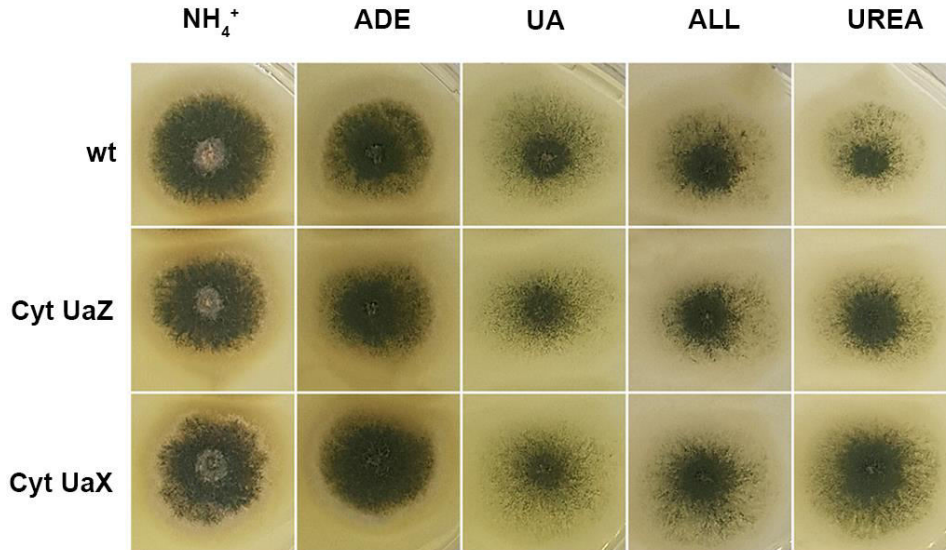


**Figure 3.14** Comparative growth tests of a standard wild-type control strain with isogenic strains expressing the cytoplasmic versions of UaZ or UaX, named Cyt UaZ and Cyt UaX, respectively (3 days at 37°C). N sources shown are: 10 mM ammonium (NH<sub>4</sub><sup>+</sup>), 0.5 mM adenine (ADE), 0.5 mM uric acid (UA), 0.5 mM allantoin (ALL), 10 mM urea. In all N source tests, 1% glucose is used as a C source.

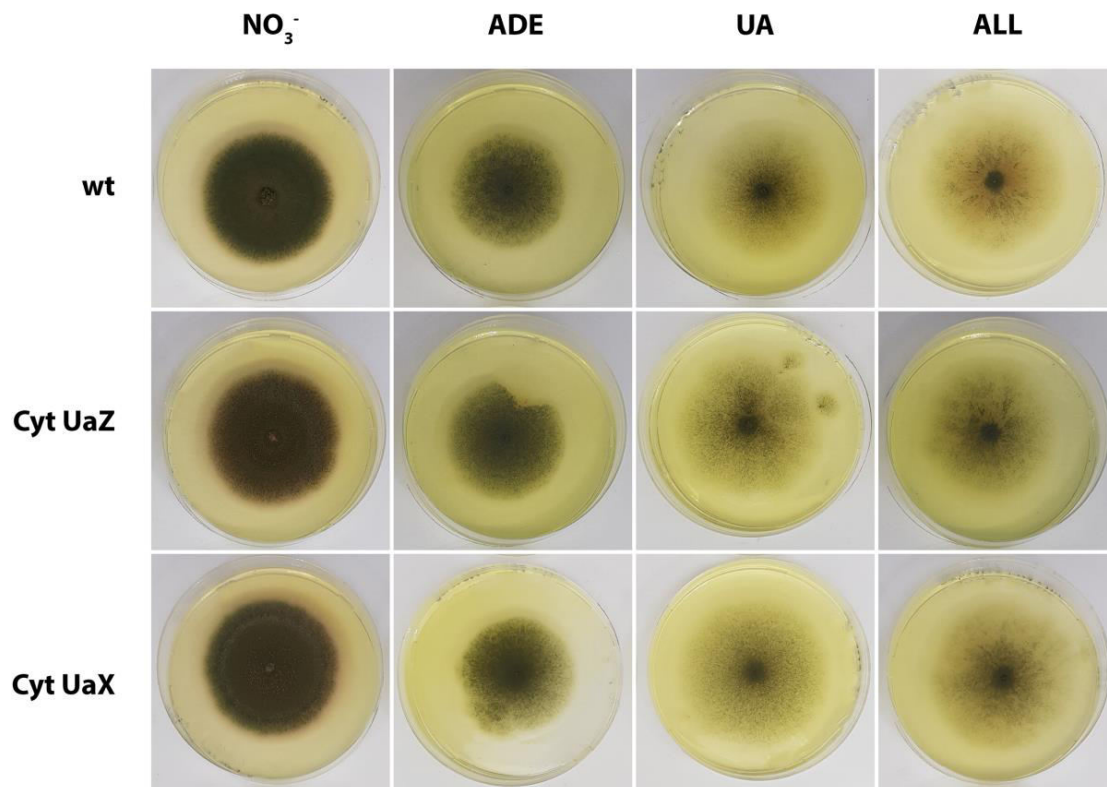


**Figure 3.15** Prolonged growth (7 days at 37°C) of a standard wild-type control strain with isogenic strains expressing the cytoplasmic versions of UaZ or UaX, named Cyt UaZ and Cyt UaZ. Media are prepared as shown in Figure 3.14.

This finding is somehow paradoxical as these enzymes and their orthologues have a highly conserved peroxisomal localization in fungi and other eukaryotes with few exceptions, as we discuss in more detail later. In addition, these results reveal also that uric acid or HIU can be catabolized in the cytoplasm of *A. nidulans* with no apparent cellular defect. This might justify why none peroxisomal purine transporter has ever been identified genetically.

We subsequently thought of testing whether cytoplasmically expressed UaZ could somehow have an effect on the mutant phenotype of  $\Delta wscA$  mutant, specifically on uric acid growth media. The rationale behind this idea was based on the hypothesis that the prominent reddish phenotype of  $\Delta wscA$  mutant on uric acid might be related to a higher demand for peroxisome-specific metabolism. Apparently, the characteristic coloration of colonies of  $\Delta wscA$  after growth for 3 days at 37°C was reduced when uric acid was cytoplasmically oxidized to HIU by cytoplasmic UaZ (Figure 3.16). This phenotype indicates that the need for WscA activity might indeed be higher when uric acid is catabolized in peroxisomes rather than in cytoplasm.

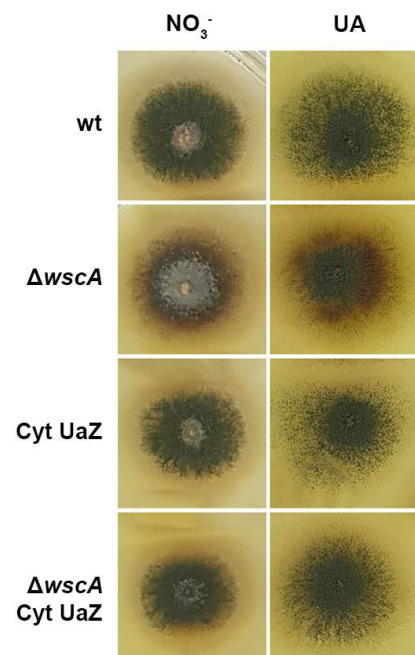


**Figure 3.16** Apparent synthetic effect of genetic absence of interaction of WscA ( $\Delta wscA$ ) with cytoplasmically expressed UaZ. Notice the suppression of reddish coloration in the double mutant  $\text{cyt-UaZ } \Delta wscA$  compared to the single mutant  $\Delta wscA$  (3 days at 37°C). N sources used were: 10 mM sodium nitrate ( $\text{NO}_3^-$ ) and 0.5 mM uric acid (UA).

However, when the same growth test was repeated for a longer period of time (7 days) at the same conditions, the characteristic reddish appearance became apparent also in the  $\Delta wscA$  mutant expressing cytoplasmic UaZ (Figure 3.17).

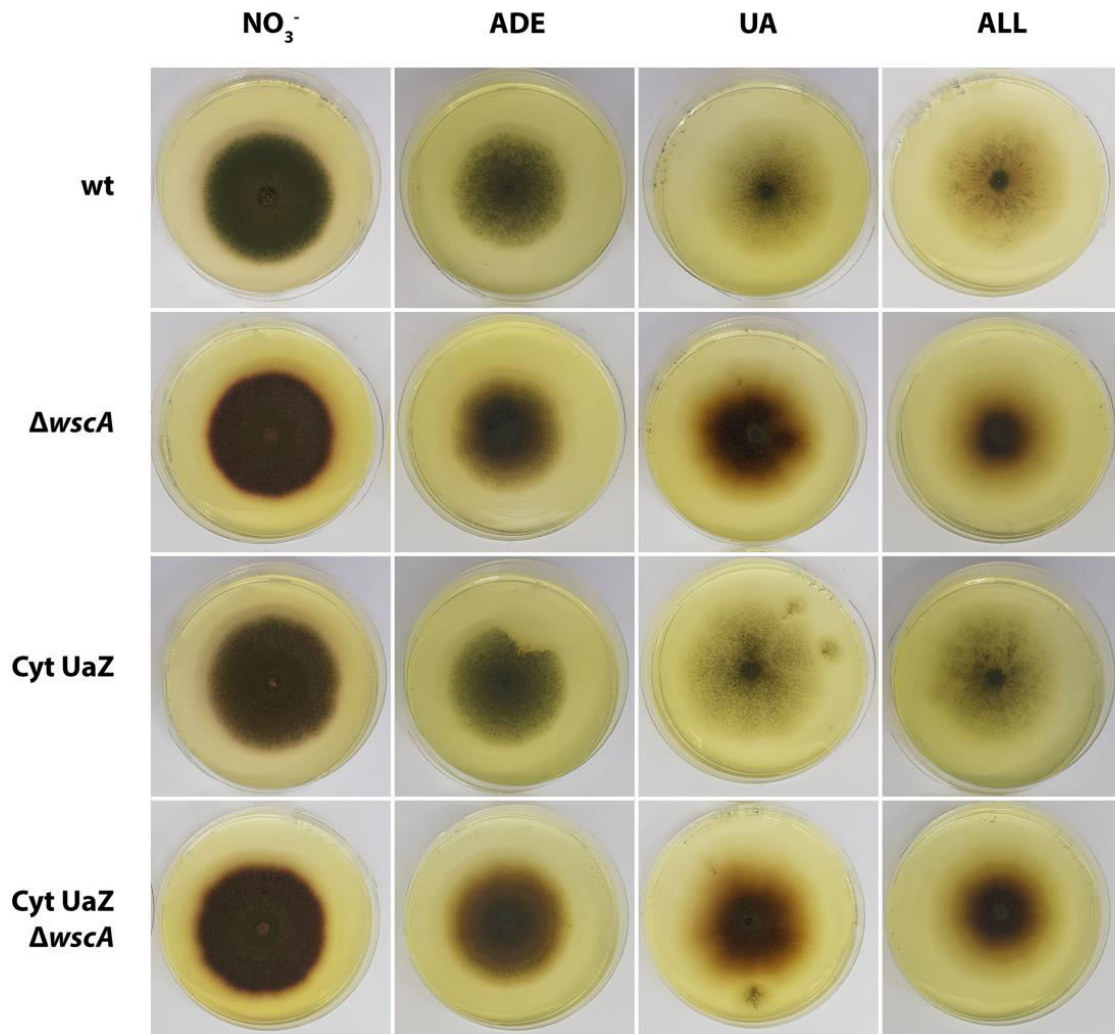


**Figure 3.17** Growth phenotypes of strains expressing cytoplasmic UaZ in the  $\Delta wscA$  background after prolonged 7-day growth at 37°C on purine related metabolites as N sources. Notice that the reddish appearance due to the  $\Delta wscA$  allele becomes apparent also the in strain expressing cytoplasmically UaZ. N sources used were: 10 mM sodium nitrate ( $\text{NO}_3^-$ ) and 0.5 mM uric acid (UA).

### 3.6 WscA expression does not depend on transcriptional regulation of purine catabolism

The fact that WscA was found to be redundant for uric acid or purine utilization and is probably involved in septal pore sealing, did not formally exclude that it might have a cryptic role, as a channel, in metabolite facilitated transport across the peroxisomal membrane. Our final effort in the investigation of the possible involvement of WscA in peroxisomal transport of uric acid or other purine-metabolites was based on the idea that its expression may be affected by conditions or mutations regulating purine catabolism.

Regulation of purine related transporters and enzymes is well established in *A. nidulans*. The transcription of all genes encoding plasma membranes transporters and enzymes of the purine catabolic pathway are known to be induced in the presence of uric acid via the action of the pathway specific transcription factor UaY [53]. Their repression on the other hand, occurs in the presence of preferred N sources, such as



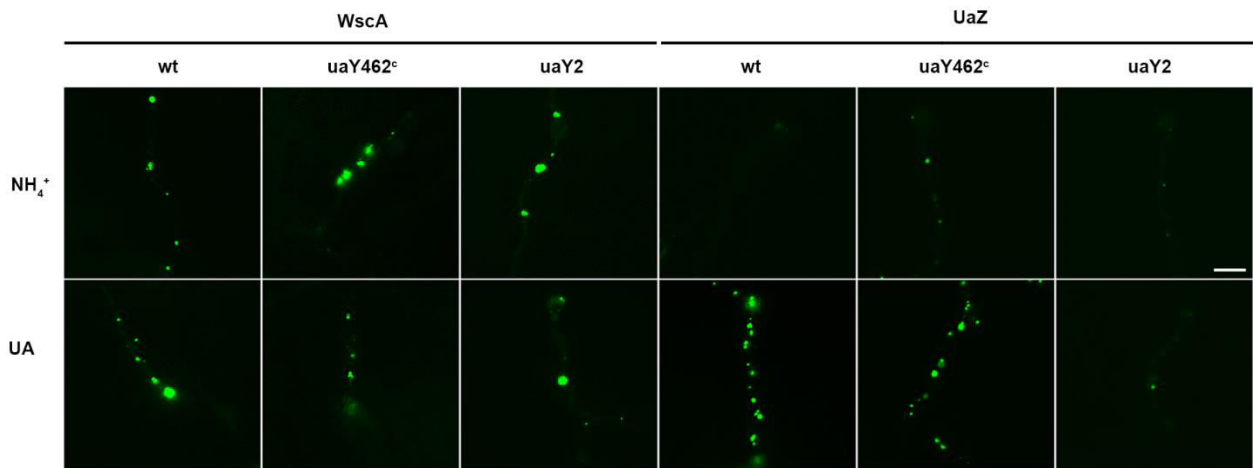


**Figure 3.20** Expression and subcellular localization of WscA and UaZ, followed by epifluorescence microscopy, in wild-type and mutant backgrounds *uaY462c* and *uaY2* leading to constitutive induction or non-induction of purine catabolic genes, respectively [51, 52], under repressing ( $\text{NH}_4^+$ ) or inducing (UA) conditions. Notice the WscA expression and subcellular localization, unlike UaZ, is practically the same in all genetic backgrounds and under all conditions tested.

Quantification of peroxisomal surface (Figure 3.21), which is indicative of *wscA* or *uaZ* expression under each genetic background, confirms our previous observations, based on the epifluorescence microscopy images (Figure 3.20). It is clear that *wscA* expression is practically the same, irrespective of the presence of an active or inactive UaY transcription factor. On the contrary, *uaZ* cannot be expressed without UaY, even under inducing conditions (uric acid).

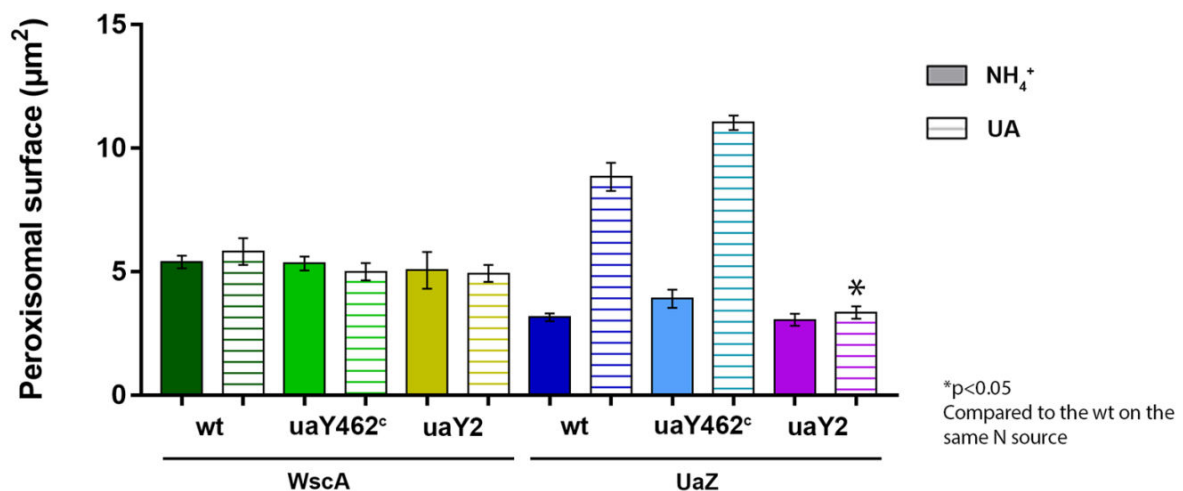


**Figure 3.21.** Quantification of peroxisomal surface in each strain under repressing ( $\text{NH}_4^+$ ) or inducing (UA) conditions confirms the constitutive purine catabolism-independent expression of WscA.

These findings further support that WscA is not specific for purine catabolism. Although, we still cannot exclude the possibility that WscA might be implicated, as a promiscuous channel, in facilitating the transport of uric acid and any other small metabolites across the peroxisomal membrane.

### 3.7 WscA is essential for peroxisome localization on septal pores

The observation of WscA localization frequently on septal pores, combined with the current bibliography about its orthologues in other filamentous ascomycetes, triggered us to examine its function in Woronin bodies. Its function in Pezizomycotina seems to be directly related to Woronin body biogenesis and localization [38, 39, 62], while its

relation to metabolite transport across the peroxisomal membrane has been reported only for higher eukaryotes [44].

In order to examine the function and/or physical association of WscA with HexA, which is the core matrix protein in Woronin bodies, we performed a series of experiments, starting with the investigation of the possible co-localization of WscA-mRFP with GFP-HexA. The fact that the strain expressing GFP-HexA proved only partially functional, as judged by a moderate growth defect on several N sources when compared to an isogenic control strain (Figure 3.22), did not have any effect on HexA subcellular localization. The GFP-HexA marker showed a typical peroxisomal localization, characterized by an abundance in apical compartments, that is already noted in *N. crassa*, due to the apically-biased hexA gene expression [64] and a high endosome-driven motility of smaller peroxisomes [84]. Thus GFP-HexA could be certainly used for colocalization studies with WscA-mRFP.

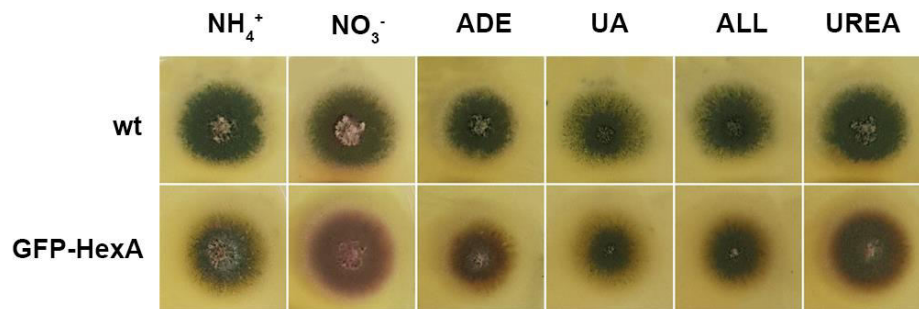


**Figure 3.22** Growth tests (3 days at 37°C) showing that GFP-HexA is not fully functional, as judged by the reddish appearance of relative strains and the similarity to the phenotype of a  $\Delta$ hexA mutant, shown in Figure 3.24. N sources shown are: 10 mM ammonium (NH<sub>4</sub><sup>+</sup>), 10 mM sodium nitrate (NO<sub>3</sub><sup>-</sup>), 0.5 mM adenine (ADE), 0.5 mM uric acid (UA), 0.5 mM allantoin (ALL), 10 mM urea. 1% glucose is used as a C source.

Figure 3.23 shows that HexA and WscA show a very high-colocalization, close to 75%, which is practically 100% on septal pores. Taking into consideration peroxisomal motility, that underrates the actual co-localization between the two markers, we could say that WscA and HexA are found almost always together. We also found that GFP-HexA, similar to WscA-mRFP, co-localizes but at a lower degree (~60%) with other molecular markers of peroxisomes such as mRFP-PTS1 (not shown).

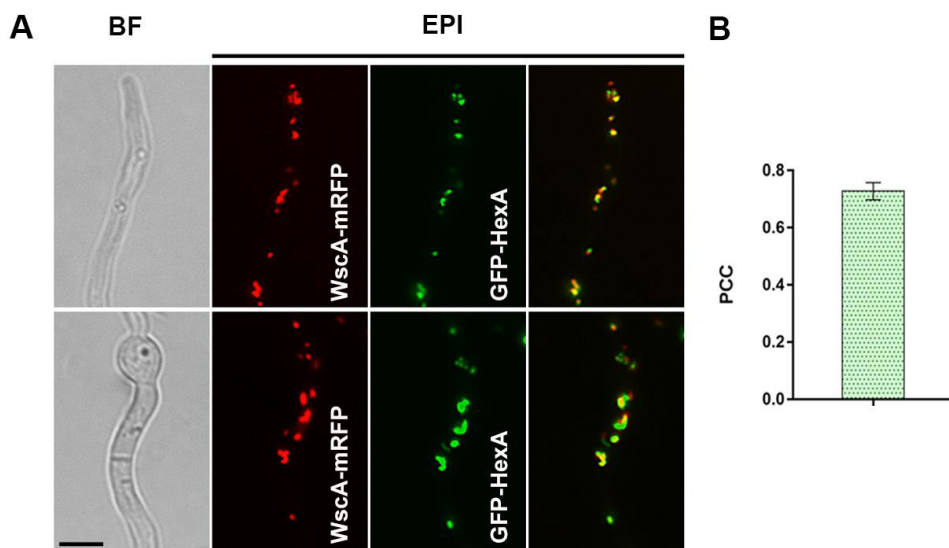


**Figure 3.23 (A)** Epifluorescence microscopy of germlings of strains of strains co-expressing WscA-mRFP and GFP-HexA. Notice the very high colocalization of the two peroxisomal markers. Bar = 5µm **(B)**

Quantification of co-localization between WscA-mRFP and GFP-HexA, by calculating Pearson's Correlation Coefficient (PCC) for n=12 hyphae. P-value is p<0.00014

The co-localization of GFP-HexA with RFP-PTS1 was also observed in *A. fumigatus* [71] with the latter being normally excluded from HexA assemblies in *N. crassa* [38].

Total deletion of *hexA* led to a distinct growth phenotype, mostly on purines and urea, characterized by reddish colony appearance (Figure 3.24). This phenotype resembles the one we saw on the  $\Delta wscA$  mutant, suggesting the absence of these proteins leads to the same cellular defect, apparently septal pore closure.

Phenotype of knock-out mutants of orthologues of *hexA* have been described also. In *N. crassa* the *hex1* null mutant was capable of producing aerial hyphae and conidia [69], but the growth was less vigorous than the wild-type and conidiation was poor [70], while in *A. fumigatus* the phenotype was less dramatic [71]. Under standard conditions, growth of the *hexA* mutant was comparable to that of the wild type, but in the presence of stressors, like Congo red or SDS, growth of the mutant was clearly impaired [71]. Concerning *A. oryzae*, the null mutant colony morphology on agar media was fluffy and more compact than the wild type, while a complete block in conidiation was detected [72]. Additionally, this strain was sensitive to Congo red and micafungin, but not to Calcofluor white [72].

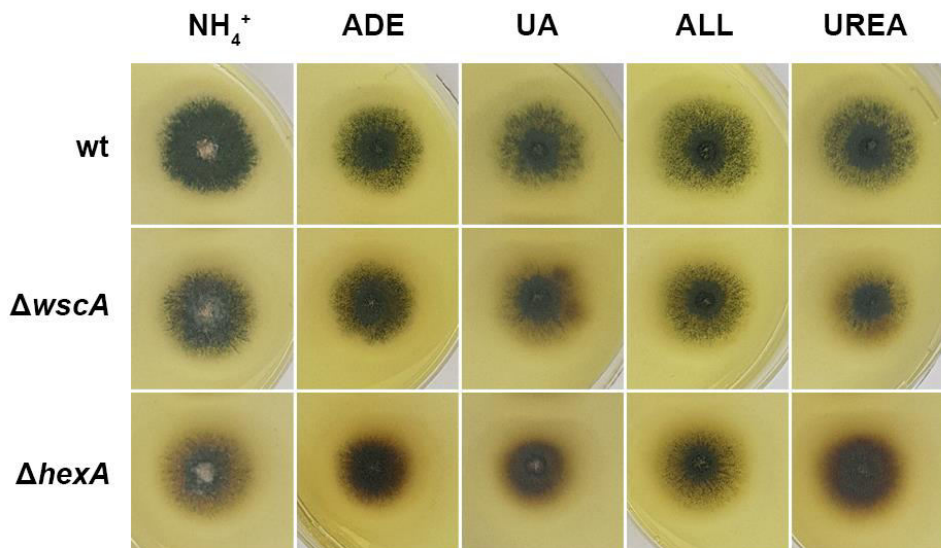


**Figure 3.24** Comparative growth phenotypes of the  $\Delta hexA$  and  $\Delta wscA$  mutants and isogenic wild-type control strains (3 days at 37°C). N sources shown are: 10 mM ammonium (NH<sub>4</sub><sup>+</sup>), 0.5 mM adenine (ADE), 0.5 mM uric acid (UA), 0.5 mM allantoin (ALL), 10 mM urea. As C source, 1% glucose is used.

We consequently tested the effect of WscA and/or HexA loss on septa sealing, as the two proteins are thought to be essential for Woronin bodies. For this purpose, we measured the percentage of closed septa in strains harboring GFP-UaZ as a peroxisomal marker under a wild-type background as well as  $\Delta wscA$  and/or  $\Delta hexA$ . To our surprise, deletion of *hexA* led to only a minor reduction in apparent septal pore plugging with peroxisomes, as ~ 50% septal pores were still plugged, as measured using GFP-UaZ as a peroxisomal marker, under conditions of its induction (Figure 3.25). In wounded hyphae of a  $\Delta hexA$  mutant in *A. fumigatus* closed septa were also found [71]. This contrasts the nearly absolute need of WscA for peroxisomal septal pore sealing, observed in the  $\Delta wscA$ , where > 90% septal pores are open [Figure 3.26 (A)]. Quantitative immunofluorescence analysis of  $\Delta wscA$  hyphae in *A. fumigatus* revealed also the importance of WscA in Woronin bodies positioning, as in the  $\Delta wscA$  mutant 93% of septa lacked HexA assemblies, whereas 87% of all septa in the parental strain were

associated with Woronin bodies [62]. In respect to our results, this quantification proves that regardless of using a typical WB marker (HexA) or a peroxisomal one (UaZ), septa sealing ranges at quite similar percentages in the wild-type strain as well as in the  $\Delta wscA$  mutant. Taken together, these findings show that WscA, but not HexA, is necessary for positioning of peroxisomes in septal pores. However, the actual localization pattern of Woronin bodies on the septal pores remains still a mystery, albeit the scenarios proposed in *N. crassa* [38] and *A. fumigatus* [65].

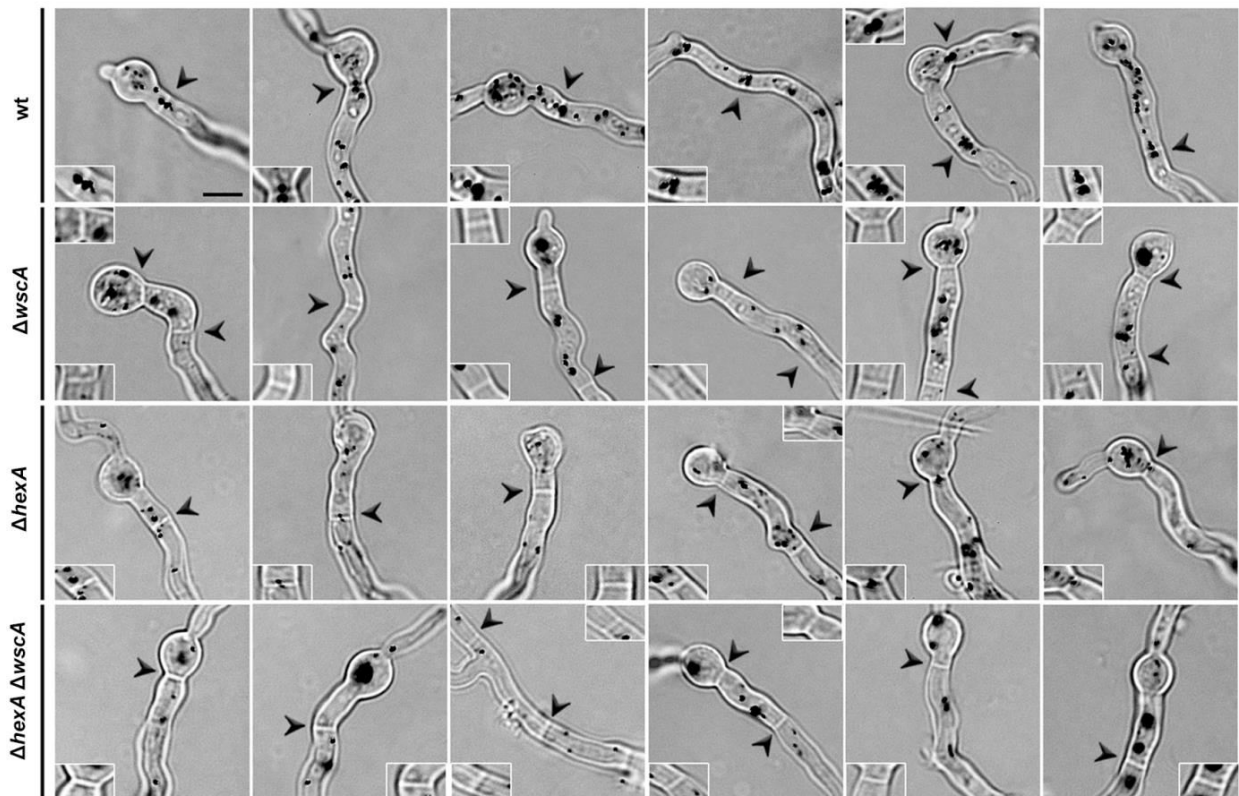


**Figure 3.25** Epifluorescence microscopy of germlings of strains expressing GFP-UaZ, under transcriptional inducing conditions, in isogenic strain deleted for *wscA* and/or *hexA*, compared to a control strain. Bar = 5 $\mu$ m

The double null mutant was totally incapable of sealing its septal pores [Figure 3.26 (A)]. Quantification of peroxisome number per 40  $\mu$ m of hypha length revealed that WscA has also an impact on peroxisome biogenesis, whereas HexA is not critical for this process [Figure 3.26 (B)].

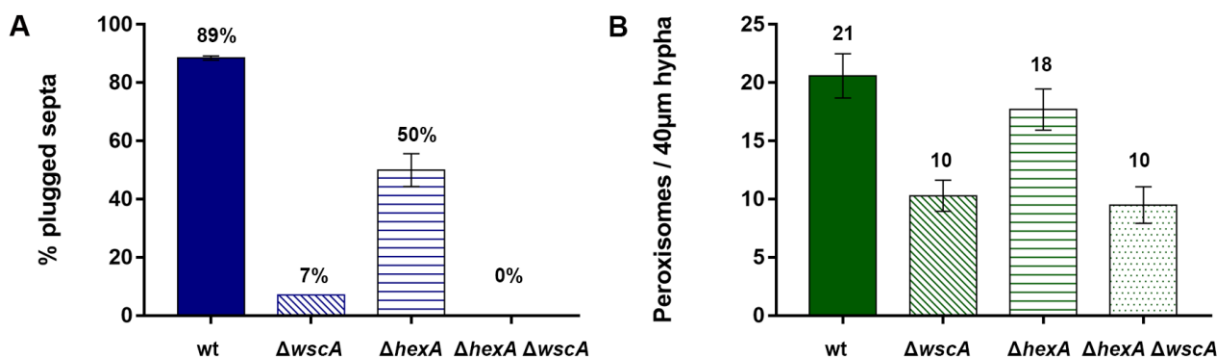


**Figure 3.26. (A)** Quantification of the number of apparently open versus closed septal pores shows that WscA, but not HexA, is essential for pore sealing by peroxisomes. Septa were counted as closed, if UaZ was found on both sides of the septal pore. The percentages of closed septa were determined based on the analysis of 120 septa for each strain. **(B)** Quantification of the total number of peroxisomes per 40  $\mu$ m of hypha length in relative strains. Notice the nearly 50% reduction in strains that *wscA* is deleted.

Since we came to the conclusion that WscA is essential for localization of Woronin bodies to the septal pores, we decided further to investigate which factors affect septa sealing under normal growth conditions, due to the fact that septa are mainly sealed in the wild-type strain. It is well established that septal pore sealing happens during hyphal wounding in order to prevent cytoplasmic loss, but the reasons behind this process throughout vegetative growth are not clarified.

Using WscA-mRFP as a marker, we tried to quantify the percentage of plugged septa under different environmental conditions. Taking into consideration the  $\Delta wscA$  reddish phenotype on several N sources we thought that this may relate on an inability of the strain to seal its septal pores. As shown in Figure 3.27, this is not true, as septal pores remain closed at ~ 90%, regardless of the N source.

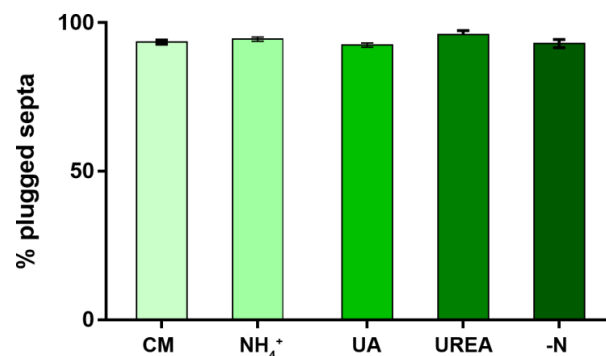


**Figure 3.27.** Quantification of the number of closed septal pores in a strain expressing WscA-mRFP under various N sources (CM, NH<sub>4</sub><sup>+</sup>, Uric acid, Urea and Nitrogen starvation). Septa were counted as closed, if WscA was found on both sides of the septal pore. The percentages of closed septa were determined based on the analysis of 150 septa for each strain.

A similar approach was followed in *A. oryzae*, where it was assessed whether septa in intact growing hyphae are open or closed [41]. In this case, only apical septa were examined under various environmental conditions, including 4°C or 45°C, hypo- or hypertonic conditions and pH 2.0 or 11.0. Laser dissection showed that none of the conditions significantly influenced the septal plugging incidence of the first (apical) septum [40], in accordance to our results.

Another factor, we thought that may affect septal pore sealing was cell cycle, due to the fact that all nuclei within a cellular compartment enter and exit mitosis synchronously, while nuclei in apical and subapical cells are arrested at different phases of the cell cycle. Open septal pores definitely pose a challenge on how nuclei in connected cells that share the same cytoplasm are independently regulated during growth [73]. Recent work on this subject demonstrated for the first time that septal pores are regulated to be opened during interphase, but closed during mitosis, providing a diffusion barrier between adjacent connected cells, that allows them to maintain their mitotic autonomy [73]. A model was proposed, where NIMA kinase seems to be critical for this process, remaining at septa during interphase, thus keeping them open, while its removal from them during mitosis, due to localization to nuclei, leads to septal pore sealing [73]. NIMA kinase is a mitotic regulator, promoting mitotic nuclear pore complex (NPC) disassembly that is required for entry into mitosis in *A. nidulans* [74]. Common cell cycle regulatory mechanisms might control septal pores and nuclear pores in a way that they are opened and closed out of phase to each other during cell cycle progression [73].

Having seen that WscA seals septal pores, we came to the idea that this protein might be the possible substrate of NIMA at septa that has not been identified yet. Using WscA-GFP as a marker for septa sealing, we tried first to verify the mitotic regulation of cell to cell connectivity. In order to arrest cells during different phases of the cell cycle,

we expressed WscA-GFP in two different genetic backgrounds. One harboring the temperature-sensitive mutation, *nimA5* (*never in mitosis*), which blocks the G2 to M transition at restrictive temperature, 42°C, arresting cells at interphase [55], while the other, also a thermosensitive mutation, *bimE7* (*blocked in mitosis*), causes chromosome condensation and pre-anaphase spindle formation at restrictive temperature, leading cells to a mitotic arrest [56]. In these strains, histones were marked with mRFP, in order to confirm that cells were actually arrested at interphase or mitosis. Due to the fact that these conditional mutations lead to an inability of spore germination at restrictive temperature, all experimental manipulations were conducted either near this temperature (37°C instead of 42°C) or after a 4 h exposure of germinated spores at 42°C (for microscopic analysis).

As Figure 3.28 shows, at permissive temperature (25°C) there is no difference between the control strain and the cell cycle mutants on septal pore sealing, as expected. On the contrary, at restrictive temperature (42°C for 4 h), cells arrested at interphase (*nimA5*) tend to have half of their septal pores open, whereas in cells arrested at mitosis (*bimE7*), all pores were sealed. This result is in line with findings reported in Osmani et al. [73], confirming that cell cycle regulates septal pore opening and additionally shows that WscA has a crucial role in this process.

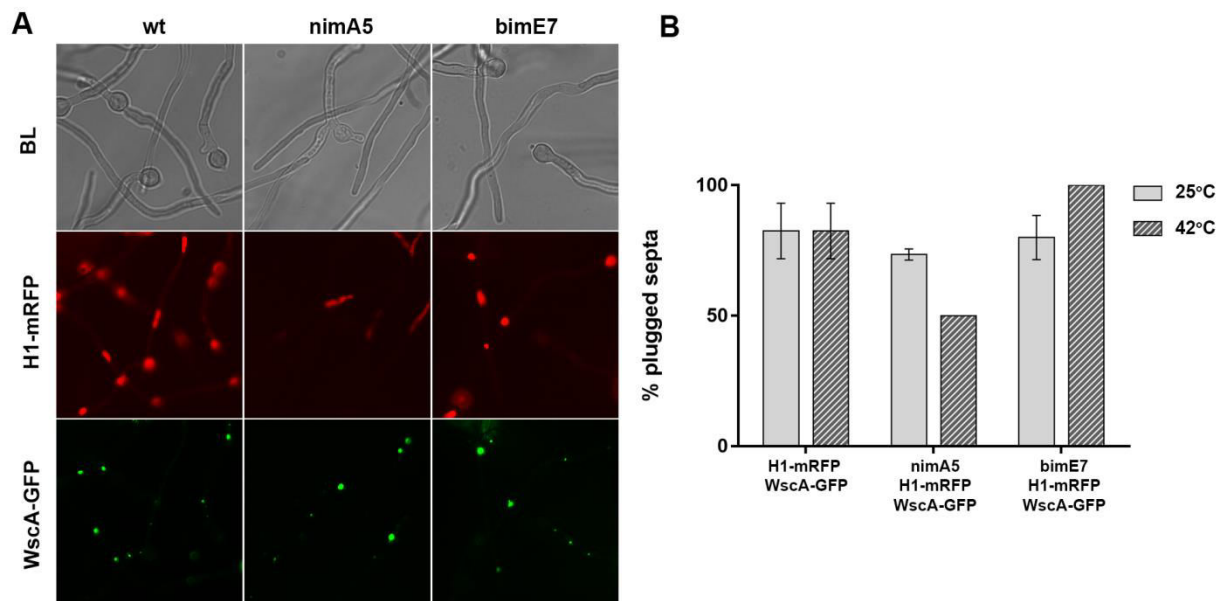


**Figure 3.28. (A)** Epifluorescence microscopy of WscA-GFP H1-mRFP, *nimA5* WscA-GFP H1-mRFP and *bimE7* WscA-GFP H1-mRFP expressing strains after a 4h shift at the restrictive temperature (42°C) **(B)** Quantification of the percentage of closed septa of each strain at permissive (25°C) and restrictive temperature (42°C). Notice the difference on septal pore sealing at 42°C on the cell cycle mutants, *nimA5* (fewer plugged septa) and *bimE7* (all septa plugged). The percentages of closed septa were determined based on the analysis of 60 septa for each strain.

Next, we proceeded to a more ambitious project, concerning the possibility that WscA might act as a substrate for NIMA at septal pores. According to this hypothesis, phosphorylation of WscA might be the factor that determines whether Woronin bodies will localize on septa or not. In such a scenario, NIMA is removed from septa during mitosis to promote the disassembly of nuclear pore complex (NPCs), leaving WscA unphosphorylated and ready to trigger septal pore closing via Woronin bodies. During mitotic exit, NIMA locates back to septa and phosphorylates WscA, rendering it inactive and incapable of plugging septal pores.

In order to investigate this hypothesis, we performed Western blot analysis, using GFP-antibody, on strains expressing WscA-GFP in genetic backgrounds with defects in cell

cycle (*nimA5* and *bimE7*) as well as in a wild-type background. All strains were incubated under two different temperatures, 25°C and 37°C. Western blot immunodetection was performed after total protein extraction. Western blot analysis is shown in Figure 3.29, where no differences in protein size and thus in the phosphorylation state of WscA can be detected at 37°C between the wild-type and the cell cycle mutants.

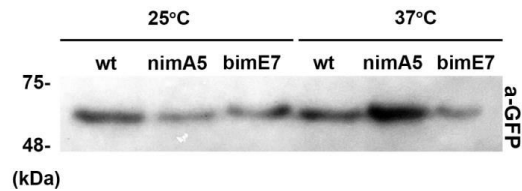


**Figure 3.29** Western blot analysis of WscA-GFP in wt, *nimA5* and *bimE7* genetic backgrounds.

WscA does not seem to be phosphorylated when cells are arrested at interphase (*nimA5*) or unphosphorylated when they are blocked at mitosis (*bimE7*). Thus, the NIMA substrate in septal pores remains unknown.

## 4. DISCUSSION

Peroxisome-based metabolism, which is essential for all eukaryotic cells, requires the transport of metabolites, ions and cofactors across the peroxisomal membrane [75, 76]. As most of these solutes are, in principle, unable to diffuse freely through the lipid bilayer, specific transport proteins are needed for their membrane passage. According to the current knowledge, small solutes, with molecular masses up to 300-400 Da, cross the peroxisomal membrane via facilitated diffusion carried by rather promiscuous channels, whereas “bulky” metabolites, including ATP, cofactors like NAD/H, NADP/H or CoA as well as fatty acids, are translocated by specific transporters [45]. For instance, peroxisomes harbor ATP binding cassette (ABC) transporters, which use ATP to actively transport CoA esters of fatty acids across the membrane [77]. Still however, very little is known on specific transporters related to peroxisomal metabolism at the molecular level. Rather surprisingly, years of fungal genetics have led to practically no information concerning genes encoding putative peroxisomal transport proteins.

One of the best characterized metabolic processes related to peroxisomes is that of purine catabolism in *A. nidulans*, where all genes encoding the relative enzymes, regulatory proteins and plasma membrane transporters have been characterized in great detail [16]. The way, although, by which specific intermediate metabolites of this catabolic pathway cross the peroxisomal membrane is still totally ignored, as we do not have any clue on how uric acid or HIU are translocated between cytoplasm and peroxisomal matrix. Given the failure of classical genetics or biochemical approaches to identify peroxisomal uric acid transport proteins, we tried here to investigate whether an *in silico* approach of correlated gene loss with UOX might lead us to the “missing” peroxisomal transport systems. Using this approach and based on best hits relative to putative transport proteins, we functionally characterized the PMP22 homologue of *A. nidulans*.

This protein, named WscA, had all the characteristics of a putative transmembrane channel and was indeed shown to be a major peroxisomal protein, as might have been expected from analogous studies of its orthologues in other filamentous ascomycetes as well as higher eukaryotes. Most importantly, we obtained genetic and physiological evidence that this protein is redundant for uric acid catabolism and that its expression is unrelated to regulation of purine catabolism. In other words, we failed to associate WscA with peroxisomal transport of uric acid or other related metabolite. Noticeably, WscA was found to be redundant not only for purine metabolites but also for other metabolites involved in known peroxisomal pathways, such as the catabolism of long chain fatty acids or D-amino acids. This redundancy strongly suggests that WscA is not the major transporter/channel of the relative metabolites. Similar lack of evidence against an association of WscA homologue with peroxisomal transport was obtained in the methylotrophic yeast *Hansenula polymorpha* [78]. There, deletion of the *wsc* gene did not affect growth on methanol or ethanol, which necessitate several metabolites to be transported across the peroxisomal membrane, such as formaldehyde, dihydroxyacetone, glyceraldehyde-3-phosphate and xylulose-5-phosphate. Also, the metabolism of D-amino acids, D-choline or methylamine by peroxisomal oxidases was not defective in the  $\Delta wsc$  mutant, indicating that a role of Wsc in solute transport is very unlikely, also in *H. polymorpha*. Instead,  $\Delta wsc$  lead to morphological changes in peroxisomes which appeared to possess an irregular shape with long tubular extensions [78]. The redundancy of WscA/Wsc in purine and specific metabolite utilization or biosynthesis, processes supposed to take place, at least partly, in the peroxisomes, establishes that this protein is *not* a major transporter/channel of the peroxisomal membrane. The indirect but strong evidence against WscA being a channel

for peroxisomal metabolites in *A. nidulans* and *H. polymorpha*, coupled with the technical difficulty in performing direct uptake assays with isolated peroxisome ascomycetes, leave open whether WscA acts as a *bona fide* channel at all.

Conclusions concerning a potential role of WscA specifically in purine peroxisomal transport in *A. nidulans* become even more difficult to draw under the light of the unexpected finding that purines can be normally catabolized in genetically modified strains that express peroxisomal enzymes, such as UoX or HIU hydrolase, in the cytoplasm. Similar doubts concern the biochemical role of PMP22 proteins in eukaryotes, in general. Interestingly, PMP22 proteins possess a core structure of 4 TMS and cytosolic tails, similar to Claudins [79], which are also channel-like proteins of similar size that control selective *paracellular* transport of solutes (including uric acid; [80] ) at tight junctions of cells in many organisms, ranging from nematodes to humans [81]. Claudins however have an additional extracellular beta-sheet domain that is lacking in PMP22.

As our experiments did not demonstrate a role of WscA in purine transport and purine catabolism, other reasons may explain the link between UOX and WscA observed by coevolution analysis. A possible explanation, supported by the observations that these genes are often lost in anaerobic or micro-aerobic species, is that both proteins are relevant for oxidative metabolism in the peroxisome. Another possibility is that urate oxidation in fungi has a more general role in the maintenance of peroxisome structure as it has been observed in plants [82].

Apart from a potential role of WscA as a channel, one other observation drew our attention, concerning its function at septa. WscA was found to be absolutely essential for septal pore sealing. In parallel, WscA proved to be critical for peroxisome biogenesis, oxidative and general stress sustainability, and the proper production of conidiospores. The latter phenotypic defects observed in the null  $\Delta wscA$  mutant are apparently related to the lack of septal pore sealing. Interestingly, lack of *hexA* had a very minor apparent defect in the localization of peroxisomes at septal pores, despite encoding the core matrix protein of Woronin bodies. This means, that even without HexA, peroxisomes containing WscA find their way to septal pores. Whether the pores lacking HexA are properly sealed, remains to be shown. However, the similarity of mutant phenotypes of  $\Delta wscA$  and  $\Delta hexA$  mutants favors the idea that pores plugged with peroxisomes without HexA are not properly sealed. In this case, peroxisomes are localized at pores, but without the dense crystal lattice that HexA would form through its self-assembly, a partial communication across the two adjacent cells is still permitted. Notably, the strong growth defects of both null  $\Delta wscA$  and  $\Delta hexA$  mutants on purines or urea might be attributed to the fact that the catabolism of these metabolites is known to generate reactive oxygen species and significant oxidative stress, which apparently requires proper septal pore sealing.

In conclusion, despite the fact that our results did not give credit, at least in this work, to our original idea on how to find the 'missing' peroxisomal uric acid transporter, they established, together with work in *H. polymorpha*, that fungal PMP22 proteins do not function as peroxisomal transporters. In addition, although this work did not have the intention to functionally dissect the details on the mechanism of peroxisome-dependent septal pore sealing in ascomycetes, still a number of novel findings, such as the establishment of WscA as a HexA-independent peroxisomal sorting factor and its importance in proper peroxisome biogenesis and sustainability to oxidation, came to light. Although we still ignore the full range of cellular roles and details on the mechanism of action of WscA, one can also predict that its role extends beyond septal sealing in filamentous ascomycetes, as orthologous proteins can be readily identified in

yeast as diverse as *Kluyveromyces lactis*, methylotrophic yeast species and basidiomycetes.

## ABBREVIATIONS

HxA	xanthine dehydrogenase
AIX	allantoinase
AaX	allantoicase
UaW	ureido imidazoline decarboxylase
XanA	a-ketoglutarate Fe(II)-dependent dioxygenase
UaZ, UOX	urate oxidase
UaX, HIU	5-hydroxy-isourate hydrolase
UglA	ureidoglycolate lyase
ER	Endoplasmic reticulum
Pex	Peroxisins
PTS1	Peroxisomal targeting signal 1
PTS2	Peroxisomal targeting signal 2
mPTS1	Membrane peroxisomal targeting signal 1
mPTS2	Membrane peroxisomal targeting signal 2
PAS	Pre-autophagosomal structure
15-LOX	15-lipoxygenase
PSLP	Peroxisomal Lon protease
(V)LCFA	(very) long chain fatty acids
Wsc	Woronin sorting complex
WBs	Woronin bodies
Pyro	Pyridoxine
Paba	P-aminobenzoic acid
Panto	Pantothenic acid
Ribo	Riboflavin
Bio	Biotin
CM	Complete medium
MM	Minimal medium
ROI	Region of Interest
PCC	Pearson's relation coefficient
GFP	Green Fluorescent Protein
mRFP	Monomeric Red Fluorescent Protein
NH <sub>4</sub> <sup>+</sup>	Ammonium
NO <sub>3</sub> <sup>-</sup>	Sodium nitrate

ADE	Adenine
ALL	Allantoin
UA	Uric acid
BF	Brightfield
EPI	Epifluorescent microscopy
PAR	Paraquat
CR	Congo red
MB	Methylene blue
Cd	Cadmium
Cyt	Cytoplasmic

## APPENDIX

### Oligonucleotides used in this study for cloning purposes

Oligonucleotides	Sequence
<b><i>pGEM wscA<sup>-(5xGA)</sup>GFP::AFpyrG or pGEM wscA<sup>-(5xGA)</sup>mRFP::AFpyrG</i></b>	
wscA 5' ApaI F	GCGCGGGCCCCTGGGGTCGTAACAGCTTCC
wscA ORF NS SpeI R	GCGCACTAGTCCGGTAGTCGGGTCCAGG
wscA 3' SpeI F	GCGCACTAGTAGGATGTAATTCCTCCCGGAC
wscA 3' NotI R	GCGCGCGGCCGCGCGCGAAGCAGTGCTTCGAATATC
5xGA SpeI F	CGCGACTAGTGGAGCTGGTGCAGGCGCTGGAGCCGGTGCC
AFpyrG SpeI R	CGCGACTAGTCTGTCTGAGAGGAGGCACTGATGCG
<b><i>pGEM wscAA::AFpyrG</i></b>	
wscA 5' ApaI F	GCGCGGGCCCCTGGGGTCGTAACAGCTTCC
wscA 5' SpeI R	GCGCACTAGTGGTTGCGATGGTGGAGGAG
wscA 3' SpeI F	GCGCACTAGTAGGATGTAATTCCTCCCGGAC
wscA 3' NotI R	GCGCGCGGCCGCGCGCGAAGCAGTGCTTCGAATATC
AFpyrG SpeI F	CGCGACTAGTGCCTCAAACAATGCTCTTCACCCTC
AFpyrG SpeI R	CGCGACTAGTCTGTCTGAGAGGAGGCACTGATGCG
<b><i>pGEM hexAA::AFpyrG</i></b>	
hexA 5' ApaI F	CGCGGGGCCCCGAGTCGATCGAGGAGAACAATGTC
hexA 5' SpeI R	CGCGACTAGTCTTGCGAGCCTTGGGGTGATCTAC
hexA 3' SpeI F	CGCGACTAGTGCTGTCTACAGGGGTCTCTAAAAC
hexA 3' NotI R	CGCGGCGGCCGCCCAATCAGTACACACGAGATCGAG
AFpyrG SpeI F	CGCGACTAGTGCCTCAAACAATGCTCTTCACCCTC
AFpyrG SpeI R	CGCGACTAGTACTGTCTGAGAGGAGGCACTGATGCG
<b><i>hexAp::AFpyrG::GFP-hexA</i></b>	
GFP-hexA F	CGGCATGGACGAGCTGTACAAGAATGGGTACTACGACGACGACGG
hexA-AFpyrG R	GGGTGAAGAGCATTGTTTGAGGCTTATAGACGGGAAGAGTGGATGATC
hexA 5 nest F	GAGAGGAAGAAAAGAAGAGGCTGG
hexA 3 nest R	CTCAGTACGCCAGTAAATGGCAC
<b><i>pGEM aloAA::AFpyrG</i></b>	
aloA 5' NcoI F	CGGCCATGGGTGATATCAGCCATGTTTGGCAAGG
aloA 5' SpeI R	CGCGACTAGTCTGGCTGCTTTTGTGTGTATCGATG
aloA 3' SpeI F	CGCGACTAGTGAAAGGTACGGTTACAGCTAGCAAAC
aloA 3' NotI R	CGCGGCGGCCGCCAACCCTGATTCCCGATTTGTCTC
AFpyrG SpeI F	CGCGACTAGTGCCTCAAACAATGCTCTTCACCCTC
AFpyrG SpeI R	CGCGACTAGTACTGTCTGAGAGGAGGCACTGATGCG

## REFERENCES

- [1] Houbraken, J., R. P. de Vries, R. A. Samson, 2014 Modern taxonomy of biotechnologically important *Aspergillus* and *Penicillium* species. *Adv Appl Microbiol.* 86:199-249.
- [2] Kirk, P. M., P. F. Cannon, D. W. Minter, and J. A. Stalpers, 2008 *Dictionary of the Fungi*. 10th ed., Wallingford: CABI.
- [3] Alexopoulos, C. J., C. W. Mims, and M. Blackwell, 1996 *Introductory Mycology*. 4th ed., John Wiley and Sons, New York.
- [4] Lutzoni, F., F. Kauff, C. J. Cox, D. McLaughlin, G. Celio et al., 2004 Assembling the fungal tree of life: progress, classification, and evolution of subcellular traits. *Am J Bot.* 91: 1446-1480.
- [5] Scazzocchio, C., 2009 *Aspergillus: A Multifaceted Genus*. In *Encyclopedia of Microbiology*, Schaechter, M. (ed.). Elsevier, Oxford. Pp. 401-421.
- [6] Fischer, R. & Kues, U., 2006. Asexual sporulation in mycelial fungi. In *The Mycota, Growth, Differentiation and Sexuality*, Volume 1, Edited by R. Fischer, U. Kues. Berlin Heidelberg, FL: Springer-Verlag Berlin Heidelberg
- [7] Galagan JE, Calvo SE, Cuomo C, Ma LJ, Wortman JR, Batzoglou S, Lee SI, Basturkmen M, Spevak CC, Clutterbuck J, Kapitonov V, Jurka J, Scazzocchio C, Farman M, Butler J, Purcell S, Harris S, Braus GH, Draht O, Busch S, D'Enfert C, Bouchier C, Goldman GH, Bell-Pedersen D, Griffiths-Jones S, Doonan JH, Yu J, Vienken K, Pain A, Freitag M, Selker EU, Archer DB, Penalva MA, Oakley BR, Momany JM, Tanaka T, Kumagai T, Asai K, Machida M, Nierman WC, Denning DW, Caddick M, Hynes M, Paoletti M, Fischer R, Miller B, Dyer P, Sachs MS, Osmani SA, Birren BW, 2005. Sequencing of *Aspergillus nidulans* and comparative analysis with *A. fumigatus* and *A. oryzae*. *Nature* 438: 1105–1115.
- [8] Pontecorvo, G., Roper, J.A., Hemmons, L.M., MacDonald, K.D. & Bufton, A.W.J. The genetics of *Aspergillus nidulans*. *Adv. Genet.* 5, 141–238 (1953).
- [9] Todd RB, Davis MA, Hynes MJ. Genetic manipulation of *Aspergillus nidulans*: meiotic progeny for genetic analysis and strain construction. *Nat Protoc.* 2007;2(4):811–21.
- [10] Casselton L and Zolan M. (2002). The art and design of genetic screens: filamentous fungi. *Nat Rev Genet* 3:683-69
- [11] Marzluf G. A. (1997). Genetic regulation of nitrogen metabolism in the fungi. *Microbiology and molecular biology reviews : MMBR*, 61(1), 17–32.
- [12] Arst HN Jr, Cove DJ (1973) Nitrogen metabolite repression in *Aspergillus nidulans*. *Mol Gen Genet* 126:111–141
- [13] Todd R.B. (2016) 11 Regulation of Fungal Nitrogen Metabolism. In: Hoffmeister D. (eds) *Biochemistry and Molecular Biology. The Mycota (A Comprehensive Treatise on Fungi as Experimental Systems for Basic and Applied Research)*, vol III. Springer, Cham
- [14] Scazzocchio, C., Sdrin, N., and Ong, G. (1982) Positive regulation in a eukaryote, a study of the *uaY* gene of *Aspergillus nidulans*: I. Characterization of alleles, dominance and complementation studies, and a fine structure map of the *uaY-oxpA* cluster. *Genetics* 100: 185–208.
- [15] Pantazopoulou, A., and Diallinas, G. (2007) Fungal nucleobase transporters. *FEMS Microbiol Rev* 31:657–75.
- [16] Galanopoulou, K, C Scazzochio, ME Galinou, W Liu, F Borbolis, M Karachaliou, N Oestreicher, DG Hatzinikolaou, G Diallinas, and S Amillis. 2014. Purine utilization proteins in the Eurotiales: Cellular compartmentalization, phylogenetic conservation and divergence. *Fungal Genetics and Biology* 69: 96-108
- [17] Gournas, C., Oestreicher, N., Amillis, S., Diallinas, G., and Scazzocchio, C. (2011) Completing the purine utilisation pathway of *Aspergillus nidulans*. *Fungal Genet Biol* 48: 840–8.
- [18] Hayashi, S., Fujiwara, S., Noguchi, T., 2000. Evolution of urate-degrading enzymes in animal peroxisomes. *Cell Biochem. Biophys.* 32, 123–129.
- [19] Titorenko, V. I., & Rachubinski, R. A. (2001). The life cycle of the peroxisome. *Nature Reviews Molecular Cell Biology*, 2(5), 357–368
- [20] Maruyama, J., & Kitamoto, K. (2013). Expanding functional repertoires of fungal peroxisomes: contribution to growth and survival processes. *Frontiers in physiology*, 4, 177.
- [21] Hu, J., Baker, A., Bartel, B., Linka, N., Mullen, R. T., Reumann, S., & Zolman, B. K. (2012). Plant peroxisomes: biogenesis and function. *The Plant cell*, 24(6), 2279–2303.
- [22] Wanders R. J., Waterham H. R. (2006). Biochemistry of mammalian peroxisomes revisited. *Annu. Rev. Biochem.* 75, 295–332
- [23] Costello, J. L., & Schrader, M. (2018). Unloosing the Gordian knot of peroxisome formation. *Current opinion in cell biology*, 50, 50–56.
- [24] Eckert J.H., Erdmann R. (2003) Peroxisome biogenesis. In: *Reviews of Physiology, Biochemistry and Pharmacology*. Reviews of Physiology, Biochemistry and Pharmacology, vol 147. Springer, Berlin, Heidelberg

- [25] Dimitrov, L., Lam, S. K., & Schekman, R. (). The role of the endoplasmic reticulum in peroxisome biogenesis. *Cold Spring Harbor perspectives in biology*, 5(5), a013243.
- [26] Lazarow, Paul. (2016). Peroxisomes. *Encyclopedia of Cell Biology*.
- [27] Islinger, M., Grille, S., Fahimi, H.D. et al. *Histochem Cell Biol* (2012) The peroxisome: an update on mysteries 137: 547.
- [28] Bartoszewska, M., Opaliński, L., Veenhuis, M., & van der Klei, I. J. (2011). The significance of peroxisomes in secondary metabolite biosynthesis in filamentous fungi. *Biotechnology letters*, 33(10), 1921–1931.
- [29] Farmer, L. M., Rinaldi, M. A., Young, P. G., Danan, C. H., Burkhart, S. E., & Bartel, B. (2013). Disrupting autophagy restores peroxisome function to an Arabidopsis lon2 mutant and reveals a role for the LON2 protease in peroxisomal matrix protein degradation. *The Plant cell*, 25(10), 4085–4100.
- [30] De Duve, C., & Baudhuin, P. (1966). Peroxisomes (microbodies and related particles). *Physiological Reviews*, 46(2), 323–357.
- [31] Islinger, M., Cardoso, M. J. R., & Schrader, M. (2010). Be different—The diversity of peroxisomes in the animal kingdom. *Biochimica et Biophysica Acta (BBA) - Molecular Cell Research*, 1803(8), 881–897.
- [32] Wanders, R. J. A. (2014). Metabolic functions of peroxisomes in health and disease. *Biochimie*, 98, 36–44.
- [33] Kunze, M., Pracharoenwattana, I., Smith, S. M., & Hartig, A. (2006). A central role for the peroxisomal membrane in glyoxylate cycle function. *Biochimica et Biophysica Acta (BBA) - Molecular Cell Research*, 1763(12), 1441–1452.
- [34] Lee, I. R., Yang, L., Sebetso, G., Allen, R., Doan, T. H., Blundell, R., Fraser, J. A. (2013). Characterization of the complete uric acid degradation pathway in the fungal pathogen *Cryptococcus neoformans*. *PLoS one*, 8(5), e64292.
- [35] Knowles J. R. (1989). The mechanism of biotin-dependent enzymes. *Annu. Rev. Biochem.* 58, 195–221
- [36] Tanabe Y., Maruyama J., Yamaoka S., Yahagi D., Matsuo I., Tsutsumi N., et al. (2011). Peroxisomes are involved in biotin biosynthesis in *Aspergillus* and *Arabidopsis*. *J. Biol. Chem.* 286, 30455–30461
- [37] Stehlik, T., Sandrock, B., Ast, J., & Freitag, J. (2014). Fungal peroxisomes as biosynthetic organelles. *Current Opinion in Microbiology*, 22, 8–14.
- [38] Liu, F., Ng, S. K., Lu, Y., Low, W., Lai, J., & Jedd, G. (2008). Making two organelles from one: Woronin body biogenesis by peroxisomal protein sorting. *The Journal of cell biology*, 180(2), 325–339.
- [39] Maruyama, Jun-ichi & Kitamoto, Katsuhiko. (2019). The Woronin Body: A Fungal Organelle Regulating Multicellularity, *Biology of the Fungal Cell*, pp.3-14
- [40] Ng, S. K., Liu, F., Lai, J., Low, W., & Jedd, G. (2009). A Tether for Woronin Body Inheritance Is Associated with Evolutionary Variation in Organelle Positioning. *PLoS Genetics*, 5(6), e1000521.
- [41] Bleichrodt R, van Veluw GJ, Recter B, Maruyama J, Kitamoto K, Wösten HAB (2012) Hyphal heterogeneity in *Aspergillus oryzae* is the result of dynamic closure of septa by Woronin bodies. *Mol Microbiol* 86:1334–1344
- [42] Jedd, G. (2011). Fungal evo–devo: organelles and multicellular complexity. *Trends in Cell Biology*, 21(1), 12–19.
- [43] Antonenkov VD, Sormunen RT, Hiltunen JK (2004) The rat liver peroxisomal membrane forms a permeability barrier for cofactors but not for small metabolites in vitro. *J Cell Sci* 117:5633–5642
- [44] Rokka A, Antonenkov VD, Soininen R, Immonen HL, Pirila PL, Bergmann U, Sormunen RT, Weckstrom M, Benz R, Hiltunen JK (2009) Pxmp2 is a channel-forming protein in mammalian peroxisomal membrane. *PLoS ONE* 4:e5090
- [45] Antonenkov, V. D., & Hiltunen, J. K. (2012). Transfer of metabolites across the peroxisomal membrane. *Biochimica et Biophysica Acta (BBA) - Molecular Basis of Disease*, 1822(9), 1374–1386.
- [46] Kemp S, Theodoulou FL, Wanders RJ (2011) Mammalian peroxisomal ABC transporters: from endogenous substrates to pathology and clinical significance. *Br J Pharmacol* 164:1753–1766
- [47] Palmieri L, Rottensteiner H, Girzalsky W, Scarcia P, Palmieri F, Erdmann R (2001) Identification and functional reconstitution of the yeast peroxisomal adenine nucleotide transporter. *EMBO J* 20:5049–5059
- [48] Visser WF, van Roermund CW, Waterham HR, Wanders RJ (2002) Identification of human PMP34 as a peroxisomal ATP transporter. *Biochem Biophys Res Commun* 299:494–497
- [49] Linka N, Theodoulou FL, Haslam RP, Linka M, Napier JA, Neuhaus HE, Weber AP (2008) Peroxisomal ATP import is essential for seedling development in *Arabidopsis thaliana*. *Plant Cell* 20:3241–3257
- [50] Futagami, T., Nakao, S., Kido, Y., Oka, T., Kajiwara, Y., Takashita, H., Goto, M. (2011). Putative stress sensors WscA and WscB are involved in hypo-osmotic and acidic pH stress tolerance in *Aspergillus nidulans*. *Eukaryotic cell*, 10(11), 1504–1515.

- [51] Nayak, T., Szewczyk, E., Oakley, C. E., Osmani, A., Ukil, L., Murray, S. L., Oakley, B. R. (2006). A versatile and efficient gene-targeting system for *Aspergillus nidulans*. *Genetics*, 172(3), 1557–1566.
- [52] Oestreicher, N., Sealy-Lewis, H. M., & Scazzocchio, C. (1993). Characterisation, cloning and integrative properties of the gene encoding urate oxidase in *Aspergillus nidulans*. *Gene*, 132(2), 185–192.
- [53] Suárez, T., de Queiroz, M. V., Oestreicher, N., & Scazzocchio, C. (1995). The sequence and binding specificity of UaY, the specific regulator of the purine utilization pathway in *Aspergillus nidulans*, suggest an evolutionary relationship with the PPR1 protein of *Saccharomyces cerevisiae*. *The EMBO journal*, 14(7), 1453–1467.
- [54] Nayak, T., Edgerton-Morgan, H., Horio, T., Xiong, Y., De Souza, C. P., Osmani, S. A., & Oakley, B. R. (2010). Gamma-tubulin regulates the anaphase-promoting complex/cyclosome during interphase. *The Journal of cell biology*, 190(3), 317–330.
- [55] Osmani, S. A., May, G. S., & Morris, N. R. (1987). Regulation of the mRNA levels of *nimA*, a gene required for the G2-M transition in *Aspergillus nidulans*. *The Journal of cell biology*, 104(6), 1495–1504.
- [56] Osmani, S. A., Engle, D. B., Doonan, J. H., & Morris, N. R. (1988). Spindle formation and chromatin condensation in cells blocked at interphase by mutation of a negative cell cycle control gene. *Cell*, 52(2), 241–251.
- [57] Yu, J.H., Hamari, Z., Han, K.H., Seo, J.A., Reyes-Domínguez, Y., Scazzocchio, C., (2004). Double-joint PCR: a PCR-based molecular tool for gene manipulations in filamentous fungi. *Fungal Genet. Biol.* 41, 973-981.
- [58] Koukaki, M., Giannoutsou, E., Karagouni, A., and Diallinas, G., (2003). A novel improved method for *Aspergillus nidulans* transformation. *J. Microbiol. Methods.* 55, 687-695.
- [59] Bradford, M. M. (1976). A rapid and sensitive method for the quantitation of microgram quantities of protein utilizing the principle of protein-dye binding. *Analytical Biochemistry*, 72(1-2), 248–254.
- [60] Kriventseva, E. V., Kuznetsov, D., Tegenfeldt, F., Manni, M., Dias, R., Simão, F. A., & Zdobnov, E. M. (2019). OrthoDB v10: sampling the diversity of animal, plant, fungal, protist, bacterial and viral genomes for evolutionary and functional annotations of orthologs. *Nucleic acids research*, 47(D1), D807–D811.
- [61] Date, S. V., & Marcotte, E. M. (2003). Discovery of uncharacterized cellular systems by genome-wide analysis of functional linkages. *Nature Biotechnology*, 21(9), 1055–1062.
- [62] Leonhardt, Y., Beck, J., & Ebel, F. (2016). Functional characterization of the Woronin body protein WscA of the pathogenic mold *Aspergillus fumigatus*. *International Journal of Medical Microbiology*, 306(3), 165–173.
- [63] Han, P., Jin, F. J., Maruyama, J., & Kitamoto, K. (2014). A large nonconserved region of the tethering protein Leashin is involved in regulating the position, movement, and function of Woronin bodies in *Aspergillus oryzae*. *Eukaryotic cell*, 13(7), 866–877.
- [64] Tey WK, North AJ, Reyes JL, Lu YF, Jedd G (2005) Polarized gene expression determines Woronin body formation at the leading edge of the fungal colony. *Mol Biol Cell* 16: 2651–2659.
- [65] Beck, J., Echtenacher, B., & Ebel, F. (2013). Woronin bodies, their impact on stress resistance and virulence of the pathogenic mould *Aspergillus fumigatus* and their anchoring at the septal pore of filamentous Ascomycota. *Molecular Microbiology*, 89(5), 857–871.
- [66] Szewczyk, E., Nayak, T., Oakley, C.E., Edgerton, H., Xiong, Y., Taheri-Talesh, N., Osmani, S.A., Oakley, B.R., 2006. Fusion PCR and gene targeting in *Aspergillus nidulans*. *Nat. Protoc.* 1, 3111-3120.
- [67] Huh, W.K., Lee, B.H., Kim, S.T., Kim, Y.R., Rhie, G.E., Baek, Y.W., Hwang, C.S., Lee, J.S., Kang, S.O., (1998). D-Erythroascorbic acid is an important antioxidant molecule in *Saccharomyces cerevisiae*. *Mol. Microbiol.* 30, 895-903.
- [68] Ravagnani, A., Gorfinkiel, L., Langdon, T., Diallinas, G., Adjadj, E., Demais, S., Gorton, D., Arst, H.N.Jr., Scazzocchio, C., (1997). Subtle hydrophobic interactions between the seventh residue of the zinc finger loop and the first base of an HGATAR sequence determine promoter-specific recognition by the *Aspergillus nidulans* GATA factor AreA. *EMBO J.* 16, 3974-3986.
- [69] Jedd, G., & Chua, N.-H. (2000). A new self-assembled peroxisomal vesicle required for efficient resealing of the plasma membrane. *Nature Cell Biology*, 2(4), 226–231.
- [70] Tenney, K., Hunt, I., Sweigard, J., Pounder, J. I., McClain, C., Bowman, E. J., & Bowman, B. J. (2000). *hex-1*, a Gene Unique to Filamentous Fungi, Encodes the Major Protein of the Woronin Body and Functions as a Plug for Septal Pores. *Fungal Genetics and Biology*, 31(3), 205–217.
- [71] Beck, J & Echtenacher, Bernd & Ebel, Frank. (2011). The HexA protein of *Aspergillus fumigatus* and its role in stress resistance and virulence. 11-11.
- [72] Maruyama, J., Juvvadi, P. R., Ishi, K., & Kitamoto, K. (2005). Three-dimensional image analysis of plugging at the septal pore by Woronin body during hypotonic shock inducing hyphal tip bursting in the filamentous fungus *Aspergillus oryzae*. *Biochemical and Biophysical Research Communications*, 331(4), 1081–1088.

- [73] Shen, K. F., Osmani, A. H., Govindaraghavan, M., & Osmani, S. A. (2014). Mitotic regulation of fungal cell-to-cell connectivity through septal pores involves the NIMA kinase. *Molecular biology of the cell*, 25(6), 763–775.
- [74] Govindaraghavan, M., Lad, A. A., & Osmani, S. A. (2013). The NIMA Kinase Is Required To Execute Stage-Specific Mitotic Functions after Initiation of Mitosis. *Eukaryotic Cell*, 13(1), 99–109.
- [75] Theodoulou, F. L., Carrier, D. J., Schaedler, T. A., Baldwin, S. A., & Baker, A. (2016). How to move an amphipathic molecule across a lipid bilayer: different mechanisms for different ABC transporters?. *Biochemical Society transactions*, 44(3), 774–782.
- [76] Linka, N., & Esser, C. (2012). Transport proteins regulate the flux of metabolites and cofactors across the membrane of plant peroxisomes. *Frontiers in plant science*, 3, 3.
- [77] Morita, M., & Imanaka, T. (2012). Peroxisomal ABC transporters: Structure, function and role in disease. *Biochimica et Biophysica Acta (BBA) - Molecular Basis of Disease*, 1822(9), 1387–1396.
- [78] Manivannan, S. (2014). Yeast peroxisomes: de novo formation and maintenance. [S.l.]: s.n.
- [79] Tsukita, S., Tanaka, H., & Tamura, A. (2018). The Claudins: From Tight Junctions to Biological Systems. *Trends in Biochemical Sciences*.
- [80] Kimura, T., Tsukada, A., Fukutomi, T., Ichida, K., Ohtsuki, S., & Sakurai, H. (2019). Urate Transport via Paracellular Route across Epithelial Cells. *Biological and Pharmaceutical Bulletin*, 42(1), 43–49.
- [81] Mukendi, C., Dean, N., Lala, R., Smith, J., Bronner, M. E., & Nikitina, N. V. (2016). Evolution of the vertebrate claudin gene family: insights from a basal vertebrate, the sea lamprey. *The International Journal of Developmental Biology*, 60(1-2-3), 39–51.
- [82] Hauck, O. K., Scharnberg, J., Escobar, N. M., Wanner, G., Giavalisco, P., & Witte, C. P. (2014). Uric acid accumulation in an Arabidopsis urate oxidase mutant impairs seedling establishment by blocking peroxisome maintenance. *The Plant cell*, 26(7), 3090–3100.
- [83] Momany, M., Richardson, E. A., Van Sickle, C., & Jedd, G. (2002). Mapping Woronin body position in *Aspergillus nidulans*. *Mycologia*, 94(2), 260–266.
- [84] Salogiannis, J., Egan, M.J., Reck-Peterson, S.L., 2016. Peroxisomes move by hitchhiking on early endosomes using the novel linker protein PxdA. *J. Cell. Biol.* 212, 289-296.